IMPACT ANALYSIS OF SPATIAL-TEMPORAL RESOLUTION ON HIGH PENETRATION OF RENEWABLE ENERGY

by

GUOLONG, MA

A thesis submitted to

The University of Birmingham

for the degree of

DOCTOR OF PHILOSOPHY

Department of EESE,

School of Engineering

The University of Birmingham

September 2024

Dedicate to

My parents

ABSTRACT

The power generation of variable renewable energy (VRE) is largely affected by natural environmental factors, such as wind speed and solar irradiance, which can cause great variability, fluctuation, and intermittency, and these characteristics will become more severe as renewable energy penetration increases. These power variations will bring operational challenges to the instantaneous balance, and will also increase in intraday trading frequency, and increase re-scheduling operation costs in the electricity market. Therefore, increasing penetration of VRE will cause fundamental and structural changes to traditional power system operation regimes. This doctoral study focuses on the investigation of increasing spatial-temporal resolution in high-penetration renewable energy systems and evaluates their impact on electricity market operations, hence providing scientific insights into the electricity market reform.

This thesis carries out a literature review and it is found: there is a lack of theoretical research on the impact of power fluctuation characteristics on the day-ahead power curve and the real-time power curve; there is a lack of quantitative scientific evaluation of the entire electricity market at different temporal granularity; Current research on increasing spatial granularity generally focuses on the regional and node electricity prices, but rarely mentions the increase of spatial network granularity, and lacks a scientific model for building spatial grid networks.

In terms of power fluctuation, this thesis proposes metrics including power incremental

statistics, coefficient of variation, and peak power duration to characterize the power variability characteristics. Based on these metrics, the mathematical relationship between these variations and net-load power curves, and real-time power imbalance curves are analysed. It is found that power variability will directly affect net-load power curves and the power gradient will affect the real-time power imbalance. For example, the solar power variability characteristics will cause the net-load power curve to look like a duck curve, while real-time power imbalance to look like a butterfly curve.

In terms of increasing temporal resolution reform in electricity markets, this thesis proposes an evaluation method for the electricity market at different time granularity, including ex-ante real-time power deviation prediction; real-time power scheduling operation and clearing; and ex-post power deviation settlement. Based on this evaluation model proposed, this thesis provides strong evidence that the higher the time granularity, the power step changes and the real-time power deviation quantities are smaller, and vice versa. Increasing the time granularity from 30 to 5 minutes will reduce the balancing cost by nearly half and reduce the power step amplitude standard deviation by nearly 80%.

In regarding the increasing spatial resolution for electricity market reform, including the space granularity of renewable generation units and the space granularity of the subnetworks, the thesis proposes the stochastic energy network theory to characterize the supply-demand adaptation balance index (SDABI) and further proposes a subnetwork networking method to evaluate the impact of increasing space granularity on reducing

power system operation costs, power flow losses, and power transmission network congestion.

In summary, this doctoral thesis for the first time provides scientific evidence to support the worldwide power market reform of the increasing spatial-temporal resolution with massive renewable energy integration systems.

ACKNOWLEDGEMENT

I would like to express my deep gratitude to my supervisor, Professor Xiao-Ping Zhang, for his valuable help, support, and guidance during my entire PhD study. My supervisor provided me with a good scientific research environment and an advanced development platform, which allowed me to explore the beauty of scientific research and the path of learning; From the words and deeds of my supervisor, I not only improved my professional level but also learned the methods and principles of dealing with people, which have benefited me throughout my life and I am deeply grateful.

I want to thank Dr. Jianing Li and Dr. Ying Xue for their guidance and help in the early stages of my PhD study. Their profound knowledge and peaceful personality have influenced me, from which I have benefited a lot.

I want to thank my colleagues and friends in my research group for all the helpful and inspiring discussions about my PhD research. Thanks to Dr. Nan Chen, Dr. Xin Ma, Dr. Shuailong Dai, Mr. Zixuan Jia, Mr. Chengyi Wu, Mr. David Li, Mr. Yiliang Fan, Mr. Mohamed Alashqar, Ms. Yinru Chen, Miss Yixin Li, etc.

I am deeply grateful to my family. They have always been my strong backing during my more than 20 years of study. It is their silent dedication and endless care that gave me the ability to choose a goal and be able to work hard for it.

I want to express my sincere thanks to all the experts and professors who reviewed this thesis and participated in the defense, as well as all the leaders, teachers, colleagues, and

friends who have cared about and helped me.

LIST OF PUBLICATIONS & OUTCOMES

[1] G. Ma, J. Li and X. -P. Zhang, "A Review on Optimal Energy Management of Multi-microgrid System Considering Uncertainties," *IEEE Access*, vol. 10, pp. 77081-77098, 2022, Doi: 10.1109/ACCESS.2022.3192638. (Some of the work corresponding to Chapter 2)

[2] G. Ma, J. Li, and X. -P. Zhang, "Energy Storage Capacity Optimization for Improving the Autonomy of Grid-Connected Microgrid," *IEEE Transactions on Smart Grid*, vol. 14, no. 4, pp. 2921-2933, July 2023, Doi: 10.1109/TSG.2022.3233910. (Some of the work corresponding to Chapter 5)

[3] G. Ma and X. -P. Zhang, "Real-Time Power Imbalance Time Series with Solar Power Penetration: Butterfly Curve," *IEEE Transactions on Sustainable Energy*, vol. 15, no. 2, pp. 1414-1417, April 2024, Doi: 10.1109/TSTE.2024.3368268. (Some of the work corresponding to Chapter 3)

[4] G. Ma and X. -P. Zhang, "Evaluation of the influence of increasing time granularity in the balanced electricity market", IET Powering Net Zero Conference 2024. (Accepted) (Some of the work corresponding to Chapter 4)

[5] G. Ma and X. -P. Zhang, " Would increasing time granularity reduce power market balancing costs and power grid frequency deviations?", (Under review in Energy Journal) (Some of the work corresponding to Chapter 4)

[6] G. Ma and X. -P. Zhang, " Evaluation of The Impact of Increasing Space Granularity Based on Supply-Demand Adaptation Balance on Power System Operation?", (Submitted to IEEE Transactions on Smart Grid) (Some of the work corresponding to Chapter 5)

CONTENTS

LIST OF FIGURES

LIST OF TABLES

1. INTRODUCTION

1.1. Research Background and Challenges

1.1.1 High Penetration Renewable Energy System

Recently, the world has suffered from a wide range of climate extremes, including heat waves, hurricanes, wildfires, and droughts, and how to mitigate the frequency of extreme weather and tackle climate change has become a global challenge that transcends national boundaries. To combat climate change, at the 21st Conference of the Parties (COP) held in Paris on December 12, 2015, 197 countries adopted the Paris Agreement. The agreement aims to significantly reduce global greenhouse gas emissions and limit global temperature rise this century to less than 2°C [1-2].

As the urgent issue of climate change continues to escalate, more and more countries have committed to achieving net zero carbon emissions in the coming years [3], The global renewable energy market has undergone qualitative changes:

(1) Renewable energy installed capacity is growing rapidly. During the whole year of 2023, 《Renewable Capacity Statistics 2024》 released by the International Renewable Energy Agency (IRENA) shows that solar energy and wind energy contribute more than 97% of the world's renewable energy installed capacity. Among them, solar energy accounts for about 73%, and wind power accounts for about 24%, total renewable installed capacity is about 473 GW [4 - 5].

(2) The cost of the entire renewable energy industry chain has been significantly reduced. From 2010 to 2022, the levelized cost of electricity (LCOE) of newly put-into-production grid-connected PV projects worldwide dropped by 88%. Wind power dropped by 68%, and offshore wind power dropped by 60% [6 - 7].

(3) Renewable energy has net-zero carbon emissions and is environmentally friendly. Based on the above characteristics, several research institutes have given renewable energy future scenarios in recent decades, as shown in **Error! Reference source not found.**.

From **Error! Reference source not found.**, this PhD study finds that variable renewable energy (VRE) will play an important role in the future energy structure, such as the Lappeenranta-Lahti University of Technology (LUT) predicts that 2050 share of renewable energy electricity will account for about 89% of the primary energy; the University of Technology Sydney predict that 2050 share of renewable energy electricity will account for about 92.3% of the primary energy; the Standard University predict that 2050 share of renewable energy electricity will account for about 99.1% of the primary energy; The institutes, International Renewable Energy Agency (IRENA) and International Energy Agency (IEA) predict that 2050 share of renewable energy electricity will account for about 90% and 88%, respectively [8 - 13].

Table 1-1 Renewable energy future scenarios in 2050

Research Institutes	Target	Energy sources	Renewable energy rate in total energy supply	Renewable energy rate in total electricity supply
LUT University	100% renewable energy	Solar photovoltaic (PV), Concentrated solar power (CSP), wind, hydropower, geothermal and bioenergy	100%	89%
University of Technology Sydney	1.5℃ target	Solar, wind, hydro, geothermal, biomass, ocean energy (tidal and wave)	100%	92.3%
Stanford University	100% WIND-WATER-SOLAR	Wind, PV, CSP, geothermal, hydro and ocean energy. Solar thermal, geothermal.	100%	~99.1%
International Renewable Energy Agency (IRENA)	1.5℃ target	Solar, wind, biogas, biomass, hydropower, geothermal, solar, ocean energy, natural gas, oil, coal and nuclear	74%	90%
International Energy Agency (IEA)	Net-zero emission	Solar, bioenergy, wind, hydropower, geothermal, other renewables, nuclear, natural gas, oil and coal.	67%	88%

1.1.2 Problems and Challenges

The main purpose of the power system is to maintain an immediate equilibrium between power supply and load demand for the security of the power system [14-15]. However, VREs face inherent challenges due to their reliance on natural environmental factors, such as solar irradiance, air temperature, wind speed, and wind directions, etc. These factors introduce significant volatility and uncertainty into the energy system [16-18]. As VREs penetrate the power grid on a massive scale, the grid will encounter greater fluctuations and intermittent than it does at present.

In the traditional power system, traditional generation such as nuclear, thermal, gas, and hydropower, etc. occupy a large proportion, and these generators have high inertia, which can use mechanical rapid rotating power to serve as automatic power generators to help keep the grid frequency stable [19]. However, with the high penetration of VREs, these generators (including wind turbines and PVs) transfer power/energy to the main grid based on an inverter technique. Through this technology, the inertia from the VREs is decoupled from the other side of the grid, therefore the moment of inertia of the total grid will be reduced and the lower rotational inertia will influence the power grid stability [20-23]. In addition, the volatility and intermittency of VRE generators will also cause higher power fluctuations, which will also cause power grid frequency fluctuations [14, 24-25]. Except for influencing the power grid frequency stability, the volatility and intermittency of VRE generators will bring higher power differences between day-ahead dispatch and real-time dispatch process, and therefore increase the re-dispatch operating cost and power deviation settlement cost, influencing the power market operation cost [26-29]. Therefore, high penetration of renewable energy systems will cause the following challenges.

(1) **Power grid operation stability:** The VRE generators (including wind turbines [21] and photovoltaics [23]) transmit power/energy to the main grid based on power electronics rectification and inverter technology. Through this technology, the inertia of the rotating parts of renewable energy units will be decoupled from the other side of the grid, resulting in a lower inertia of the total power system, which will reduce a

negative impact on the power system operation stability [14], [20], [23].

(2) **Power system operation and control:** The frequent and rapid fluctuation characteristics of high-penetration VREs will bring operational challenges to the instantaneous balance of load demand and power supply [14], [18], [30-31].

(3) **Electricity market operation and settlement:** The high penetration of VREs will cause frequent fluctuations in the power supply of the electricity market, leading to an increase in intraday trading frequency, thereby placing higher demands on the actual electricity price that reflects the operation real states of the power system [32]. Meantime, its rapid and frequent fluctuations will also increase re-scheduling operation costs in the electricity market [26-28].

1.2. Objectives, Contributions, and Thesis Outline

1.2.1 Objectives

Based on the literature in Chapter 2, the following research gaps have been identified:

(1) **Research gap 1:** The high penetration of renewable energy systems will bring more variable characteristics of modern power systems. Currently, there is a lack of theoretical research on the impact of this fluctuation characteristic on the day-ahead electricity market and the real-time electricity market operations.

(2) **Research gap 2:** Although the global electricity market is undergoing reforms to improve time granularity, there is a lack of quantitative scientific evaluation of the

entire electricity market process, including ex-ante real-time power deviation prediction, real-time power dispatch and clearing process, and ex-post power deviation settlement.

(3) **Research gap 3:** Regarding the reform of increasing spatial granularity, current research generally focuses on the reform of regional and node electricity prices, but rarely mentions the increase of spatial network granularity, and lacks a scientific model for building spatial networks.

Based on the research gaps identified, this PhD study considers the following objectives, Obj 1 and Obj 2 respond to address the research gap 1; Obj 3 respond to address the research gap 2; Obj 4 respond to address the research gap 3. The main details of the objectives are as below:

(1) **Obj 1:** Proposed metrics including power incremental statistics, coefficient of variation, and peak power duration to characterize the power variability characteristics of different flexible resources.

(2) **Obj 2:** The proposed mathematical model between these power variations and net-load power curves and real-time power imbalance curve finds that power variability will directly affect net-load power curves, and the power gradient will affect the real-time power imbalance curve.

(3) **Obj 3:** Proposed an evaluation method for the electricity market at different time granularity, including ex-ante real-time power deviation prediction; real-time power

scheduling operation and clearing; and ex-post power deviation settlement. Evaluate the effect of increasing temporal granularity on reducing balance electricity market costs and power grid frequency deviation.

(4) **Obj 4:** Proposed the stochastic energy network theory to characterize the supply-demand adaptation balance index (SDABI) and further proposes a subnetwork networking method to evaluate the impact of increasing space granularity on reducing power system operation costs, power flow losses, and power congestion.

1.2.2 Contributions

This study includes the following contributions:

(1) **Contribution 1:** Proposed metrics such as power incremental statistics, coefficient of variation, and peak power duration to characterize the variability in power output of various flexible resources.

(2) **Contribution 2:** The mathematical model, which characterizes the relationship between power variations metrics and net-load power and real-time power imbalance, providing scientific guidance to the flexibility resources reserve, is proposed. High PV penetration will make the net load curve look like a canyon and make the real-time imbalanced power curve look like a butterfly.

(3) **Contribution 3:** This thesis proposed an evaluation method for the electricity market at different time granularity, including ex-ante real-time power deviation prediction; real-time power scheduling operation and clearing; and ex-post power deviation

settlement. Evaluating the effect of increasing temporal granularity on reducing balance electricity market costs and power grid frequency deviation, for the first time provides quantitative scientific guidance to increase temporal granularity.

(4) **Contribution 4:** This thesis proposes the stochastic energy network theory to characterize the three different operating states of the sub-network, including waste of power supply (WoPS), represents renewable power supply plus energy storage is larger than energy consumption, loss of load demand (LoLD) represents renewable power supply plus energy stored in ESS is less than the load demand during a period, and supply-demand adaptation balance represents renewable energy supply with the ESS can meet the energy demand during a period, and then based on the supply-demand adaptation balance index (SDABI), further established the SDABI-based subnetwork networking method to improve spatial granularity.

(5) **Contribution 5:** This thesis evaluates the SDABI-based subnetwork networking method for increasing spatial granularity, which will reduce power system operation costs, power flow losses, and power congestion.

1.2.3 Thesis Outline

This study mainly evaluates the effect of increasing spatial-temporal resolution in high-penetration renewable energy systems. Figure 1-1 shows the research structure of this PhD thesis and the relationship between chapters.

Chapter 1 provides a background introduction to the research topic as well as issues and

challenges.

Chapter 2 presented the literature review of relevant research works.

Chapter 3 proposed metrics including power incremental statistics, coefficient of variation, and peak power duration to characterize the power variability characteristics, based on these metrics, this study analyzes the mathematical relationship between these variations and net-load power curves and real-time power imbalance curve, finds that power variability will directly affect net-load power curves and the power gradient will affect the real-time power imbalance curve, providing scientific guidance for the flexible resources reserve strategy.

Chapter 4 proposed an evaluation method for the electricity market at different time granularity, including ex-ante real-time power deviation prediction; real-time power scheduling operation and clearing; and ex-post power deviation settlement, and based on this method, provides strong evidence that the higher time granularity, the power step changes, and real-time power deviation quantities are smaller, and vice versa. Reducing the power step changes and real-time power deviations will reduce power grid frequency deviations and power market balancing costs.

Chapter 5 proposed the stochastic energy network theory to characterize the supply-demand adaptation balance index (SDABI) and further proposes a subnetwork networking method, and then combines power system operation evaluation indicators, such as power system operation costs, power flow losses, and mitigate power congestion situations, etc.

to evaluate the influence of increasing space granularity on power system reform.

Chapter 6 summarized the main conclusions that can be drawn from this research study and future research work plans. The main conclusions include the power fluctuation characteristics and their impact on power system operation and then summarize the benefits to power system operation by increasing spatial-temporal granularity reforms to solve the above power fluctuations, including reducing balance electricity market costs, reducing power grid frequency deviations, improving power system operation efficiency, providing scientific guidance for flexible reserves, etc. And then giving future challenges and work plans.

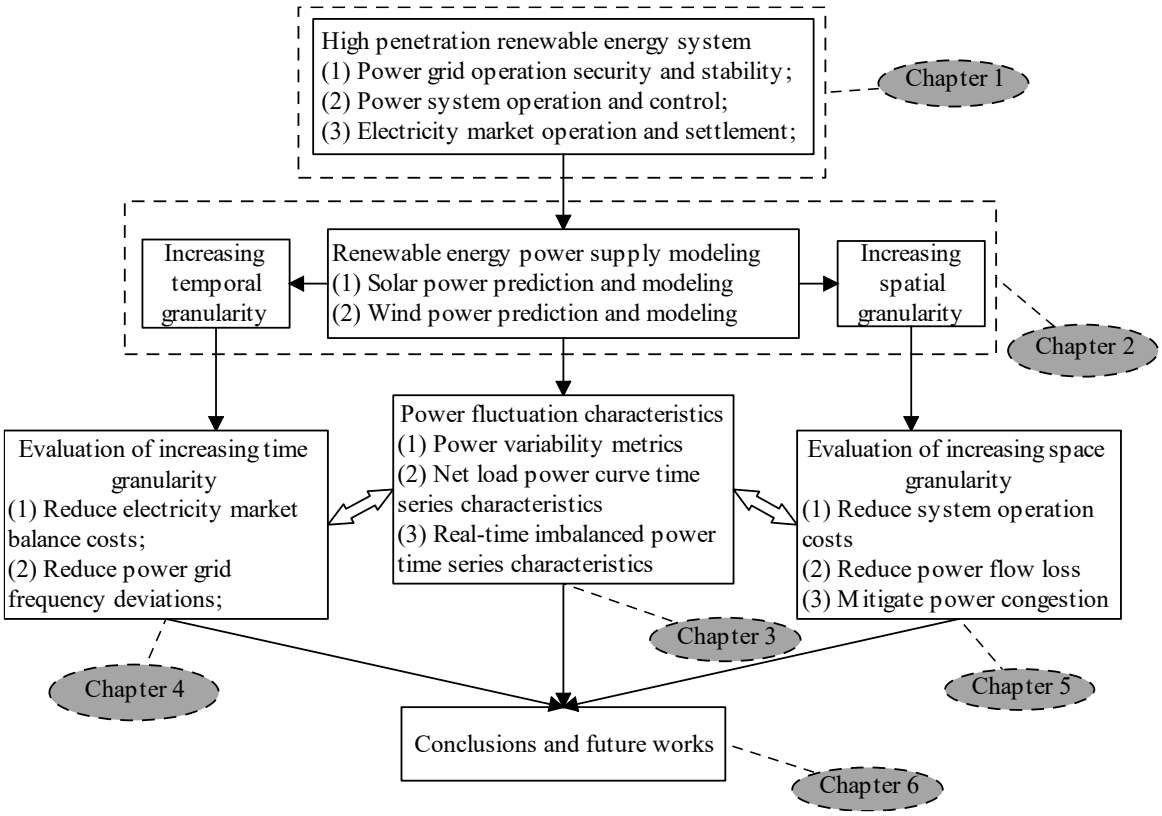

Figure 1-1 Research structure and the relationship between chapters of the thesis.

2. LITERATURE REVIEW

2.1. Renewable Energy Power Supply Prediction Model

In recent years, the capacity of renewable energy installations has been growing rapidly. From 2022 to 2023, renewables accounted for a record 86% of global power additions, among them, solar energy and wind energy contribute more than 97% of the world's renewable energy installed capacity. Solar energy accounts for about 73%, wind power accounts for about 24%, and total renewable installed capacity is about 473 GW. By the end of 2023, renewables accounted for 43% of global installed power capacity, and the solar installed capacity and wind installed capacity were more than 95% [4-5]. Therefore, in this study, renewable energy mainly focuses on solar power and wind power.

(1) Solar power

Solar power is greatly impacted by meteorological factors, especially solar radiation and ambient temperature [33-34]. The installed solar power capacity has increased year by year, and solar resources account for an increasing share of the total primary energy [4]. In this context, When meteorological conditions change, changes in solar power will directly influence the power system's operation stability [14], [23] and reduce energy security, power quality [35], etc. For example, In mid-February 2021, extreme winter storms and cold weather hit the south-central United States, causing PV, wind turbines, natural gas, etc. over 1,000 generator outages and derates across the region [36]. Luis Ceferino, etc. applied

a probabilistic framework to evaluate the performance of solar infrastructure to generate energy during hurricanes and evaluate the 2,694 counties in the 38 central and eastern US states to elucidate the risk landscape of solar generation during hurricanes [37]. Therefore, it becomes increasingly important to establish an accurate solar power generation output and prediction model, especially for the high penetration renewable energy systems operation and control.

Recently, amount of research has been carried out worldwide on the prediction and characterization of solar power generation. Among them, according to the different prediction timescales, solar power prediction can be divided into three different categories: long-term solar power prediction, medium-term solar power prediction, and short-term solar power prediction [38-41]. The medium- and long-term forecast period ranges from 30 days to 365 days, and the short-term forecast period ranges from minutes to several days. The effect of short-term prediction of solar power generation will directly affect the power consumption arrangement and dispatch plan of the power system as well as the stable operation of the system. Therefore, the short-term solar power prediction has received the focus of relevant research worldwide.

The prediction methods for short-term can be divided into indirect methods [41-43] and direct methods [40], [44-46]: In the indirect method, the solar radiation intensity is first predicted, then calculated and the short-term predicted output power based on the photoelectric conversion physical model. The direct prediction method, based on the

mathematical statistical prediction method, inputs meteorological data and historical power generation data of solar power generation into the established prediction model, and obtains short-term predicted output power from the output of the model. The indirect method model does not require a large amount of data support, but its modeling process is very complex, the amount of calculation is large, and the prediction accuracy is not high. The direct method has high prediction accuracy, a simple modeling process, and a relatively small calculation amount, but it requires the use of a large amount of historical data.

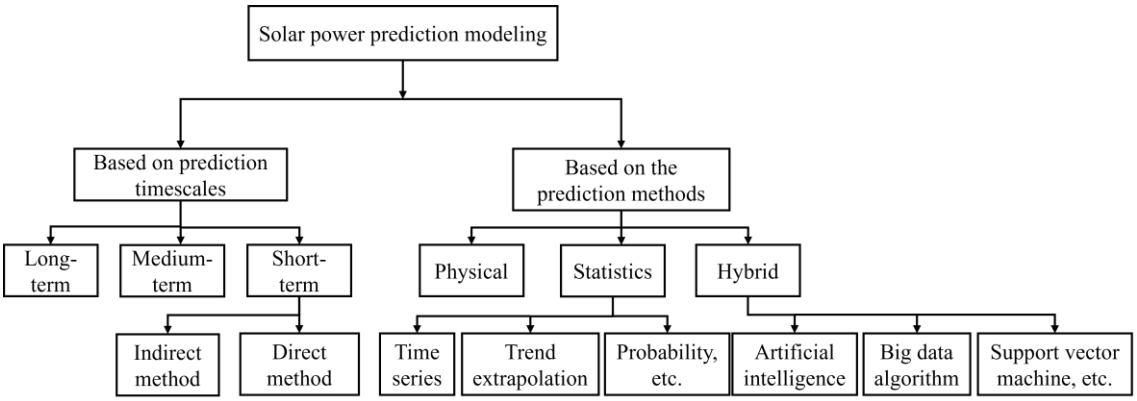

Figure 2-1 Solar power prediction modeling classifications

In addition, the differences in solar power generation prediction algorithms also include prediction methods based on physical models [47-49], prediction methods based on statistics [50-52], and prediction methods based on artificial intelligent algorithms [44], [46], [53-56]. Among them, the prediction method based on physical models adds solar radiation intensity, temperature, observation and satellite remote sensing radiation inversion data, and photovoltaic semiconductor component physical model data to the physical model for predicting solar power generation. Forecasting methods based on statistics include time series methods [51], trend extrapolation methods, and probability

forecasting methods [52]. This method mainly uses a large amount of historical data information combined with statistical principles to conduct corresponding forecasting analysis. The prediction method based on artificial intelligence algorithms combines the advantages of the above different methods and uses big data algorithms [54], support vector machine methods [44], [55], artificial neural networks [46], [53], etc., and other methods to train the parameters of the model to achieve prediction and modeling analysis of solar power. Figure 2-1 summarizes the solar power prediction models, and Table 2-1 summarizes different solar power modeling methods and classifications in recent years.

Table 2-1 Solar power prediction modeling methods and classifications.

References	Methods	Classification types
[40], [57-58]	Deep learning methods	Direct method: prediction method based on artificial intelligence algorithm
[41], [43], [49]	Photoelectric conversion model	Indirect method: prediction methods based on physical model
[44], [55], [59]	Support vector machine	Direct method: prediction method based on artificial intelligence algorithm
[45], [51-52]	Hybrid NARX-LSTM Model; time series model; Bayesian Model	Direct method: prediction methods based on statistics
[46], [53]	Artificial Neural Networks	Direct method: prediction method based on artificial intelligence algorithm

(2) Wind power

Wind power is greatly affected by meteorological natural environment factors, especially wind speed and wind direction, etc. At present, a lot of research has been carried out worldwide on the prediction and characterization of wind power generation [60-62].

Among them, according to the different prediction timescales, the wind power prediction model can be divided into three categories: long-term, medium-term, and short-term. The prediction methods for short-term can be divided into indirect methods and direct methods: In the indirect method, the wind speed is first predicted, then calculated and the short-term predicted output power is based on the physical conversion model. The direct prediction method, based on the mathematical statistical prediction method, inputs meteorological data and historical power generation data of wind power generation into the established prediction model, and obtains short-term predicted output power from the output of the model. The indirect method model does not require a large amount of data support, but its modeling process is very complex, the amount of calculation is large, and the prediction accuracy is not high. The direct method has high prediction accuracy, a simple modeling process, and a relatively small calculation amount, but it requires the use of a large amount of historical data.

After several years of research and practice worldwide, wind power generation prediction has built a series of prediction processes including numerical weather prediction (NWP) [63], wind power conversion model [64-65], prediction result application, prediction result evaluation [66], etc. Based on these above processes there are two different major technical categories of wind power prediction methods including physics [63], [67] and statistics [68-72]. NWP is mainly used in physical methods, and statistical methods mainly involve three technologies other than the NWP technique, but it is not absolute, and

the two different technical methods also combine.

Based on the definition and technical characteristics of physical prediction methods, it mainly includes three different technical parts [67]:

(1) NWP data injection, including wind speed and wind direction collection at wind turbine hub height.

(2) Wind natural resources-power conversion physical module, that is, considering information such as wind farm topography, NWP data is converted into wind resources information under actual environmental conditions, calculating the predicted power of the wind turbine based on the performance parameters of the wind turbines.

(3) Accumulate total wind farm power output to obtain the theoretically predicted power of the entire wind farm. The calculation of this method is relatively complex and requires solving a multi-dimensional partial differential equation for prediction. However, the requirements for the technical conditions of wind farm operation are lower, and it does not require a large amount of historical wind farm operation data information. It only requires the location, topography, landform, and basic information of the wind turbine capacity, etc.

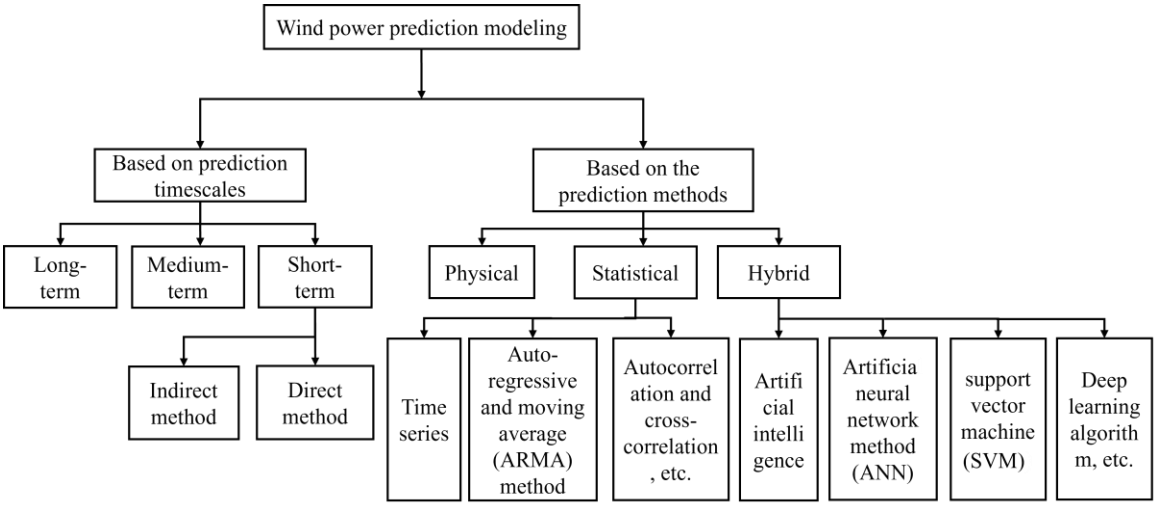

Figure 2-2 Wind power prediction modeling classifications

Different from physical prediction methods, statistical prediction methods do not need to consider the complex physical change process of wind resources and electric power. This method uses statistical algorithms to learn the characteristic patterns shown by the historical meteorological and power data of the wind farm and then combines the measured power data or NWP data to predict the wind farm's future power generation. This method does not require the construction of complex differential equations to present the wind resources exchange to electric power, but statistical learning modeling requires large amounts of data for training [61-62], [70], [73]. Statistical forecasting methods include forecasting methods based on time series characteristics [68], [74-76] and forecasting methods based on artificial intelligence algorithms [69-70], [77-79]. Among them, the time series-based method does not require natural environmental factors such as wind speed and direction. In particular, according to the definition and technology of this method, we can obtain some time series characteristics of the wind farm by training and learning its historical power sequence characteristics, and then obtain its future power output, this kind of statistical time

series characteristics can be characterized using statistical indicators, such as autocorrelation and cross-correlation [74], moment [75], probability density function and cumulative density function, etc. [72]. In addition, time series features can also be used in other ways, including continuous method, auto-regressive and moving average (ARMA) method [76], and Kalman filter algorithm [66], etc. The time series extrapolation prediction method is simple to operate. On a shorter time scale, its prediction accuracy may even exceed other complex artificial intelligence methods. However, as the time scale increases, its prediction accuracy will drop sharply, so it is only suitable for ultra-short-term wind forecasting [76].

The artificial intelligence-based prediction method combines the advantages of the above different methods, comprehensively considers relevant influencing factors such as natural environment factors and electricity uses one or more AI algorithms to train historical power output data, extracts the connection between NWP data and power generation data, and then based on the above relationship predicts wind power generation from NWP data is an important research direction, which mainly includes artificial neural network method (ANN) [69], [77], support vector machine (SVM) [78], deep learning algorithm [79], etc. The AI prediction method does not need to establish a specific analytical relationship between predicted power and meteorological data. Good prediction results can be obtained through large amounts of data training, which is suitable for different time scales wind power prediction, and the accuracy will be higher based on the massive training data and suitable

AI algorithm [61], [70]. Figure 2-2 summarizes the wind power prediction models, and Table 2-2 below summarizes different wind power modeling methods and classifications in recent years.

Table 2-2 Wind power prediction modeling methods and classifications.

References	Methods	Types
[63-64], [67]	NWP data; wind speed and direction; wind speed-power conversion module	Indirect method; physical prediction
[69], [77]	Artificial neural network method	Direct method; artificial intelligence algorithms
[71-72], [74], [76]	Statistics; Bayesian model; autocorrelation and cross-correlation; ARMA	Direct method; statistical prediction: based on time series
[70], [73]	Data-driven; Big data mining	Direct method; statistical prediction
[78], [80]	Support vector machine	Direct method; artificial intelligence algorithms
[79], [81]	Deep learning algorithm	Direct method; artificial intelligence algorithms

2.2. Increasing Spatial Granularity

Increasing space granularity mainly reflects two aspects: one is increasing renewable generation units' space granularity, that is to reduce the amount of renewable energy injected into a single node or increase the number of inject nodes for renewable generation units; the other one is increasing transmission network space granularity, that is to reduce the complexity of the transmission network or reduce the repeated power flow transmission.

Increasing renewable generation units' space granularity can help system operators find

the renewable generators' marginal electricity price, which will reduce the customers' energy costs [80]. In addition, increasing the renewable energy generation space granularity is also a key market design innovation in the electricity market, including node pricing widely used in the US market [83-85] and regional pricing widely used in the pan-European region [86-87]. For example, the Electric Reliability Council of Texas (ERCOT) implements node pricing. By adding electricity price information at different nodes across the state, it discovers the true energy usage of different nodes during the power transmission process and formulates reasonable node prices based on the energy usage, thereby improving the efficiency of the power grid operation and improving the economic benefits of the whole society [85], [88]. The New York Independent System Operator (NYISO) in the United States also uses nodal pricing in its wholesale electricity market to improve system operating efficiency and aims to help increase the penetration of variable renewable energy [84]. The pan-European electricity market increasing space granularity market innovation is implementing zonal pricing. Electricity is traded through different bidding zones and settled according to the prices in different zones. Some countries only have one bidding zone, such as France, Great Britain, and Germany, etc. Other countries divide their transmission systems into multiple bidding areas, including Denmark, Italy, Norway, Sweden, etc. By increasing space granularity and reducing the amount of renewable energy injected into a single node, this electricity market changes, on the one hand, improve the power congestion problem of adjacent lines connected to VRE injected nodes, on the other

hand, increasing renewable generation units space granularity can better discover the marginal electricity price of the units, thereby reducing energy costs. Regarding the reform of increasing spatial granularity, current research generally focuses on the reform of regional and node electricity prices, but rarely mentions the increase of spatial network granularity, and lacks a scientific model for building spatial networks.

To increase transmission network space granularity, the first idea is to construct many space subnetworks. How to divide that transmission network topology into several subnetworks and then reduce the power transmission amount, repeated power flow and electricity power transfer distance is a vital problem. The subnetwork works in one of the following three working states during a period:

(1) Waste of power supply, in this state means that if the power supply exceeds the load demand for a period, the excess power will be stored in the energy storage system (ESS) until it reaches its rated capacity, thus generating excess power [89-91].

(2) Loss of load demand, in this state means that the power supply plus energy stored in the energy storage system (ESS) is less than the load demand during a period, resulting in an energy shortage [92-93].

(3) Supply-demand adaptation balance, in this state means that the energy supply with the energy storage system (ESS) can meet the energy demand during a period. To solve the above problems, the cumulative energy production of VREs needs to meet the cumulative energy consumption of all load nodes in the subnetwork, increasing the

probability of a supply-demand adaptation balance state [91], [94-95].

2.3. Increasing Temporal Granularity

Increasing time granularity in power systems by reducing the energy settlement time unit (pricing shorter market time units) is an important energy market innovation to address the volatility, uncertainty, and intermittency challenges posed by the increased penetration of VREs [32]. On the one hand, increasing more quickly solving the closing time of the scheduling gate is more frequent and the scheduling interval is shorter, which allows system operators to more quickly solve the power imbalance problem caused by the difference between day-ahead dispatch and real-time dispatch [96]. Also, shortening the scheduling intervals means that power step change at scheduling interval points and real-time power deviation during the scheduling intervals will decrease, reducing power grid frequency deviation [27], [97-98]. On the other hand, increased time granularity in the electricity market helps system operators predict day-ahead and real-time operations more accurately based on timely information [96], [99-100]. This helps avoid the re-dispatch process, which will increase the ex-post power deviation settlement cost.

At present, across the whole world electricity markets (including the day-ahead market and intra-day market), with the increasing shares of VRE generation resulting in larger volatility and intermittency [17-19], more and more countries will focus on energy products with a higher temporal resolution [32], for example, in the day-ahead market, the California Independent System Operator (California ISO) reduce the temporal resolution of traded

energy products from hours to minutes [101]. In the intraday market, several European nations such as France [102], Germany, and the United Kingdom, had sub-hourly energy products, for example, half-hour energy products [103]. By increasing time granularity, shorter clearing, and financial settlement periods, these energy market changes, on the one hand, reduced barriers to integrating variable energy resources and addressed market inefficiencies, on the other hand, increased the granularity of prices in the wholesale energy market can increase the short-term flexibility of the electricity system. Although the global electricity market is undergoing reforms to improve time granularity, there is a lack of quantitative scientific evaluation of the entire electricity market process, including ex-ante real-time power deviation prediction, real-time power dispatch and clearing process, and ex-post power deviation settlement.

2.4. Summary

This chapter reviews the renewable energy power supply modeling methods and increasing spatial-temporal resolution reform in power systems, The renewable energy power supply modeling part, can produce and provide abundant scientific datasets to do further power fluctuation characteristics analysis when there is a lack of dataset and the amount of data is relatively small; For the increase in spatial resolution, this chapter provides a clear definition and overview of the latest research on reforms to increase spatial granularity in power systems worldwide, aiming to help researchers quickly and accurately understand the impact and role of spatial granularity reforms in power systems, but current

research generally focuses on the reform of regional and node electricity prices, but rarely mentions the increase of spatial network granularity, and lacks a scientific model for building spatial networks; For the increase in temporal resolution, this chapter reviews the reforms in electricity markets in different countries to increase time resolution, aiming to help researchers quickly and accurately establish a theoretical framework for increasing temporal resolution research by citing related articles, but there is a lack of quantitative scientific evaluation of the entire electricity market process, including ex-ante real-time power deviation prediction, real-time power dispatch and clearing process, and ex-post power deviation settlement.

3. POWER FLUCTUATION CHARACTERISTICS OF HIGH PENETRATION RENEWABLE ENERGY SYSTEM

Abstract: Compared with traditional energy systems, high-penetration renewable energy systems have brought some new opportunities and challenges to the power balance process due to power volatility, intermittency, and fluctuations. Based on high temporal resolution datasets include load demand, wind power, and solar power located in three different countries around the world. This PhD study proposes metrics including power incremental statistics, coefficient of variation, and peak power duration to characterize the power variability characteristics. Based on these metrics, the mathematical relationship between these variations and net-load power curves, and real-time power imbalance curves are analyzed. It is found that power variability will directly affect net-load power curves and the power gradient will affect the real-time power imbalance. For example, the solar power variability characteristics will cause the net-load power curve to look like a duck curve, while real-time power imbalance to look like a butterfly curve. This chapter for the first time scientifically describes the mathematical statistical characteristics of power fluctuations. And reveals the mathematical relationship between power fluctuations, net-load power curves, and real-time power imbalance curves, guiding the operation of high-penetration energy systems.

Abbreviations	
RTIP	Real-time imbalanced power
VRE	Variable renewable energy
LD	Load demand
CoV	Coefficient of variation
PPD	Peak power duration
CAISO	California Independent System Operator
Variables, Parameters and Functions	
$P(t)$	The t-th power
$\Delta P\tau$	Power increment of two adjacent points lagged by a time interval τ
μ	Mean value
σ	Standard deviation
β	The third moment/ skewness
κ	The fourth moment/ kurtosis
$P_{\max}$	The maximum power
$\boldsymbol{P}$	Probability
$P_{\mathrm{LD},i,t}$	load demand under the sampling rate of i-th day and t-th time spot
$P_{\mathrm{PV},i,t}$	PV power under the sampling rate of i-th day and t-th time spot
$P_{\mathrm{WT},i,t}$	Wind power under the sampling rate of i-th day and t-th time spot
α	The penetration rate of photovoltaic
γ	The penetration rate of wind power
$P_{\mathrm{U},t}$	Upward flexibility
$P_{\mathrm{D},t}$	Downward flexibility
$\Delta P_{WT,t}^{+}$	Wind power real-time part larger than the day-ahead part
$\Delta P_{PV,t}^{+}$	PV power real-time part larger than the day-ahead part
$\Delta P_{WT,t}^{-}$	Wind power real-time part smaller than the day-ahead part
$\Delta P_{PV,t}^{-}$	PV power real-time part smaller than the day-ahead part
$\Delta P_{LD,t}^{+}$	Load demand the real-time part larger than the day-ahead part
$\Delta P_{LD,t}^{-}$	Load demand the real-time part smaller than the day-ahead part

3.1. Introduction

The primary purpose of the power system is to maintain an immediate equilibrium between the supply of electrical energy and the demand from consumers [14]. Compared with traditional energy systems, high-penetration renewable energy systems have brought some new opportunities and challenges to the power balance process due to the power volatility, intermittency, and fluctuations, mainly reflected in the higher requirement of flexible resources, including day-ahead dispatch process and real-time dispatch process. During the day-ahead dispatching process, the net load power curve will show fluctuation characteristics as renewable energy penetration increases, manifesting as an increase in the demand for flexible ramping resources; During the real-time dispatch process, the renewable energy variability increase will also lead to an increase in the amount of real-time imbalanced power (RTIP).

For the day-ahead dispatching process, the net load power curve represents the total electricity demand minus whatever renewable energy is on the grid [104]. Its characteristics guide flexible resources reserve in the day-ahead process. Based on the definition, the net load power is influenced by variable renewable energy (VREs) and load demand, which will be affected by natural meteorological resources and production schedules, having timing characteristics. For photovoltaic resources, since their output is mainly affected by light intensity [33-34], they exhibit the following distinct time series characteristics. The photovoltaic power generation gradually increases from 0 to the maximum power

(corresponding to zero solar irradiance to the strongest light intensity); then decreases from the maximum power to 0 (corresponding to the light intensity from highest to 0). The characteristics of photovoltaic resources result in the net load power curves in different load zones around the world showing deeper duck curve characteristics in high penetration of solar power systems [105-106].

For the real-time dispatch process, unlike the net load power curve, the RTIP curve refers to the deviation in power between the day-ahead and real-time scheduling process, resulting from changes in power levels [107]. According to its definition, the amount of RTIP is mainly proportional to the power increment, that is, the power gradient, also has time series characteristics. For photovoltaic resources, since their output is mainly affected by light intensity, they exhibit the following distinct time series characteristics:

(1) Photovoltaic power gradient is often 0 when the power is minimum and maximum, and this period is often in the early morning, evening, and noon.

(2) When the light intensity gradually increases or weakens, although the photovoltaic power generation is not high, the power change rate of photovoltaic is relatively larger [48], [51].

Wind power generation has different features in different geographical areas based on natural wind resources. It also has these features:

(1) When the wind speed is relatively high, the wind power will be relatively large, while the change rate of wind power will be relatively small.

(2) When the wind speed is relatively small, the wind power will be relatively small, and the power change rate will be relatively small [63], [67].

Compared with PV power and wind power, the load demand variability is not obvious, but load demand also has time series characteristics at different locations based on the production schedule:

(1) Load demand has peak periods and valley periods in time series.

(2) The amount of power change in load demand during peak/valley periods is relatively small [14], [108].

In this chapter, we use the high temporal resolution dataset including load demand, wind power, and solar power located in three different countries around the world to calculate the influence of power variability on the high penetration renewable energy systems. First, we established several metrics including power increment statistics, coefficient of variation (CoV), and peak power duration (PPD) to characterize the power variability of renewable energy supply and load demand. Second, based on these countries' variability resources time series datasets, we analyze the net load power curves' time series characteristics under different renewable energy penetrations. Then we analyze the timing characteristics of RTIP quantities under different renewable energy penetrations based on the power variability in these different countries. The main findings include three aspects: (1) Power variability characteristics will be different for different types of resources, solar power has the highest power variability, and the load demand has the lowest power variability, based

on the metrics established in this chapter; (2) Renewable power generations have time series characteristics: wind power generates higher power when the wind speed is higher, and solar power generates relatively larger power when the light intensity is higher, so its power changes directly affect the shape of the net-load power curve and it has obvious time series characteristics, such as the canyon curve characteristics with massive solar power; (3) The power variability will directly affect the amount of RTIP; The lowest power variability means the lowest RTIP value, and vice versa. For example, the solar power variability characteristics will cause the RTIP curve to look like a butterfly.

3.2. Data Setting and Description

In this chapter, we independently analyze the high temporal resolution dataset including wind power, solar power, and load demand, which is in three different countries around the world, including California Independent System Operator (CAISO), Czech grid, and Qatar grid. Observing the power variability characteristics, and based on this variability, this chapter will evaluate their impact on the net load power curve and RTIP curve timing characteristics and draw some conclusions for the reform of high penetration renewable energy systems. The description of the dataset in this chapter is as follows.

(1) Load demand time series dataset

CAISO: The load demand is in the California Independent System Operator (CAISO) grid. The temporal resolution is 1 minute. The dataset includes nearly two years between 01/01/2018 and 31/12/2019 [109].

Czech: The load demand is in the Czech grid. The temporal resolution is 1 minute. The dataset includes nearly one year between 01/01/2021 and 31/12/2021 [110].

Qatar: The load demand is in the Qatar grid. The temporal resolution is 1 minute. The dataset includes nearly one month between 20/11/2022 and 18/12/2022.

(2) Renewable energy time series dataset

CAISO: The renewable energy time series dataset in the CAISO grid has a high temporal granularity, and the frequency rate is equal to 1 minute. The dataset includes nearly two years between 01/01/2018 and 31/12/2019 [109]. For solar power, based on the dataset from the National Solar Radiation Database (NSRDB), light intensity data information can be obtained, and solar power is estimated based on solar radiation-related data through a physical model [43]. For wind power, wind speed information is first collected from weather stations at different locations, and then estimated wind power output through wind turbine power curves associated with that location.

Czech: The renewable energy time series dataset in the Czech grid has a high temporal granularity, the frequency rate is equal to 1 minute. The dataset includes nearly one year between 01/01/2021 and 31/12/2021. This dataset includes solar and wind power data aggregated from multiple photovoltaic and wind farms respectively.

Qatar: The renewable energy time series dataset in the Qatar grid has a high temporal granularity, the frequency rate is equal to 1 minute. The dataset includes nearly one month between 20/11/2022 and 18/12/2022. The dataset includes solar power output from

Alkarsaah PV farm [111].

Based on the above datasets, we can calculate the per unit load demand and unit renewable energy power by dividing the load power by the peak load power and the renewable energy power by the renewable energy installed capacity, respectively. The per-unit power curves from the above dataset in this section are shown below.

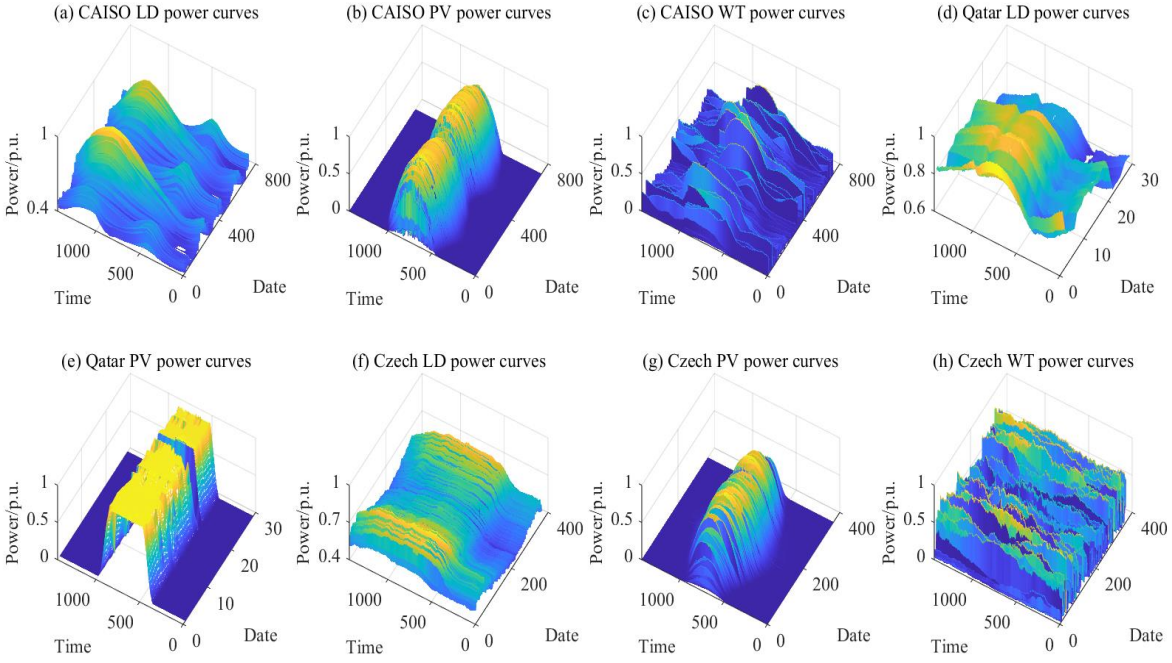

Figure 3-1. Per unit power curves from different countries and different resources

3.3. Methods

3.3.1 Power Variability Metrics

Variable resources in high-penetration renewable energy power systems mainly include wind power, solar power, and load demand. For our research, there are two main ways to characterize power variability: (1) local power variability curve, mainly characterized by power increments under different time lags (2) overall power curve fluctuation

characteristics; mainly characterized by the overall power curve statistical characteristics, including coefficient of power variation and peak power duration.

(1) Power increment statistics

To characterize these local power variabilities, we use the power increment of two adjacent points lagged by a certain time interval τ for statistical analysis, represents, $\Delta P\tau = P(t)-P(t-\tau)$. From the current state $P(t)$, the power increment value $\Delta P\tau$ at lag τ time can have positive and negative values, representing the system requires upward flexibility resources and downward flexibility resources. And the higher the $\Delta P\tau$, that means the more flexibility resources need. The value of $\Delta P\tau$ will only give the information of power variability degree at time point t, while the distribution of the $\Delta P\tau$ in the whole dataset will tell us the whole power variability degree [112]. An effective way in statistics to characterize the statistical properties of power increments at lag time τ is called the n-order power increment moment, which represents, ΔP_τ^n, and its n-th moment is defined as below [113].

$$\mu_n = \frac{1}{N}\sum_{i=1}^{N} \Delta P_{\tau i}^n \tag{3.1}$$

where μ_n represents a statistical n-th moment, the first moment of the power increment distribution refers to the mean value, that is $\mu_1=\mu$. In statistics, standard deviation is usually used to characterize second-order moments. it is defined as below,

$$\sigma^2 = \frac{1}{N}\sum_{i=1}^{N} (\Delta P_{\tau i} - \mu)^2 \tag{3.2}$$

where σ is the standard deviation. Finally, we use the normalized third and fourth moments, β and κ, respectively, which are defined as:

$$\beta = \frac{1}{N}\sum_{i=1}^{N}\left(\frac{\Delta P_{\tau i} - \mu}{\sigma}\right)^3 \tag{3.3}$$

$$\kappa = \frac{1}{N}\sum_{i=1}^{N}\left(\frac{\Delta P_{\tau i} - \mu}{\sigma}\right)^4 \tag{3.4}$$

(2) Coefficient of variation

In statistics, the standard power deviation is an indicator, which is used to measure the power series variation and dispersion. When the power series has a low standard deviation, it means that all the power values in the dataset tend to be close to the average value, while when the power series has a high standard power deviation, it means that all the power values tend to be spread out over a wider range.

$$\sigma = \sqrt{\frac{1}{N}\sum_{i=1}^{N}(P_i - \mu)^2} \tag{3.5}$$

$$\mu = \frac{1}{N}\sum_{i=1}^{N}P_i \tag{3.6}$$

where P_i represents the i-th value in the power series; μ represents the average power; N represents the power series number. σ represents the standard power deviation.

To characterize the total power curve variability, we define the coefficient of power variation (CoV), which is equal to the ratio of the standard deviation σ to the mean value. This indicator combines the characteristics of the standard deviation and the means to

describe the fluctuation characteristics of the total power curve. Based on these two indicators, the coefficient of power variation can normalize different amplitudes, different measurements, and different units of power curves to characterize volatility and fluctuation [114]. It can be calculated by the equation below:

$$\mathrm{CoV} = \frac{\sigma}{\mu} = \sqrt{\frac{1}{N}\sum_{i=1}^{N}(P_i - \mu)^2} \Big/ \frac{1}{N}\sum_{i=1}^{N} P_i \tag{3.7}$$

(3) Peak power duration

The peak power duration (PPD) is used to characterize the proportion of peak power duration in the whole power curve, this index is another one to characterize the total power curve variability. This duration can be arranged in descending order by the power curves within the scheduling time interval, and then a probability statistical analysis is performed according to the power time series sorted in descending order to guide the distribution of different power requirements. According to the form of the descending power curve, there are two representation calculation methods: (1) continuous probability density function integration; (2) discrete probability mass function summation. These two forms of peak power duration are as follows:

$$PPD_\alpha = \boldsymbol{P}(\alpha P_{max} \le P \le P_{max}) = \int_{\alpha P_{max}}^{P_{max}} f(P)dP \tag{3.8}$$

$$PPD_\alpha = \boldsymbol{P}(\alpha P_{max} \le P \le P_{max}) = \sum_{i=1} \boldsymbol{P}(\alpha P_{max} \le P_i \le P_{max}) \tag{3.9}$$

where $\boldsymbol{PPD_\alpha}$ represents larger and equal to α times peak power duration. $\boldsymbol{P}$ represents the probability, $\boldsymbol{f(P)}$ represents the power curve continuous probability density function.

3.3.2 Net Load Power and Real-time Imbalanced Power Analysis

Power fluctuations will challenge power system operation and balance settlement to solve instantaneous power balance. In this chapter, based on the power variability characteristics, we analyze the net load power curve and RTIP curve, and based on these curves' time series characteristics, give reasonable suggestions to system operators. We assume that the energy measurement is correct based on the sampling frequency. Using the dataset obtained at the sampling rate (1-minute) as the benchmark, we can get the day-ahead dispatched power by equation (3.10), based on the definition of net load power and RTIP [27], [104], [107], we can calculate them by the following equation (3.11) and (3.12) respectively.

$$P_{T_n} = \frac{1}{n}\sum_{i=1}^{n}(P_i), T_n = nT_0 \tag{3.10}$$

$$NLP_{T_n} = P_{LD,T_n} - P_{RES,T_n} \tag{3.11}$$

$$\begin{aligned}\Delta P_j = P_j - \frac{1}{n}\sum_{i=1}^{n}(P_i) = \frac{nP_j - \sum_{i=1}^{n}(P_i)}{n} \\ = \frac{(1-j)\Delta P_{\tau(j-1)}}{n} + \frac{(2-j)\Delta P_{\tau(j-2)}}{n} + \cdots + \frac{-\Delta P_{\tau 1}}{n} + \cdots \\ + \frac{(n-j)\Delta P_{\tau j}}{n} + \cdots + \frac{\Delta P_{\tau(n-1)}}{n}\end{aligned} \tag{3.12}$$

3.3.3 Renewable Energy Penetration

The variability from the power supply is mainly influenced by the VREs penetration, therefore, with the increased penetration of VREs, the power supply variability will also increase. The penetration rate of renewable energy is often characterized as the proportion

of renewable energy power generation to load demand [115]. Therefore, this chapter will define α and γ respectively to characterize the penetration rates of photovoltaic and wind power. Their calculation methods are as follows:

$$\alpha = \left(\sum_{i\in I}\sum_{t} P_{PV,i,t}\right)/\left(\sum_{i\in I}\sum_{t} P_{\mathrm{LD},i,t}\right) \tag{3.13}$$

$$\gamma = \sum_{i\in I}\sum_{t\in T} P_{\mathrm{WT},i,t} \Big/ \sum_{i\in I}\sum_{t\in T} P_{\mathrm{LD},i,t} \tag{3.14}$$

where α and γ represent the photovoltaic and wind power penetration rate, respectively. $P_{\mathrm{LD},i,t}$, $P_{\mathrm{PV},i,t}$ and $P_{\mathrm{WT},i,t}$ represent the load demand, PV power, and wind power under the sampling rate of i-th day and t-th time spot, respectively.

3.4. Results

3.4.1 Power Variability Characteristics

The power increment under different time lags can describe the degree of power fluctuations. Based on the methods part, we can calculate power increment at different time lags, as shown in Figure 3-2. Comparing the power fluctuation characteristics of different resources in Figure 3-2 ((a)-(c); (d) and (e); (f)-(h)), we found that, at the same time lag, the different resources power increment probability density function (pdf) is different, that is, there are differences in the wind, PV, and load demand power fluctuation. Specifically, in the CAISO grid, the PV power increment standard deviation is more than 10 times the demand power increment at a 1-minute time lag. The wind power increment standard deviation is nearly 2.5 times the load demand power increment. That is, the power

fluctuation degree in the CAISO grid, PV power is higher than wind power, and wind power is higher than the load demand. Observing the skewness index, we found that the skewness of load demand and photovoltaic power is small, and its absolute value is generally lower than 0.5, while the skewness of wind power is larger and higher than 1.5. Observing the kurtosis index, we found that the load demand has the smallest kurtosis (the kurtosis coefficient is close to 24 with a 1-minute lag, and the kurtosis coefficient is close to 3 with a 10-minute lag), followed by photovoltaic power (the kurtosis coefficient is close to 52 with a 1-minute lag, the kurtosis coefficient is close to 26 under the 10-minute time lag), and the wind power increment distribution kurtosis value is the largest, even as high as 150 under the 1-minute time lag. The skewness and kurtosis values of different resources in the CAISO grid indicate that the wind power increment and the PV power increment distribution is characterized by a peaked and thick-tailed distribution, that is, the probability of extreme values in wind power increment and PV power increment is high [113], mainly because of its relatively large power fluctuation.

In the Czech grid, the PV power increment standard deviation is more than 2.6 times the load demand power increment at a 10-minute time lag. The wind power increment standard deviation is nearly 2.9 times the load demand part. This means that the power fluctuation degree in the Czech grid, PV power, and wind power are higher than the load demand part. Observing the skewness index, we found that the absolute skewness value of different resources is generally lower than 0.2 at a 1-minute time lag. Observing the kurtosis index,

we found that the load demand has the smallest kurtosis (the kurtosis coefficient is close to 13 with a 1-minute lag, and the kurtosis coefficient is close to 6 with a 10-minute lag), followed by wind power (the kurtosis coefficient is close to 9 with a 1-minute lag), and the PV power increment distribution kurtosis value is the largest, even as high as 19 under the 1-minute time lag. The skewness and kurtosis values of different resources in the Czech grid indicate that the wind power increment and the PV power increment distribution is characterized by a peaked and thick-tailed distribution, that is, the probability of extreme values in wind power increment and PV power increment is high, mainly because of its relatively large power fluctuation.

In the Qatar grid, the PV power increment standard deviation is close to 3.6 times the load demand power increment at a 1-minute time lag and is close to 10 times the load demand power increment at a 10-minute time lag. Observing the skewness index, we found that the skewness of load demand and photovoltaic power is small, and its absolute value is generally lower than 0.1 at a 1-minute time lag. Observing the kurtosis index, we found that the load demand has the smaller kurtosis (the kurtosis coefficient is close to 5 with a 1-minute lag, and the kurtosis coefficient is close to 3 with a 10-minute lag), followed by photovoltaic power (the kurtosis coefficient is close to 100 with a 1-minute lag, the kurtosis coefficient is close to 24 under the 10-minute time lag). The skewness and kurtosis values of different resources in the Qatar grid indicate that the PV power increment distribution is characterized by a peaked and thick-tailed distribution, that is, the probability of extreme

values in PV power increment is high, mainly because of its relatively large power fluctuation.

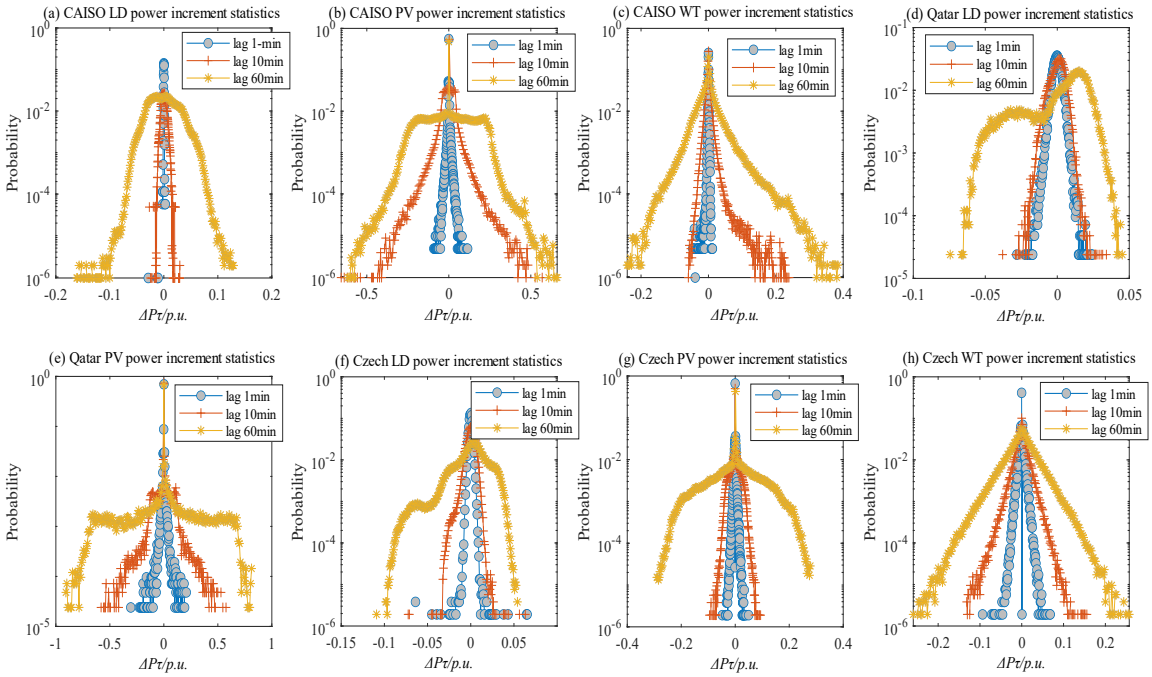

Figure 3-2. Load demand, wind power, and solar power increment statistics in time lag 1-min, 10-min, and 60-min probability density function (PDF) in the CAISO grid, Qatar grid, and Czech grid.

Power increment describes the degree of adjacent continuous power fluctuations, which reflects the local characteristics of power fluctuation. This chapter constructs other indicators such as coefficient of variation (CoV) and peak power duration (PPD) in the methods part to describe the overall power curve fluctuation characteristics of different resources. Figure 3-3 and Figure 3-4 show the results.

In Figure 3-3, we can find that the CoV of the PV daily power curve is generally high (the value generally between 1.2-2.0), followed by the wind power daily curve (the value generally between 0.3-1.2), and the load demand daily curve is the smallest (the value generally lower than 0.2). The above characteristics are mainly due to the renewable energy

variability is higher than the load demand part, As for the fluctuation characteristics of photovoltaic power and wind power, they mainly have the following different characteristics: (1) Photovoltaic power has obvious time series characteristics within a day: solar power is maximum at noon, while in the early morning and evening, its power is equal to 0; (2)wind power fluctuates strongly within a day, the overall difference is not obvious, that is, there is not much difference between the maximum power and the minimum power. What is more, the above feature of PV will not change with the increase of PV capacity, but wind power and load demand will reduce power fluctuation degree through complementary characteristics. We can further observe that the value of CoV of the PV daily power curve will be relatively low in summer and relatively high in winter. The main reason is that the light irradiance is sufficient in summer and the average daily power of PV is relatively high.

Observing Figure 3-4, we can find that PV power and load demand show obvious seasonal characteristics, that is, in summer in CAISO, the value of PPD is relatively high, while in winter, its value is relatively low. The above characteristics are mainly due to the demand in summer in CAISO is relatively high and peak load duration time is longer, and PV power output be greater in summer. There are also differences in the fluctuation characteristics of different types of resources. Among them, the load demand PPD value is generally longer than that of renewable energy sources, such as, in the CAISO grid, the PPD of load demand above 95% is close to 17%, while the PPD of wind power and PV

power above 95% is about 3.6% and 6.1%, respectively; in the Czech grid, the PPD of load demand above 95% is close to 28%, while the PPD of wind power and PV power above 95% is about 2.3% and 4.5%, respectively; in the Qatar grid, the PPD of load demand above 95% is close to 30%, while the PPD of PV power above 95% is about 23%. The PV power PPD is relatively higher in the Qatar grid than in other grids, the above characteristics are mainly due to the solar irradiation in Qatar is relatively abundant.

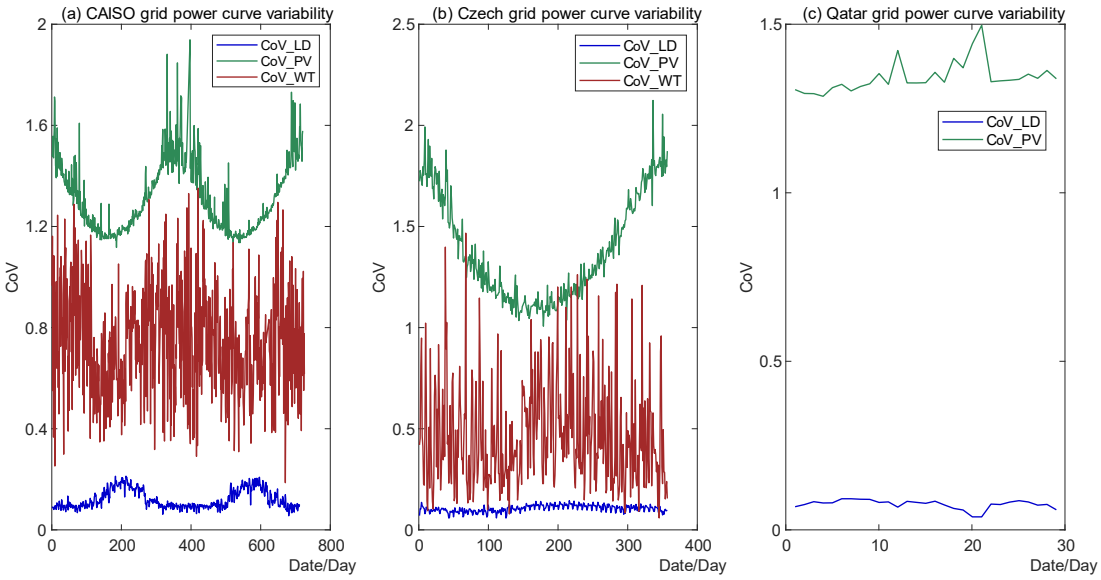

Figure 3-3. Load demand, wind power, and solar power daily power coefficient of variation (CoV) in the CAISO grid, Czech grid, and Qatar grid.

The PPD indicator comprehensively describes the duration of variable resources under different power degrees. Based on the load PPD characteristics, it can help system operators formulate reasonable demand response market strategies and incentive intensity, reduce peak load power, and reduce transmission line rated capacity, thereby improving the system operation stability; Based on the renewable energy PPD characteristics, it can effectively

configure the energy storage capacity, reduce the peak power of renewable energy output, and improve the system operation economy.

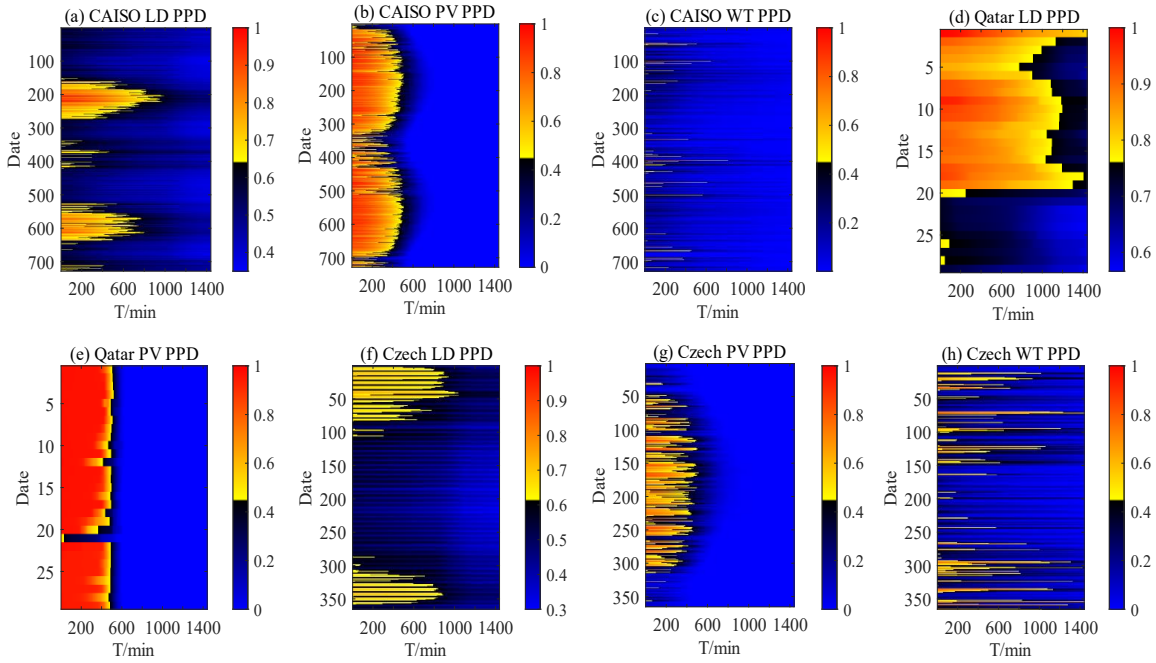

Figure 3-4. Load demand, wind power, and solar power daily peak power duration (PPD) distribution in the CAISO grid, Qatar grid, and Czech grid.

3.4.2 Net Load Power Curve Time Series Characteristics

Load demand is influenced by industrial structure and production plans in different countries, and renewable energy power supply is influenced by natural indicators, therefore, these power curves will have different time series characteristics, shown in Figure 3-5 below. In the CAISO grid, peak load demand usually occurs close to 17:00-20:00. In addition, there will also be a local short-term load peak around 6:00-8:00. The valley of load demand usually occurs at 23:00-4:30 and 13:30-15:30. While the peak power of PV usually occurs close to 11:00-13:00, during this time, the load demand is not higher, but when the load demand reaches to peak, the PV power supply is usually smaller, even to

zero (during 19:00-6:00); Wind power is relatively large between periods 9:00-17:00 and relatively small during period 20:00-6:00, but the overall difference is not clear. In the Czech grid, peak load demand usually occurs close to 10:30-13:00. The valley of load demand usually occurs at 23:00-4:30. And the peak power of PV usually occurs close to 11:00-13:00, during this time, the load demand is also higher, so in the Czech grid, the PV can better match with the load demand, and wind power does not change significantly throughout the day. In the Qatar grid, peak load demand usually occurs close to 12:00-14:00. and the peak power of PV usually occurs close to 9:30-13:30, during this time, the load demand is also higher.

By comparing the time series characteristics of different resources, we can further calculate and get the net load power curve shown in Figure 3-6. In the CAISO grid, the net load curve changes greatly in the period [8:00-18:00] and changes very little in the period [19:00-6:00]. The main reason is that the PV penetration rate in the CAISO grid is high (nearly 17.8%), and its power output is mainly concentrated in the period [8:00-18:00]. The wind power penetration rate is low (almost 3.1%), so its impact on the net load power curve in the period [19:00-6:00] is minimal. In the Czech grid and the Qatar grid, there is the same change trend, the PV power output has a higher impact on the net load power curve than wind power in these three countries.

Considering the renewable energy development trends in the above three countries, we further analyzed the changing characteristics of the net load power curve under different

renewable energy penetration rates, as shown in Figure 3-7. In the CAISO grid, PV penetration increase will cause a higher requirement of flexibility resources, it will look like the canyon curve [105]. By comparing different cases (case 1: α=0.178, γ=0.031; case 2: α=0.178, γ=0.1; case 3: α=0.178, γ=0.2, different cases means different renewable energy penetrations), with the increase of wind penetration, the net load power curve changes greatly in the period [9:00-16:00] and changes very little in the period [20:00-6:00], the main reason is that during above different period, the wind power will be different, as shown in Figure 3-5. With the PV penetration increase, by comparing the cases (case 1: α=0.178, γ=0.031; case 5: α=0.3, γ=0.031; case 6: α=0.5, γ=0.031), we can find that the net load power curve has a deep decrease and increase during the period [8:00-18:00]. That is, PV power has a bigger influence on the net load power curve than wind power. As the PV penetration rate increases, the net load power curve shows the characteristics: high on both sides and low in the middle; while the lowest time point often corresponds to the point with the largest PV power, close to 11:30-13:00, the net load power curve gradient will become very large at certain points due to the timing characteristics of PV power, which is reflected in the power system operation process, that is, the requirement of flexible ramping resources will become very large. This section analyzes the net load power curves with different renewable penetration rates in different countries, to guide the future reserve of flexible resources in these countries.

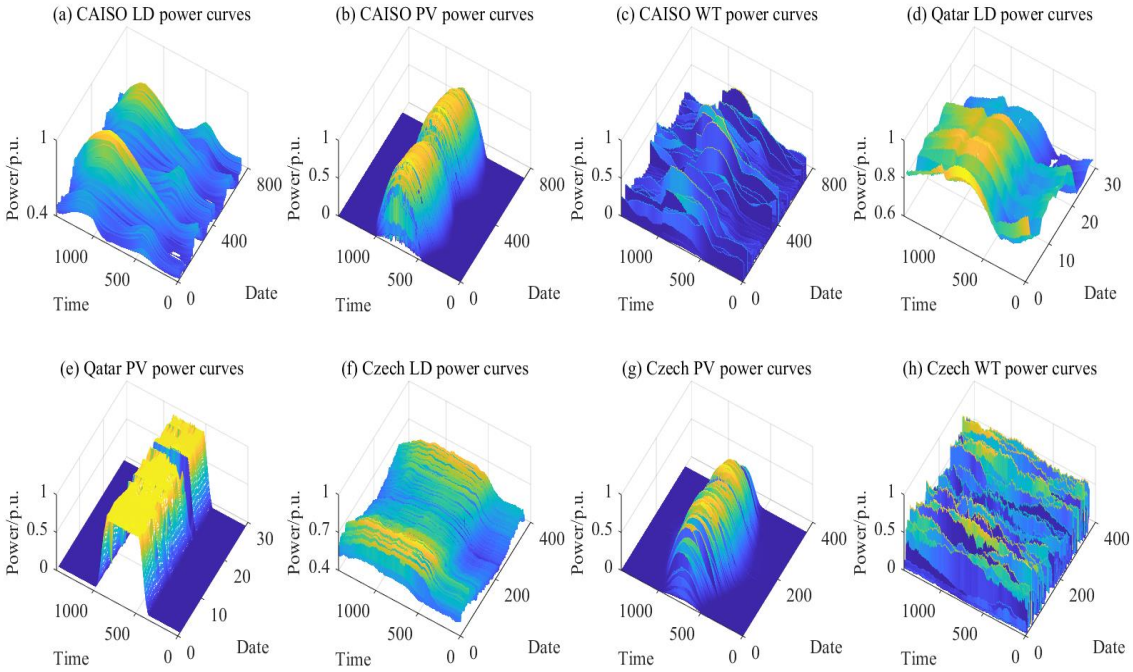

Figure 3-5. Per unit power curves in different countries and different types of resources.

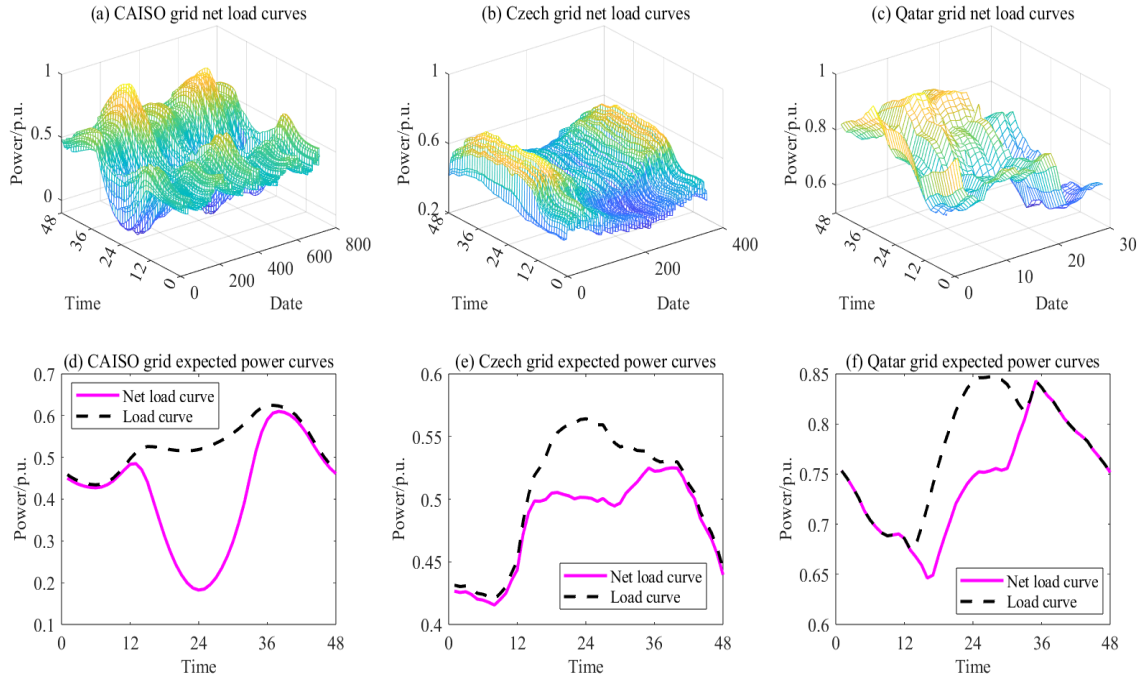

Figure 3-6. Net-load power curves. In the CAISO grid, the PV ratio is equal to 17.8%; the WT ratio is equal to 3.1%; in the Czech grid, the PV ratio is equal to 3.6%, WT ratio is equal to 0.9%; in the Qatar grid, the PV ratio is equal to 10.3%.

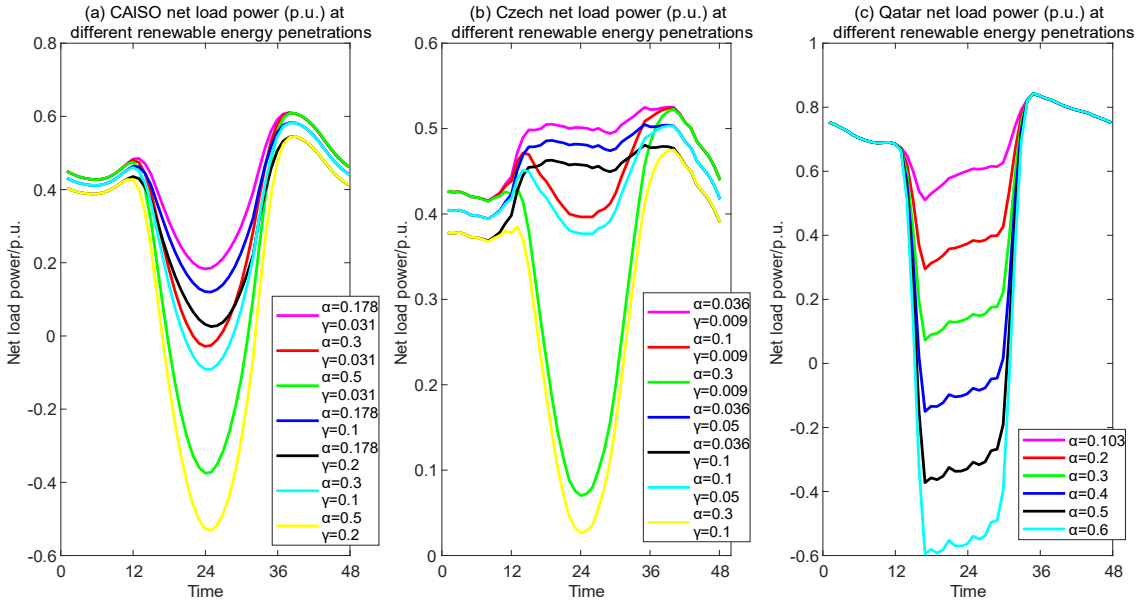

Figure 3-7. Expected daily net load power curves at different renewable penetration

3.4.3 Real-time Power Curve Time Series Characteristics

The main challenge of high-penetration renewable energy systems is the variability, fluctuation, and intermittent brought by renewable energy. This characteristic will not only affect the net load power curve, but its rapidly changing characteristics will also directly lead to the difference between real-time power and day-ahead power scheduling process, which means the system requires real-time imbalanced power backup. In this section, we will analyze different flexible resources and their real-time imbalanced power time series characteristics.

(1) Load demand real-time imbalanced power curve characteristics

The load peak and valley will have the minimum power gradient, affecting the real-time imbalanced power curve, which minimizes real-time power imbalance reserve requirements at these time points. The load peak/valley timing distribution characteristics

of different countries are shown in Figure 3-8 below. By comparing Figure 3-8,

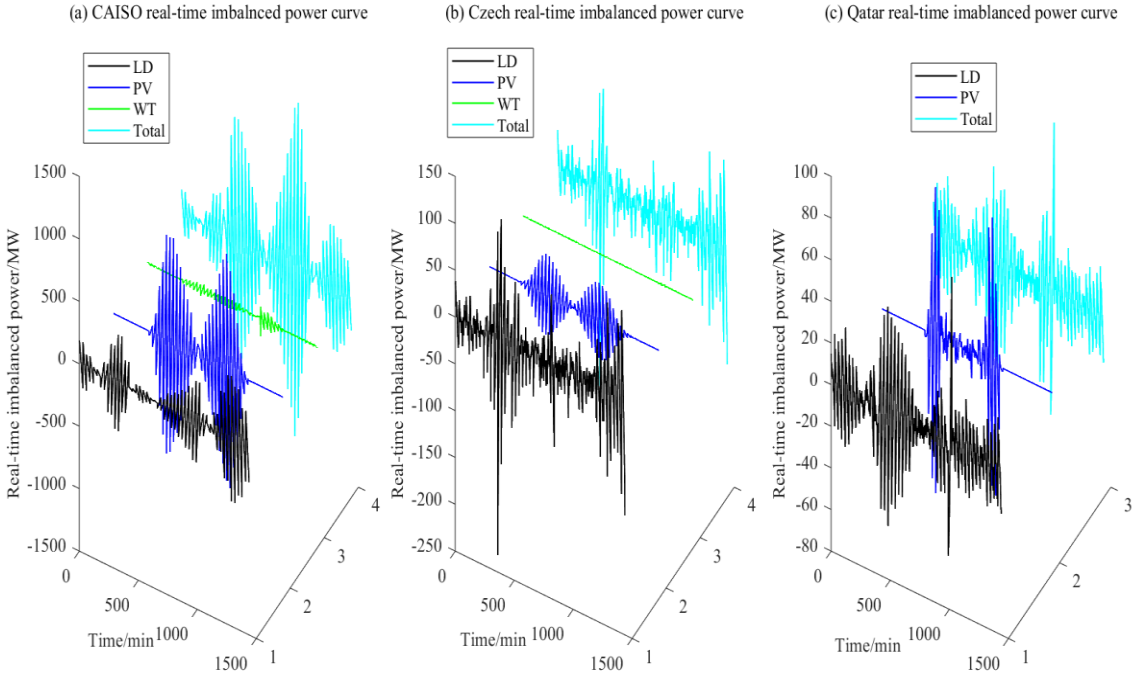

Figure 3-9, and Figure 3-10, we can find the power gradient at the peak/valley load periods is the smallest, resulting in a lower real-time imbalanced power amount in the corresponding period. From the above Figures, we can find that the load demands real-time imbalanced power time series curves have these characteristics:

(1) In the CAISO grid, peak load demand usually occurs close to 17:00-20:00. In addition, there will also be a local short-term load peak around 6:00-8:00. The valley of load demand usually occurs at 23:00-4:30 and 13:30-15:30. Between the valley and peak, the power gradient will increase from zero to a large value and then decrease to zero again. Between the peak and valley, the power gradient will decrease from zero to a small value and then increase to zero again. Therefore, the load demand RTIP has four lower periods, namely [2:00-3:00], [7:00-8:00], [14:00-15:00], and [18:00-19:00]. From Figure 3-5, we can find during periods [7:00-8:00] and [14:00-15:00], the load power gradient changes little, so the

real-time power imbalance is not large, but the period from [2:00-3:00] to [7:00-8:00], period from [14:00-15:00] to [18:00-19:00], and period from [18:00-19:00] to [2:00-3:00], the load power gradient changes significantly, so the real-time power imbalance is large, as shown in the

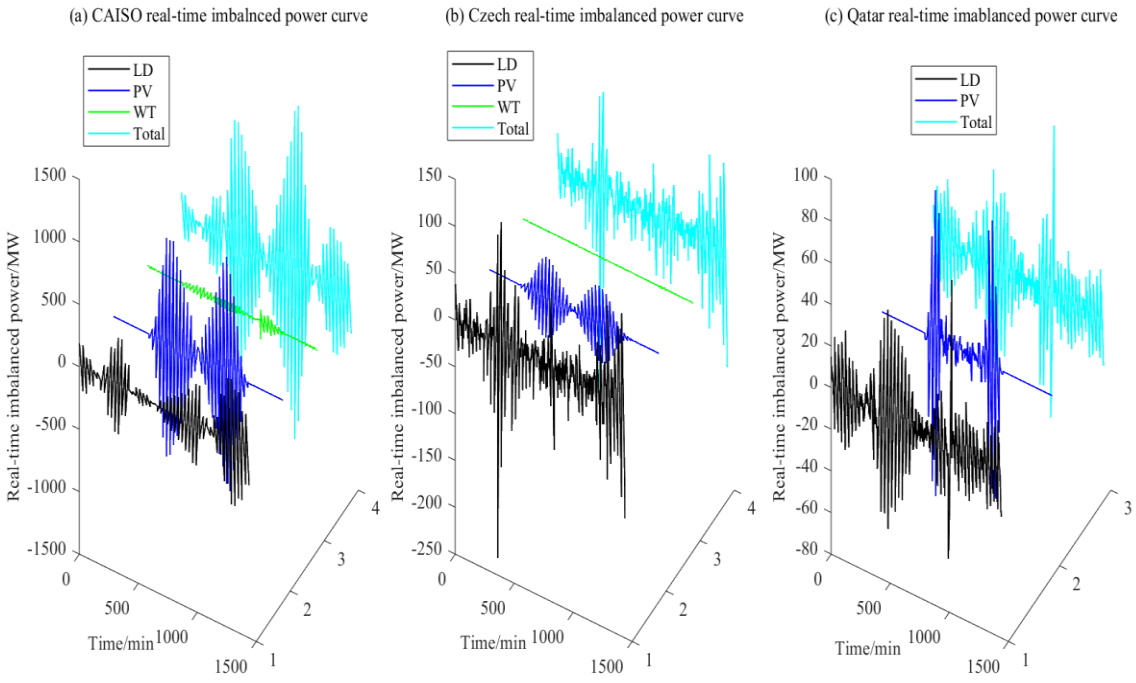

Figure 3-9 and Figure 3-10.

(2) In the Czech grid, peak load demand usually occurs close to 10:30-13:00. The valley of load demand usually occurs at 23:00-4:30. Between the valley and peak, the power gradient will increase from zero to a large value, and then decrease to zero again. Between the peak and valley, the power gradient will decrease from zero to a small value and then increase to zero again. Therefore, the load demand RTIP has two lower periods, namely [10:00-11:00] and [2:30-4:00]. From Figure 3-5, we can find during periods [10:00-11:00] and [19:00-20:00], the load power gradient changes little, so the real-time power imbalance is not large, but the period from [2:30-4:00] to [10:00-11:00], period from [19:00-20:00] to 24:00, the load power gradient changes significantly, so the real-time power imbalance is

large, as shown in Figure 3-9 and Figure 3-10.

(3) In the Qatar grid, peak load demand usually occurs close to 12:00-14:00. The valley of load demand usually occurs at 4:00-6:00. Between the valley and peak, the power gradient will increase from zero to a large value, and then decrease to zero again. Between the peak and valley, the power gradient will decrease from zero to a small value and then increase to zero again. Therefore, the load demand RTIP has two lower periods, namely [4:00-6:00] and [12:00-14:00], as shown in Figure 3-9 and Figure 3-10.

We can find that the amount of load demand RTIP has a linear relationship with the load demand power gradient. The greater the load power fluctuation, the greater the real-time power imbalance quantities. Based on the time series of the load demand power curve, especially the peak and valley points, the results of this chapter can give scientific guidance for the balance market to prepare flexibility resources in advance.

(2) Solar power real-time imbalanced power curve characteristics

Solar power is mainly affected by natural resources such as light intensity, and its power output is approximately proportional to light intensity [33], [38-39], [41-42], [47]. Therefore, its power output has obvious time series characteristics: The photovoltaic power generation gradually increases from 0 to the maximum power (corresponding to zero solar irradiance to the strongest light intensity); then decreases from the maximum power to 0 (corresponding to the light intensity from highest to 0); 2) The PV power change rate, that is, the PV power gradient, is often relatively small when the power is maximum (i.e., noon);

3) When there is no light intensity (from evening to early morning), the photovoltaic power generation is approximately 0, and its change rate is also 0; 4) When the light intensity gradually increases or weakens, although the photovoltaic power generation is not high, the PV power change rate is relatively large. Based on the above features, the PV power peak/valley timing distribution characteristics and real-time imbalanced power timing characteristics of different countries are shown in Figure 3-8 and Figure 3-9 below.

Comparing the PV power peak/valley distribution characteristics in different countries from Figure 3-8, it can be seen that even though there are differences in solar resources in different countries, their PV power timing characteristics show the same trend: (1) the PV power peak distribution is mainly concentrated at noon (11:00-13:00); (2) the PV power output is 0 in the early morning and evening.

From Figure 3-9 and Figure 3-10, we can find that the PV real-time imbalanced power time series curves have these same characteristics:

The changing trend of real-time imbalanced power reserve requirement of solar power is consistent in three different countries: (a) During the early morning and night periods, the real-time imbalanced power reserve requirement of photovoltaic power is 0; (b) During the period close to noon, the real-time imbalanced power reserve requirement for photovoltaic power is very small; (c) From early morning to noon, whether upward flexibility or downward flexibility requirement, the real-time imbalanced power reserve requirement for photovoltaic power first increases and then decreases; (d) From noon to the

afternoon, whether it is an upward flexibility requirement or downward flexibility requirement, the real-time imbalanced power reserve requirement of photovoltaic first increases and then decreases to 0. (e) The change trend of the real-time imbalance amount of photovoltaic power generation over time: first slowly increases from 0 to the maximum (the maximum point corresponds to the maximum photovoltaic power gradient, generally at [9:00-10:00]), and then slowly decrease from maximum point to 0 (The corresponding point is the largest solar intensity, usually at [11:30-13:00]), and then slowly increases from 0 to maximum (the maximum point corresponds to the largest photovoltaic power gradient, usually at [15:30-17:00]), and finally slowly decreases to 0 (corresponding to photovoltaic power is equal to 0 and power gradient also equal to 0, usually after 19:00). The solar power real-time imbalanced power curve looks like butterfly curve [115].

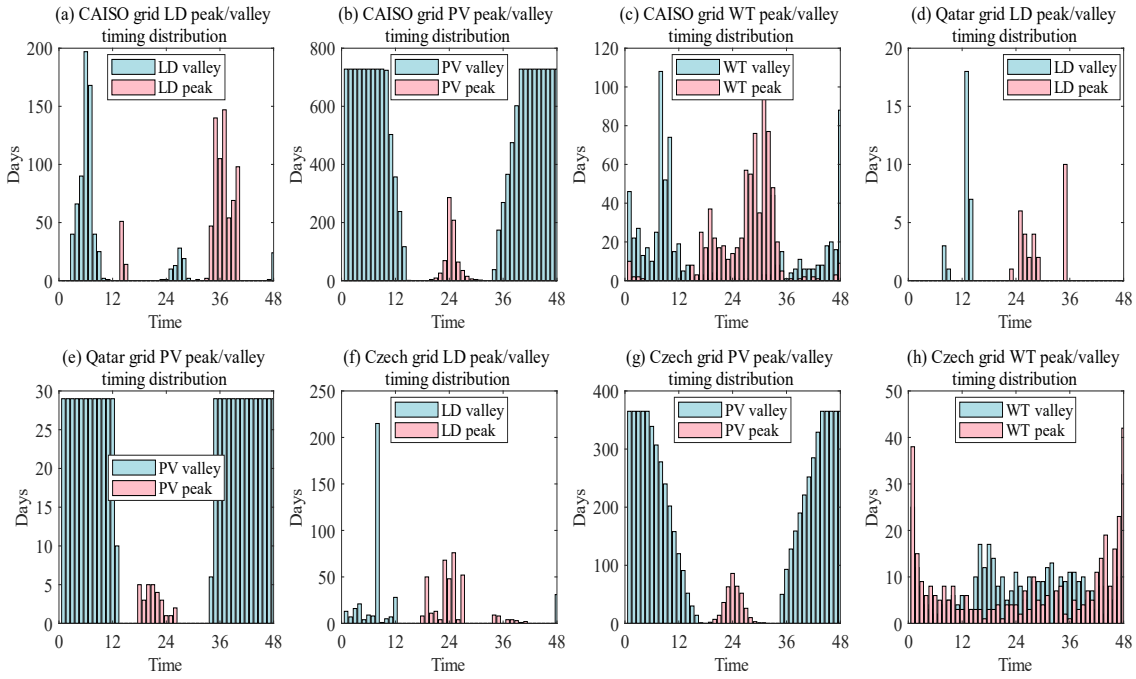

Figure 3-8. Peak/valley power timing distribution characteristics of different countries.

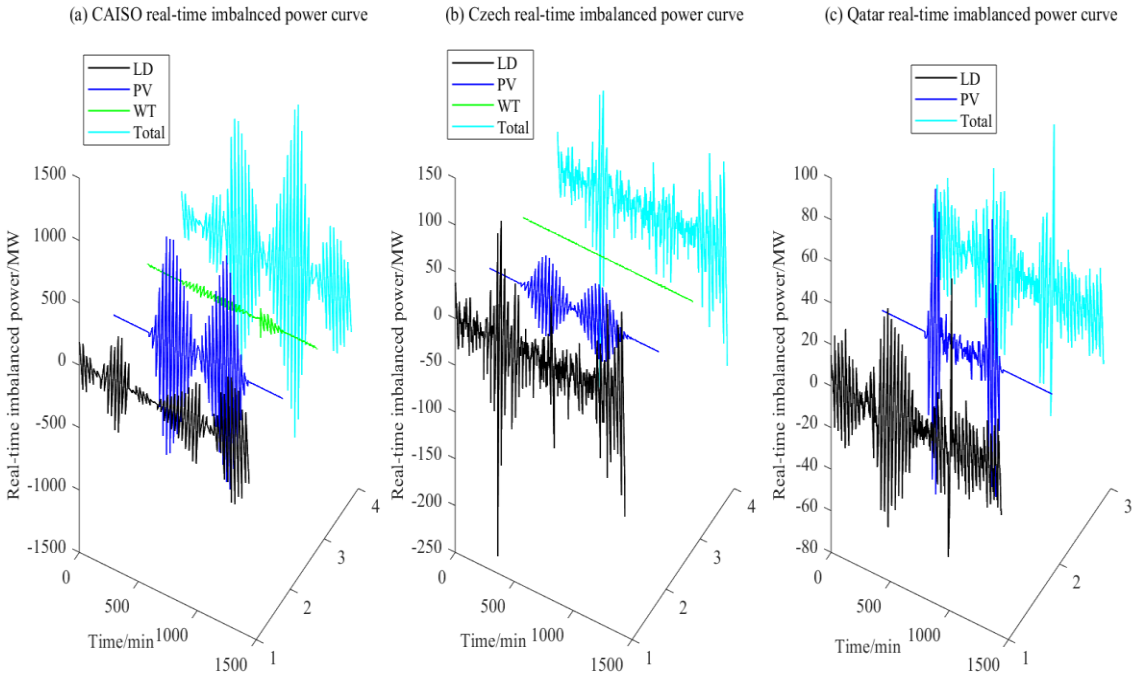

Figure 3-9. Real-time imbalanced power curves.(In the CAISO grid, the PV ratio is equal to 17.8%; the WT ratio is equal to 3.1%; in the Czech grid, the PV ratio is equal to 3.6%, WT ratio is equal to 0.9%; in the Qatar grid, the PV ratio is equal to 10.3%.)

(3) Wind power real-time imbalanced power curve characteristics

Wind power does not have obvious time series characteristics like load power curve and PV power, and there are differences in different countries. In Figure 3-8, we can find that the wind power in the CAISO grid is usually larger during periods 9:00-17:00 and relatively smaller during periods 20:00-6:00. But in the Czech grid, the wind power has an abundant peak or valley points, mainly because the power output is fluctuation heavily. The characteristic of wind power that many peak and valley powers appear alternately means that the difference between adjacent peak and valley powers in the wind curve will not be large. On the other hand, the real-time imbalanced power quantities will not be very large either, as shown in Figure 3-9 (a) and (b).

The amount of RTIP is relatively small when the wind power gradient is small

(combining Figure 3-5 (c) and Figure 3-10 (a), observation period 21:00-5:00), and is relatively large when the wind power gradient is large (combining Figure 3-5 (c) and Figure 3-10 (a), the observation period 18:00-20:00), but its absolute value is also affected by the power difference of the adjacent peak and valley. For example, in the CAISO grid, The difference in real-time imbalanced power between periods 8: 00-12:00 and 18:00-20:00; and in the Czech grid, there are many peak and valley power points, but the adjacent peak and valley differences are small, making the real-time imbalanced power of wind power is generally small, as can be seen by comparing Figure 3-5 (h) and Figure 3-10 (c).

The fluctuation characteristics of wind power will not bring obvious differences to the RTIP, mainly due to: (1) Peak and valley alternations occur frequently; (2) The power difference between adjacent peaks and valleys is not large; in the Czech grid, When the wind power penetration rate is as high as 10%, the real-time imbalanced power quantity caused by wind power fluctuations is even less than 0.1% of the load peak.

(4) The RTIP timing characteristics in the CAISO grid, Czech grid, and Qatar grid with renewable energy penetration increase

The whole power system power variability is defined as the overall external representation of all the variability resources in this area. There are differences in energy structure and peak load in different countries' grids, and therefore their external real-time imbalanced power reserve time series characteristics are also different. Considering that the power variability characteristics from traditional generators (such as gas, thermal, and

nuclear, etc.) are not obvious, that is, the power output is stable within the scheduling time window. VREs (such as wind power, solar power, etc.) have large variability characteristics, and with the penetration increases, their variability characteristics will become more obvious. Therefore, the real-time imbalanced power reserve requirement in three different countries' grids mainly comes from VREs' power variability and load demand variability. When the real-time load demand becomes smaller while the renewable energy power becomes larger, the real-time imbalanced power reserve needs upward flexibility $P_{\mathrm{U},t}$; when the real-time demand becomes larger while the renewable energy power becomes smaller, the real-time imbalanced power reserve needs downward flexibility $P_{\mathrm{D},t}$. As shown in the following equations (3.15) and (3.16).

$$P_{\mathrm{U},t} = \Delta P^{+}_{\mathrm{WT},t} + \Delta P^{+}_{\mathrm{PV},t} - \Delta P^{-}_{\mathrm{LD},t} \tag{3.15}$$

$$P_{\mathrm{D},t} = \Delta P^{+}_{\mathrm{LD},t} - \Delta P^{-}_{\mathrm{PV},t} - \Delta P^{-}_{\mathrm{WT},t} \tag{3.16}$$

where $\Delta P^{+}_{WT,t}$ and $\Delta P^{+}_{PV,t}$ represent wind power and PV power real-time part larger than the day-ahead part, respectively; $\Delta P^{-}_{WT,t}$ and $\Delta P^{-}_{PV,t}$ represent wind power and PV power real-time part smaller than the day-ahead part, respectively; $\Delta P^{+}_{LD,t}$ and $\Delta P^{-}_{LD,t}$ represent load demand real-time part larger than the day-ahead part and smaller than the day-ahead part, respectively.

Based on the different variable resources in different grids, we can obtain their real-time imbalanced power reserve requirement time series characteristics shown in Figure 3-9. At the current renewable energy penetration (In the CAISO grid, the PV ratio is equal to 17.8%;

the WT ratio is equal to 3.1%; in the Czech grid, the PV ratio is equal to 3.6%, WT ratio is equal to 0.9%; in the Qatar grid, the PV ratio is equal to 10.3%.), it can be seen that, in the CAISO grid, the real-time imbalanced power quantity has a higher value from 7:30-9:30 and 15:00-17:00, and in other periods, such as 20:00-6: 00, the real-time imbalanced power is generally low. The higher periods are mainly affected by the PV imbalance component, and the lower periods are mainly affected by the imbalance part caused by load power fluctuations. In the Czech grid, the real-time imbalanced power quantity has a higher value from 3:00 to 10:30 and a period from 20:00 to 24:00, these higher periods are mainly affected by the load demand imbalance component, and the wind power and PV power imbalances parts are relatively small. But when the PV penetration rate increases (increase to 10%, and even up to 30%), shown in Figure 3-10 (c) and (d), the Czech grid's real-time imbalanced power will be influenced by PV imbalanced characteristics, shown in the butterfly curve. In the Qatar grid, the real-time imbalanced power quantity has a higher value from 7:00-8:00 and 15:00-16:30, these higher periods are mainly affected by the PV imbalance component, look like butterfly curve, in other periods, such as 17:00-6: 00, the real-time imbalanced power is generally low, these periods are mainly affected by the load demand power fluctuations. When the PV penetration rate increases (increase to 20%, and even up to 60%), as shown in Figure 3-10 (e) and (f), the Qatar grid real-time imbalanced power quantities curve will be clearly shown as the butterfly curve.

In areas with abundant solar resources, the real-time imbalanced power curve will show

a butterfly curve, such as the CAISO grid and the Qatar grid (PV penetration rate more than 10%). However, in areas with relatively less abundant solar resources, such as the Czech grid, the real-time imbalanced power curve characteristics will also be greatly affected by the PV power fluctuation. The above features are mainly due to the PV power fluctuation characteristics having obvious timing characteristics and the amount of RTIP caused by its fluctuation are generally large, but the amount of RTIP caused by wind power and load demand fluctuations is relatively small.

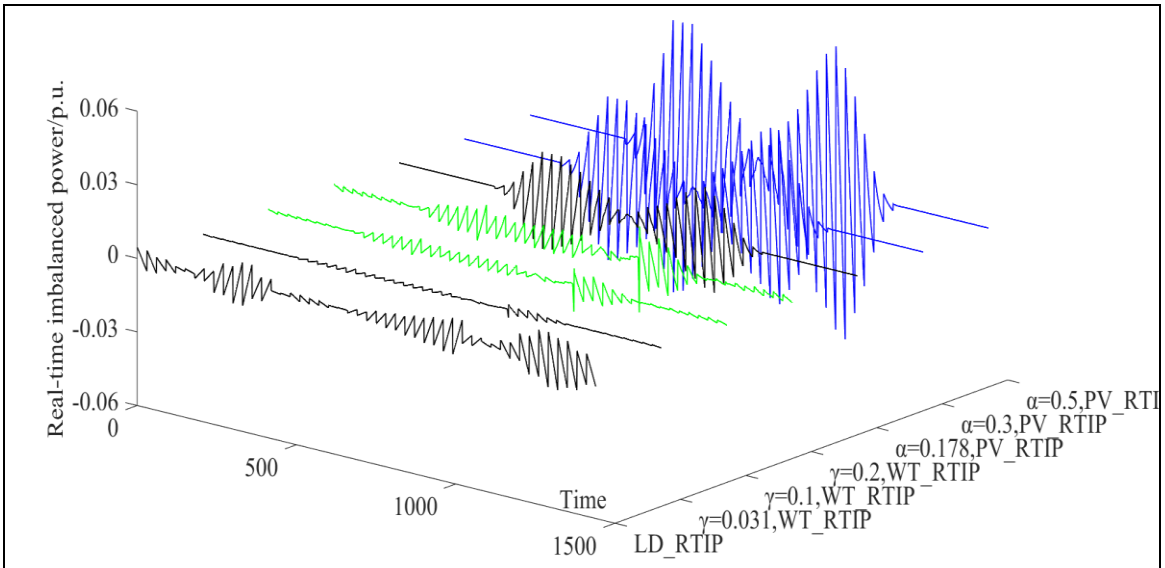

(a) CAISO grid different flexible resources real-time imbalanced power (p.u.)

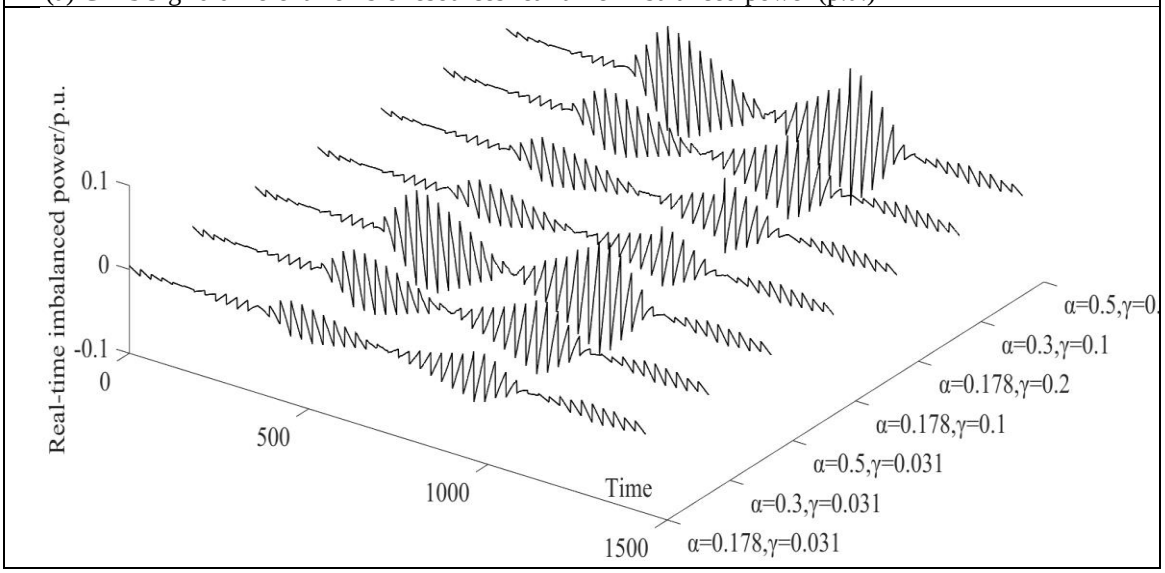

(b) CAISO grid real-time imbalanced power (p.u.) at different renewable energy penetration rates

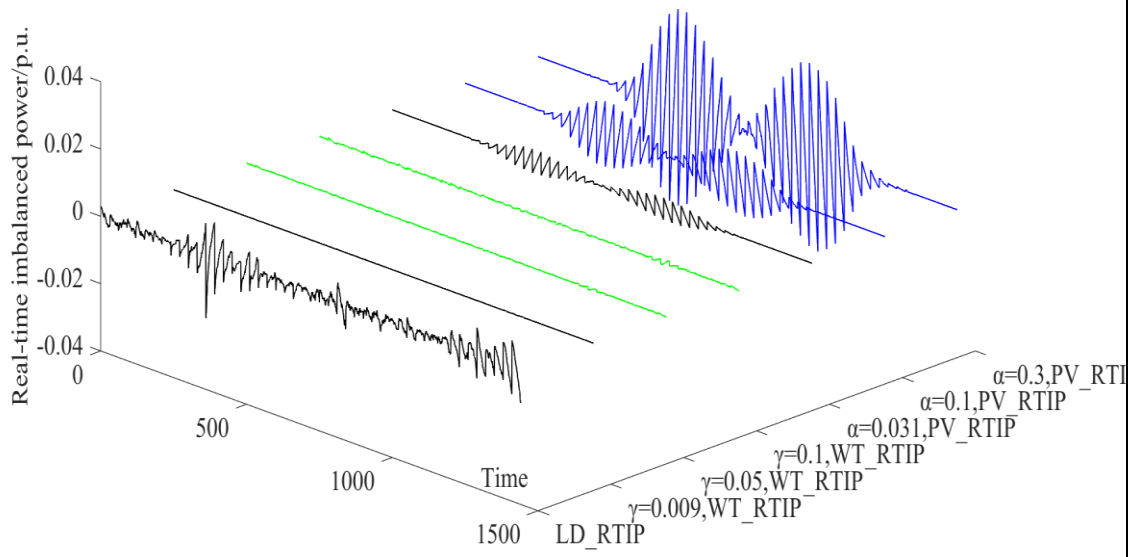

(c) Czech grid different flexible resources real-time imbalanced power (p.u.)

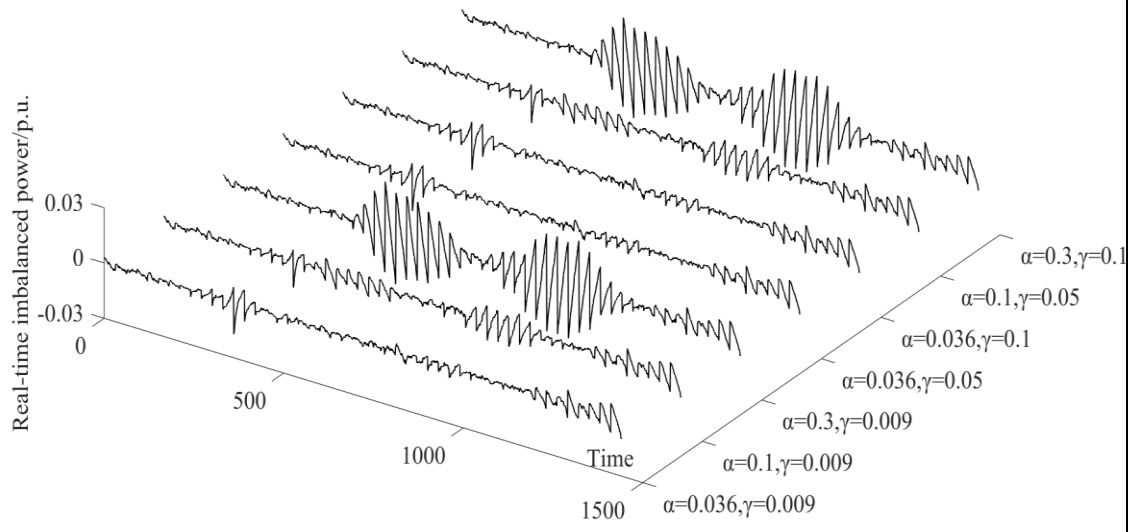

(d) Czech grid real-time imbalanced power (p.u.) at different renewable energy penetration rates

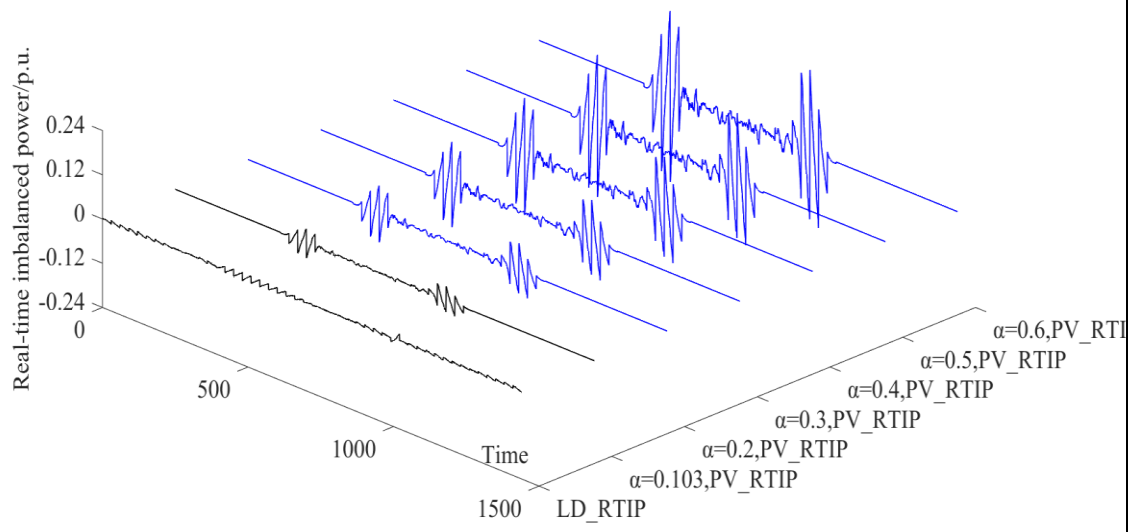

(e) Qatar grid different flexible resources real-time imbalanced power (p.u.)

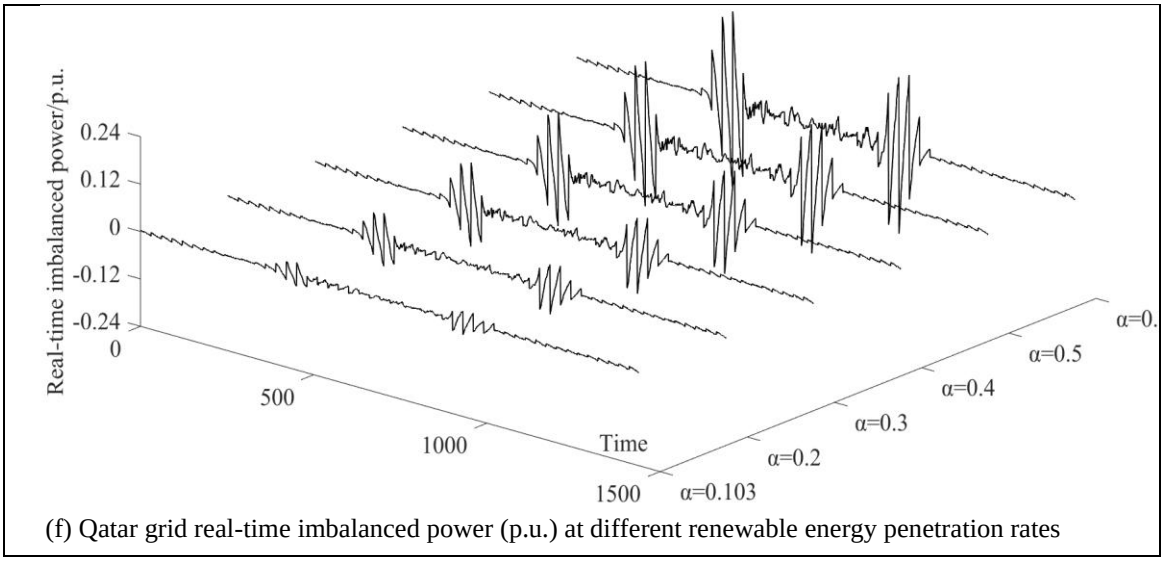

(f) Qatar grid real-time imbalanced power (p.u.) at different renewable energy penetration rates

Figure 3-10. Real-time imbalanced power curves at different renewable energy penetrations.

3.5. Summary

This chapter proposed metrics including power incremental statistics, coefficient of variation, and peak power duration to characterize the power variability characteristics. Based on these metrics, we analyze the mathematical relationship between these variations and net-load power curves and real-time power imbalance curves, finding that power variability will directly affect net-load power curves and the power gradient will affect the real-time power imbalance curve. The main conclusions are as follows:

(1) The different types of resources in different countries have different power fluctuation characteristics, PV power has the largest fluctuation, followed by wind power, and load power has the smallest fluctuation.

(2) The time series characteristics of PV power are relatively obvious, which directly affects the net load power curve. There is a higher flexible power requirement near noon (that is, around the maximum PV power), and this feature will increase as the PV

penetration rate increases. These features make the net load curve look like the canyon curve; the timing characteristics of wind power in different countries are different, but the overall impact of wind power on the net load power curve is not as obvious as that of PV power.

(3) The real-time imbalanced power quantities of different types of resources are proportional to their power gradient. The real-time power imbalance caused by PV power has timing characteristics and looks like a butterfly curve.

(4) The method proposed in this chapter can effectively help system operators rationally arrange flexible resource reserves, such as helping system operators prepare ramp power requirement reserve based on net-load power curve time series results; and prepare real-time power balance reserve based on the real-time imbalanced power curve time series results.

4. IMPACT ANALYSIS OF INCREASING TIME GRANULARITY ON HIGH PENETRATION RENEWABLE ENERGY

Abstract: The power system operation and settlement will face fundamental challenges with increasing variable renewable energy (VRE). In this chapter, we propose an evaluation method for the electricity market at different time granularity, including ex-ante real-time power deviation prediction; real-time power scheduling operation and clearing; ex-post power deviation settlement. Based on this evaluation model, we analyze high temporal resolution datasets and find strong evidence that the higher the time granularity, the power step changes and the real-time power deviation quantities are smaller, and vice versa. Reducing the power step changes and real-time power deviations will reduce power grid frequency deviations and power market balancing costs. Moreover, increasing the time granularity from 30 to 5 minutes would reduce the balancing cost by nearly half, and reduce the power step amplitude standard deviation by nearly 80%. This chapter for the first time provides scientific evidence to support the worldwide reform of the electricity market with massive renewable energy integration by increasing time granularity.

Abbreviations	
VRE	Variable renewable energy
RTPD	Real-time power deviation
MCM	Markov chain mixture distribution model
Variables, Parameters, and Functions	
T_0	Power sampling rate
T_n	Power scheduling time granularity
P_i	The *i*-th sampling power
PS	Power step changes between adjacent scheduling intervals
B_t	Bounded limit of power at the *t*-th time spot
N_t	Divide the power into *N* bins at *t*-th time spot
$\mathbf{M}_t$	The transfer matrix at *t*-th time.
$\Delta P(t)$	Real-time power deviation at the t-th time spot
$P_{\mathrm{U},s,t}$	Upward regulation power requirement at the *t*-th time spot under the *s*-th scene
$P_{\mathrm{D},s,t}$	Downward regulation power requirement at the *t*-th time spot under the *s*-th scene
$\Delta P^{+}_{\mathrm{VREs},s,t}$	VRE real-time power is larger than the day-ahead part
$\Delta P^{-}_{\mathrm{VREs},s,t}$	VRE real-time power is smaller than the day-ahead part
$\Delta P^{+}_{\mathrm{LD},s,t}$	Load demand real-time power larger than the day-ahead part
$\Delta P^{-}_{\mathrm{LD},s,t}$	Load demand real-time power smaller than the day-ahead part
$P^{U}_{B,i,s,t}$	The *i*-th flexible resources to provide upward flexible power at *t*-th time slot and in the *s*-th scene
$P^{D}_{B,i,s,t}$	The *i*-th flexible resources to provide downward flexible power at *t*-th time slot and in the *s*-th scene
N_s	The number of scenes
C_B	The real-time power scheduling cost
$\lambda^{D}_{B,s,t}$	Downward regulation unit power price at the *t*-th time slot in the *s*-th scene
$\lambda^{U}_{B,s,t}$	Upward regulation unit power price at the *t*-th time slot in the *s*-th scene
$\Delta P^{+}_{\mathrm{VREs},real,t}$	The VRE ex-post actual power is larger than the day-ahead part

$\Delta P^{-}_{\mathrm{VREs},real,t}$	The VRE ex-post actual power is smaller than the day-ahead part
$\Delta P^{+}_{\mathrm{LD},real,t}$	Load demand ex-post actual power larger than the day-ahead part
$\Delta P^{-}_{\mathrm{LD},real,t}$	Load demand ex-post actual power smaller than the day-ahead part
C_P	The ex-post power deviation settlement cost
$\Delta P_{\mathrm{D},s,t}$	The downward regulation deviation at the *t*-th time slot in the *s*-th scene
$\Delta P_{\mathrm{U},s,t}$	The upward regulation deviation at the *t*-th time slot in the *s*-th scene

4.1. Introduction

Recently, more countries have declared that they will achieve net-zero carbon emissions to mitigate the urgency of climate change. To align with this global effort, variable renewable energy (VRE) sources must be pivotal [3-5]. However, VREs face inherent challenges due to their reliance on natural environmental factors, such as solar irradiance, air temperature, wind speed and directions, etc. These factors introduce significant volatility and uncertainty into the energy system [16-19], [31], [33]. As VREs penetrate the power grid on a massive scale, the grid will encounter greater fluctuations and intermittent than it does presently.

Based on the definition and technical of the power system, it is important to maintain an immediate equilibrium between the supply of electrical energy and the demand from consumers [14]. Therefore, the variability and intermittency of the VREs will bring huge challenges to the stability and operation of the power system. Traditional generation such as nuclear, thermal, gas, hydropower, etc. occupy a large proportion of traditional power systems, and these generators have high inertia, which can use mechanical rapid rotating power to serve as automatic power generators to help keep the grid frequency stability. However, with the high penetration of VREs, these generators (including wind turbines and

PVs) transfer power/energy to the main grid based on an inverter technique. Through this technology, the inertia from the VREs is decoupled from the other part of the grid, therefore the moment of inertia in the total system will be reduced and the lower rotational inertia will influence the power grid stability [14], [20-22], [25]. In addition, the volatility and intermittency of VRE generators will also cause higher power fluctuations, which will also cause power grid frequency fluctuations. Except for influencing the power grid frequency stability, the volatility and intermittency of VRE generators will bring higher power differences between day-ahead dispatch and real-time dispatch and increase the re-dispatch operating cost and power deviation settlement cost, influencing the power market operation cost [26-28], [107].

Recently, increasing time granularity in power systems by reducing the energy settlement time unit (pricing shorter market time units) is an important energy market innovation to address the volatility, uncertainty, and intermittency challenges posed by the increased penetration of VREs [32]. On the one hand, increasing time granularity means the closing time of the scheduling gate is more frequent and the scheduling interval is shorter, which allows system operators to more quickly solve the power imbalance problem caused by the difference between day-ahead dispatch and real-time dispatch. Also, shortening the scheduling intervals means that power step change at scheduling interval points and real-time power deviation during the scheduling intervals will decrease, reducing power grid frequency deviation. On the other hand, increased time granularity in the electricity market helps system operators predict day-ahead and real-time operations more accurately based on

timely information. This helps avoid the re-dispatch process, which will increase the ex-post power deviation settlement cost.

In this chapter, we use the minute-level temporal resolution datasets including load demand, wind power, and solar power located in three different countries around the world to how we can reduce balancing electricity market costs and power grid frequency deviations by increasing time granularities. First, based on the historical datasets, we used the statistics method and found that increasing the time granularity will reduce the power step change at the scheduling interval points and real-time power deviation during the scheduling interval, increasing time granularity from 30 minutes to 5 minutes would reduce the power step amplitude by nearly 80%, improving power grid frequency stability. Then, based on the electricity balance market model, including ex-ante real-time power deviation prediction, real-time power scheduling, and ex-post power deviation settlement, we observe that increasing time granularity will improve real-time power deviation prediction accuracy (shorter time will provide more accurate forecast information); reduce real-time power scheduling operation costs and reduce ex-post power deviation settlement cost, increasing time granularity from 30 minutes to 5 minutes would reduce the balancing cost by nearly half. This chapter for the first time provides scientific evidence to support the reform of the global electricity market by increasing the time granularity.

4.2. Data Setting and Description

This chapter contains power datasets time series information from three different

countries: Qatar power grid, Czech power grid, and California Independent System Operator (California ISO) grid, these three different grides cover power information and grid frequency information. Detailed information on these datasets is described below.

Dataset I: The dataset includes PV power (PV farm) and load demand in the Qatar grid; the temporal resolution is 1 minute. (here, the dataset includes the 2022-2023 two-year data). The peak load in the Qatar grid is about 4700MW, and the PV farm capacity is about 500MW.

Dataset II: The dataset includes several wind farms and load demand in the Czech grid. (here, the dataset includes the 2021 whole-year data) [110]. The peak load in the Czech grid is about 13000MW, the PV capacity is about 1700MW, and the wind capacity is about 300MW.

Dataset III: The dataset includes wind power, solar power, and load demand located in the California Independent System Operator (California ISO) grid. The temporal resolution is 1 minute. (Here, the dataset includes nearly two years between 01/01/2018 and 31/12/2019) [109]. The peak load in the California ISO grid is about 48000MW, the PV capacity is about 18000MW, and the wind capacity is about 8100MW.

4.3. Methods

4.3.1 Power Grid Frequency Analysis

The variation in electricity frequency is mainly caused by the instantaneous power imbalance. We can describe its relationship through the swing equation below [14], [24].

$$\begin{aligned} \frac{d\delta_i}{dt} &= \Delta\omega_i \\ \frac{d\Delta\omega_i}{dt} &= \frac{\omega_N}{T_{Ji}}(P_{Ti} - P_{ei}) \end{aligned} \tag{4.1}$$

where each node *i* represents a generalized generator node (a subsystem connected to the *i*-th node), its dynamic process is characterized by two independent variables: the first is phase δ_i and the second is relatively angular velocity $\Delta\omega_i=2\pi(f_i-f_R)$. For relatively angular velocity, f_R represents the grid base frequency, which is equal to 50Hz or 60Hz, based on the grid system. f_i represents the frequency of the nodes $i=1, \ldots, N$. $\omega_N=2\pi f_R$ represents the reference angular velocity, it is a constant for a stable power system; T_{Ji} represents the *i*-th generator's inertia constant. P_{Ti} represents *i*-th mechanical power; P_{ei} represents the electrical power of the *i*-th generator. Since the change speed of P_{ei} is much higher than that of mechanical power P_{Ti}, frequency stability is mainly affected by inertia constant T_{Ji} and power fluctuations. The inertia constant T_{Ji} is mainly affected by the generator mechanical inertia of the whole system, which is a system-level problem; In contrast, the impact of power fluctuations exists all the time. It can be seen from equation (4.1) that the frequency change rate is directly proportional to the power fluctuation quantities and inversely proportional to the inertia constant. Therefore, reducing power fluctuations and increasing inertia constant are effective ways to improve the power grid frequency stability.

In most grid dispatch processes, dispatch runs are typically scheduled in 1-hour increments, with shorter intervals of 30 also possible [32], [101-103]. Hence at different interval widths, the power curve is steplike. From one interval point to another interval point, the power balance rapidly switches from positive to negative or vice versa, leading to large

deviations in the grid frequency; during the interval width, the power deviation curve alternates around 0, and the total integral is 0. From one sampling point to another, the real-time power deviation undergoes rapid switches between positive and negative values. These fluctuations also directly impact the grid frequency, which is evident in Figure 4-1 (also referenced as [122-123]). The daily average frequency depicted in Figure 4-1 results from averaging data based on multiple days. Notably, The electricity market behavior, including trading and regulation, has an obvious impact shown in Figure 4-1. Hourly observations in various countries reveal sharp frequency jumps—both upward and downward. During each interval, the frequency experiences an abrupt decrease or increase, followed by a gradual trend in the opposite direction for the subsequent interval. The main reason is that at each interval point, there is a power step, which will cause a frequency jump. During the interval, real-time power deviation will cause the frequency to slowly change. Therefore, there are two parts to power fluctuations that influence frequency change: the power step change at the interval points and the power deviation during the interval. These two parts can be described in the following part.

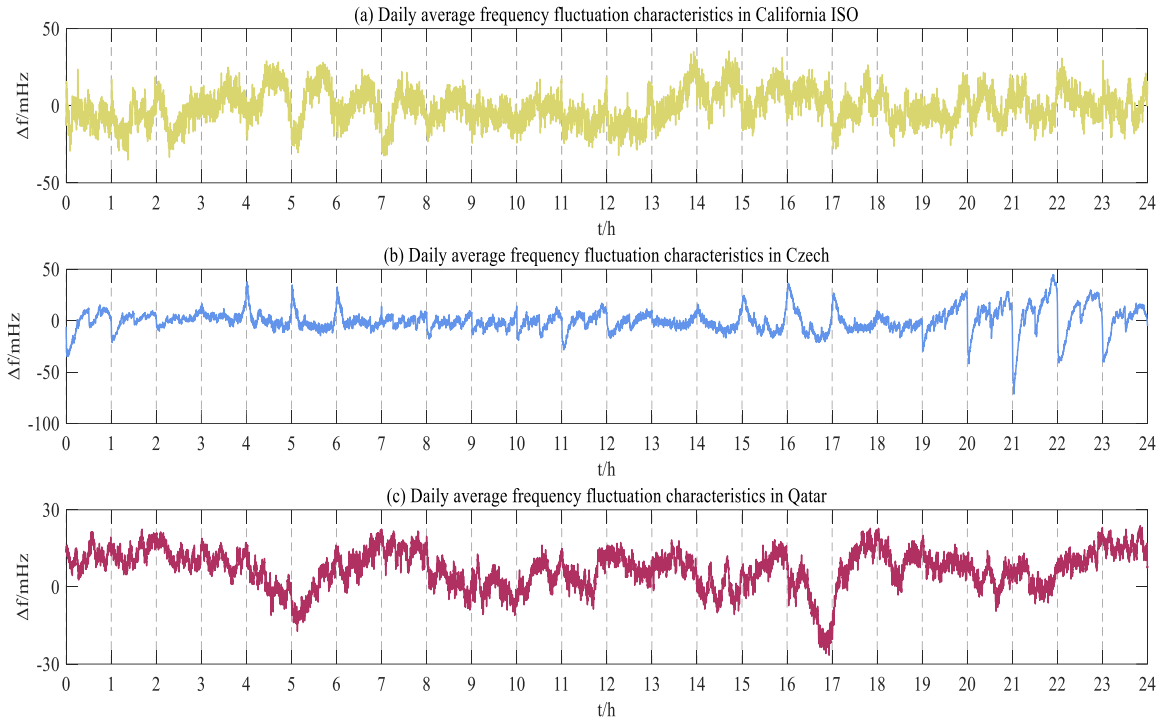

Figure 4-1 Frequency deviation timing characteristics.

4.3.2 Power Step Change and Real-time Power Deviation

Based on the electricity market operation mechanism, dispatch usually has different time intervals, such as 1 hour, 30 minutes, etc. Hence, at different interval widths, the power curve is steplike. The power step change is the power difference at different interval points. Due to power variability and uncertainty, real-time power deviation (RTPD) is equal to the power difference between the sampled power and the average power within an interval.

Therefore, we can get power step changes at different time granularities as shown in equations (4.2) and (4.3).

$$P_{T_n} = \frac{1}{n}\sum_{i=1}^{n}(P_i), T_n = nT_0 \tag{4.2}$$

$$PS = P_{T_{n+1}} - P_{T_n} \tag{4.3}$$

where T_0 represents the power sampling rate; T_n represents the power scheduling time granularities, that is the width of the scheduled intervals. P_i represents the i-th sampling power; PS represents power step changes between adjacent scheduling intervals.

By comparing real-time power and the average power in scheduled intervals, we can get real-time power deviation (RTPD) quantities at different time granularities. The details can be shown in section 3.3.2.

4.3.3 Electricity Balance Market Operation

In general, the power system operators need to schedule the system reserve power in advance according to the power deviation and guide different power units to participate in the balanced electricity market to achieve instantaneous power balancing. Uncertainties and variabilities in a large electricity system are inevitable. Therefore, the electricity balance market operation includes the following processes: (1) ex-ante real-time power deviation prediction; (2) real-time power scheduling operation and clearing; (3) ex-post power deviation settlement [27], [107]. Figure 4-2 shows the detailed process below.

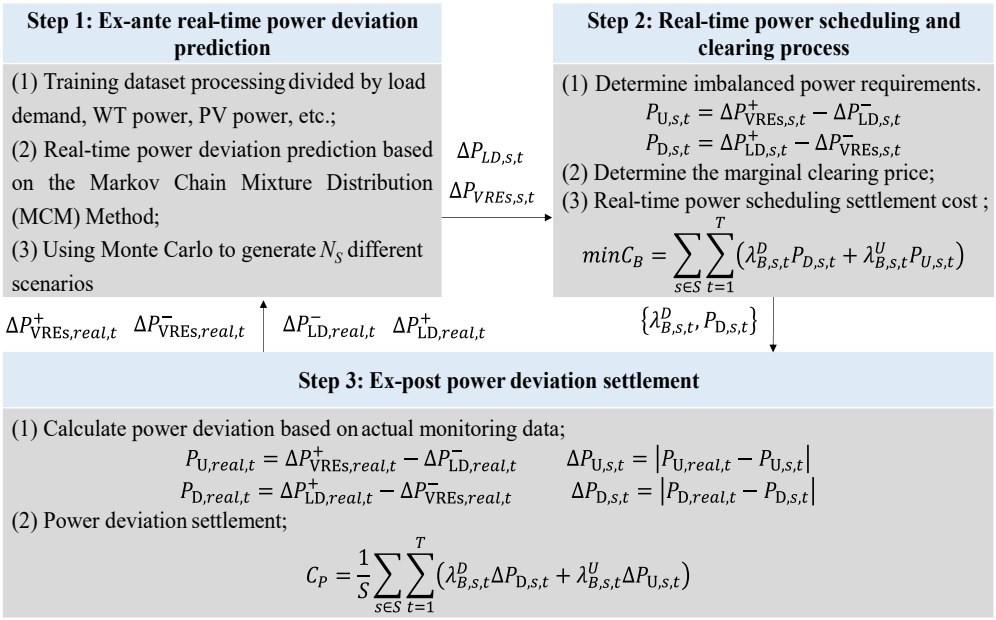

Figure 4-2. The electricity balance market operation process.

(1) Ex-ante real-time power deviation prediction

The RTPD is the power difference between sampling power and average power during the scheduling interval caused by power variability and uncertainties. Therefore, we can use equations (4.2) and (4.3) to calculate and get the RTPD training datasets at different time granularities. Then we use the Markov chain mixture distribution (MCM) model to predict real-time power deviation time series. The MCM based on *N*-state for probabilistic forecasting was widely used in forecasting solar irradiance [116-117], electricity consumption [118], etc. In this section, we will use the MCM model based on a single observation RTPD point to produce a probabilistic forecast for the next point. The MCM prediction process is shown in Algorithm 4-1 below.

Algorithm 4-1: MCM model to predict RTPD

Step 1) Define bounded within limits B_t=[a_t, b_t] based on the training time series datasets, B_t is different at different time slots.

Step 2) Choose bin N_t for the predicted model.

Step 3) Divide the training time series into N_t bins, evenly divided within the range B_t=[a_t, b_t].

Step 4) Calculate an $N_t \times N_t$ transfer matrix $\mathbf{M}_t$ based on the transfer process occurring between neighboring bins.

$$M_{t,ij} = \frac{n_{ij}}{\sum_{k=1}^{N_t} n_{ik}}, \forall i,j \in N_t \tag{4.4}$$

Step 5) Observe $\Delta P(t)$ at the t-th time point based on the test datasets, and then choose the correct bin.

Step 6) Calculate the next step predicted distribution probability, that is calculate the probability density function corresponding to the transfer matrix $\boldsymbol{M}$.

$$f\big(\Delta P(t+1)\big) = \begin{cases} P_{t+1}(x_1 \le \Delta P(t) < x_2) \\ P_{t+1}(x_2 \le \Delta P(t) < x_3) \\ \vdots \\ P_{t+1}\big(x_{N_t} \le \Delta P(t) < x_{N_t+1}\big) \end{cases} \tag{4.5}$$

$$s.t. \begin{cases} \Delta P(t) \in [a_t, b_t] \\ x_j = \dfrac{i-1}{N_t}(b_t - a_t) + a_t, i \in [1, N_t] \\ P_{t+1}\big(x_j \le \Delta P(t) < x_{j+1}\big) = M_{t,ij} \end{cases} \tag{4.6}$$

Step 7) Forecasting the real-time power deviation at the neighboring time point, we need to set the time value from t to t+1, then choose the point value $\Delta P(t+1)$ and go back from ***Step 5*** to do the same calculation.

Based on the trained model and transfer matrix $\boldsymbol{M_t}$, we can use the $\Delta P(t)$ to predict the probability distribution of the RTPD $\Delta P(t+1)$ at the next step. Through the above prediction method, we can obtain the probability distribution characteristics of the RTPD time series.

Then, we will use Monte Carlo simulation to generate S random scenarios to participate in the real-time power scheduling process.

(2) Real-time power scheduling process

Power system operators will complete real-time scheduling control and clearing processes based on the predicted RTPD and combined with the information of flexible resources in the electricity balance market. This process aims to minimize the real-time scheduling operation cost and satisfy the constraints of predicted real-time power deviation.

The primary function of a balanced electricity market is to facilitate transactions between power generation and load demand, ensuring instantaneous balance between supply and demand. Based on the predicted real-time power deviation (RTPD) from supply and demand, power imbalances in the balancing market primarily manifest in two parts [115], [119]:

1) Upward regulation ($P_{\mathrm{U},s,t}$): This part usually occurs when load demand exceeds power supply at the sampling time, to meet these power gaps, the system requires additional power generation to meet this demand. The upward regulation is shown below.

$$P_{\mathrm{U},s,t} = \Delta P^{+}_{\mathrm{VREs},s,t} - \Delta P^{-}_{\mathrm{LD},s,t} \tag{4.7}$$

2) Downward regulation ($P_{\mathrm{D},s,t}$): This part usually occurs when supply surpasses demand at the sampling time, to meet these power gaps, the system needs to reduce generation to align with demand. The downward regulation is shown below.

$$P_{\mathrm{D},s,t} = \Delta P^{+}_{\mathrm{LD},s,t} - \Delta P^{-}_{\mathrm{VREs},s,t} \tag{4.8}$$

where $\Delta P^{+}_{\mathrm{VREs},s,t}$ and $\Delta P^{-}_{\mathrm{VREs},s,t}$ represents VREs real-time power larger than the day-ahead part and smaller than the day-ahead part, respectively; $\Delta P^{+}_{\mathrm{LD},s,t}$ and $\Delta P^{-}_{\mathrm{LD},s,t}$ represents load demand

real-time power larger than the day-ahead part and smaller than the day-ahead part, respectively.

Within a scheduling window width, real-time power deviation needs to be balanced through the bidding of flexible resources, these resources need to meet the power balance constraints:

$$\sum_{i=1}^{n} P_{B,i,s,t}^{U} = P_{\mathrm{U},s,t}, \forall t \in T, \forall s \in N_s \tag{4.9}$$

$$\sum_{i=1}^{n} P_{B,i,s,t}^{D} = P_{\mathrm{D},s,t}, \forall t \in T, \forall s \in N_s \tag{4.10}$$

where $P_{B,i,s,t}^{U}$ and $P_{B,i,s,t}^{D}$ represent i-th flexible resources to provide upward and downward flexible power at t-th time slot and in the s-th scenes; N_s represents the number of scenes.

In this chapter, we use a pay-as-clear mechanism bid and participate in a real-time power scheduling process, which means the real-time power deviation clearing price is based on the most expensive offer accepted balancing unit marginal price [120]. Therefore, the real-time power scheduling operation cost is as follows, which have constraints shown in equations (4.9) and (4.10).

$$minC_B = \frac{1}{N_s} \sum\nolimits_{s=1}^{N_s} \left(\sum_{t=1}^{T} \left(\lambda_{B,s,t}^{D} P_{\mathrm{D},s,t} + \lambda_{B,s,t}^{U} P_{\mathrm{U},s,t} \right) \right) \tag{4.11}$$

where C_B represents the real-time power scheduling cost; $\lambda_{B,s,t}^{D}$ and $\lambda_{B,s,t}^{U}$ represent the downward regulation and upward regulation unit power price at the t-th time slot in the s-th scene, respectively; $P_{\mathrm{D},s,t}$ and $P_{\mathrm{U},s,t}$ represent the downward and upward regulation provided by flexible resources to participate in balance service at the t-th time slot in the s-th scene.

(3) Ex-post power deviation settlement

In large electricity systems, uncertainties are inevitable. Therefore, power system operators need to calculate additional operation costs based on the real power data collected in the SCADA system afterward. The further operation costs mainly include two parts: (1) power system reserve operation costs due to prediction errors, borne by the power system operator; (2) suppliers/consumers do not stick to their clearing given schedules during real-time power scheduling process, borne by the users. This thesis mainly evaluates the power system operation economy, therefore, the uncertainty from suppliers/consumers is ignored. Therefore, the actual upward and downward reserves are shown below:

$$P_{\mathrm{U},real,t} = \Delta P^{+}_{\mathrm{VREs},real,t} - \Delta P^{-}_{\mathrm{LD},real,t} \tag{4.12}$$

$$P_{\mathrm{D},real,t} = \Delta P^{+}_{\mathrm{LD},real,t} - \Delta P^{-}_{\mathrm{VREs},real,t} \tag{4.13}$$

where $\Delta P^{+}_{\mathrm{VREs},real,t}$ and $\Delta P^{-}_{\mathrm{VREs},real,t}$ represents VREs ex-post actual power larger than the day-ahead part and smaller than the day-ahead part, respectively; $\Delta P^{+}_{\mathrm{LD},real,t}$ and $\Delta P^{-}_{\mathrm{LD},real,t}$ represents load demand ex-post actual power larger than the day-ahead part and smaller than the day-ahead part, respectively.

By comparing the actual reserve and planned reserve, the ex-post power deviation quantities are shown in the following equations.

$$\Delta P_{\mathrm{U},s,t} = \left| P_{\mathrm{U},real,t} - P_{\mathrm{U},s,t} \right| \tag{4.14}$$

$$\Delta P_{\mathrm{D},s,t} = \left| P_{\mathrm{D},real,t} - P_{\mathrm{D},s,t} \right| \tag{4.15}$$

To simplify the analysis process, this thesis chooses the system buy price (SBP) at real-time scheduling process to achieve power deviation settlement analysis [121]. The ex-post power deviation settlement is shown below:

$$C_P = \frac{1}{N_S} \sum_{s \in N_S} \sum_{t=1}^{T} \left(\lambda^{D}_{B,s,t} \Delta P_{\mathrm{D},s,t} + \lambda^{U}_{B,s,t} \Delta P_{\mathrm{U},s,t} \right) \tag{4.16}$$

where C_P represents the ex-post power deviation settlement cost; $\Delta P_{\mathrm{D},s,t}$ and $\Delta P_{\mathrm{U},s,t}$ represent the downward and upward regulation deviation at the t-th time slot in the s-the scene.

4.4. Results

4.4.1 Impact Analysis of Increasing Time Granularity on Power Step Change And Real-Time Power Deviation Amplitude

For the power step change at the interval point, we obtain the power step change distribution characteristics at different time granularities in different countries, as shown in Figure 4-3. Overall, as time granularity increases, the power step change value will be smaller and concentrate around 0. For example, the standard deviation of the California ISO power step change value at the 30-minute granularity is nearly 5.9 times at the 5-minute granularity; the standard deviation of the Czech grid power step change value at the 30-minute granularity is almost 4.2 times at the 5-minute granularity; Next, we observe the shape of the probability density function (pdf) of the power step change at different time granularities. We can find that when there is a large power step change in different countries, the probability is generally relatively small, that is, an extreme event [113]. In a word, the larger the time granularity is, the smaller the probability of occurrence of extreme power step change events. That is, increasing time granularity can significantly reduce the occurrence of extreme events, such as higher power step changes, and improve the power system stability.

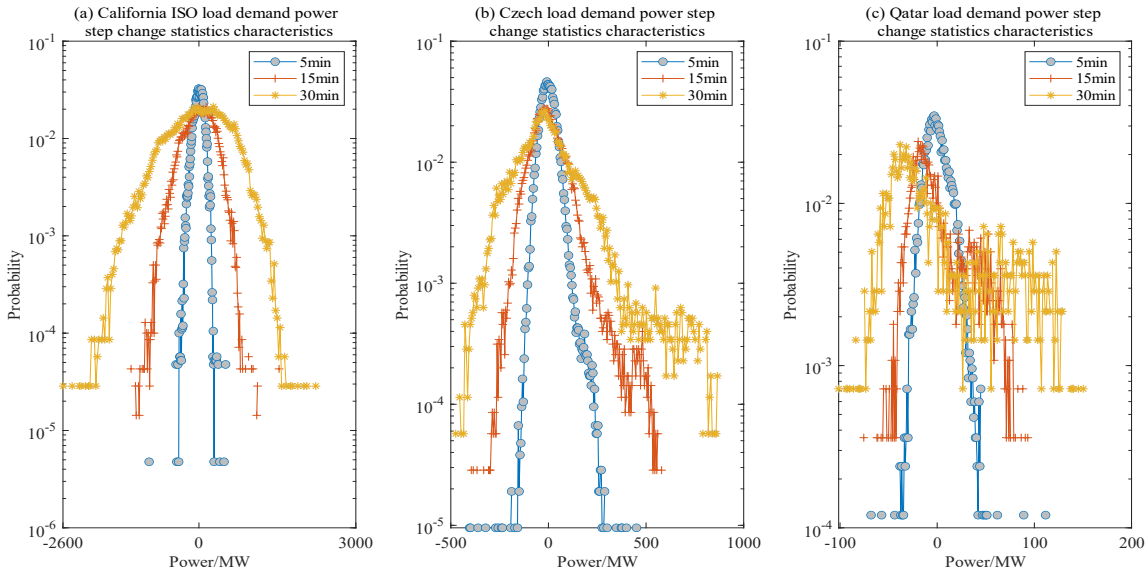

Figure 4-3. The probability density function of the load demand power step changes at different time granularities.

For the real-time power deviation during the interval, we obtain the power deviation distribution characteristics at different time granularities in different countries, as shown in Figure 4-4. As the time granularity increases, the load demand power step change (LDPS) at the interval points and the real-time power deviation (RTPD) during the interval will decrease significantly, as shown in Figure 4-4 (a-1), (a-2), and (a-3) or (b-1), (b-2), and (b-3) or (c-1), (c-2), and (c-3). At the same time granularity, the power step change will generally be larger than the real-time power deviation during the interval. Although the real-time power deviation will occasionally be no less than the power step change, the probability is extremely low, or even lower than 10^{-5}, which means in extreme events that scene will happen. The phenomenon that the power step change is larger than the real-time power deviation means that frequency jumps generally occur at interval points, as shown in **Error! Reference source not found.**. Therefore, increasing the scheduling time granularity will, on the one hand, reduce the power step change at interval points, reduce the frequency jump

degree, and on the other hand, reduce the real-time power deviation during the interval, reduce the frequency change degree, that is, improving the power grid frequency stability.

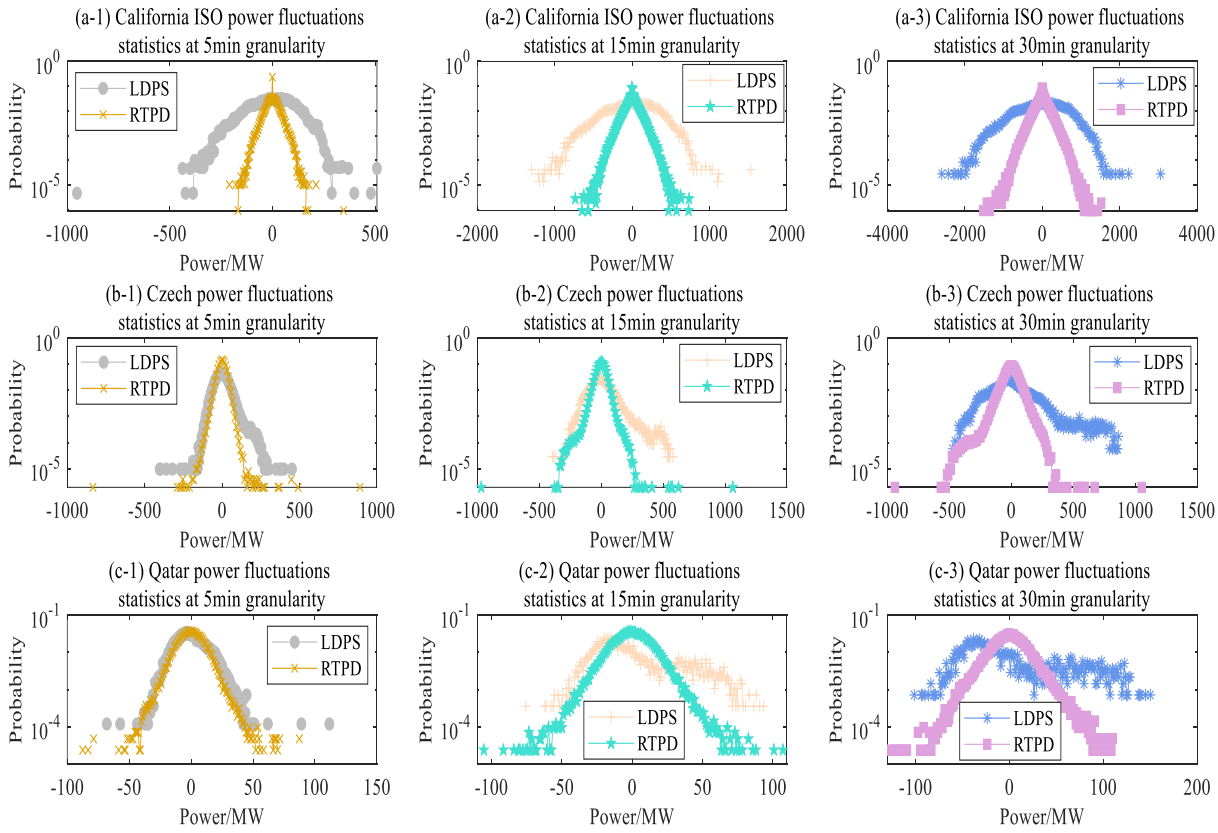

Figure 4-4. Statistical characteristics of load demand power step change at interval point and real-time power deviation during the interval width at different time granularities.

4.4.2 Impact Analysis of Increasing Time Granularity on Power Market Balancing Costs

Increasing time granularity by reducing the scheduling interval width (pricing shorter market time units) allows system operators to more quickly solve the power imbalance problem caused by the difference between day-ahead dispatch and real-time dispatch process, which can effectively address the volatility, uncertainty, and intermittency challenges. The main reason is that increasing time granularities can reduce the real-time

power deviation, as shown in Figure 4-5. Observing the time series of RTPD in different countries in Figure 4-5, we can find that the larger the time granularity, from 30-minute granularity to 5-minute granularity, the more concentrated the RTPD, which value is near 0, in other words, increasing the time granularity, the RTPD will significantly decrease; For example, the standard deviation of RTPD in the California ISO grid at the 30-minute granularity is nearly 6.2 times at the 5-minute granularity; the standard deviation of RTPD in the Czech grid at the 30-minute granularity is almost 2.3 times at the 5-minute granularity; the standard deviation of RTPD in the Qatar grid, at the 30-minute granularity is nearly 2 times at the 5-minute granularity; Reducing the RTPD value will bring new opportunities to the electricity balance market, as the power balancing market objective is to solve the power deviation problems by dispatching the dispatchable resources. Therefore, the electricity market balance cost is proportional to the RTPD quantities. We can find that the time granularity from 30 minutes to 5 minutes would reduce the balancing cost by nearly five-sixth in the California ISO grid; the time granularity from 30 minutes to 5 minutes would reduce the balancing cost by more than half in the Czech and Qatar grid.

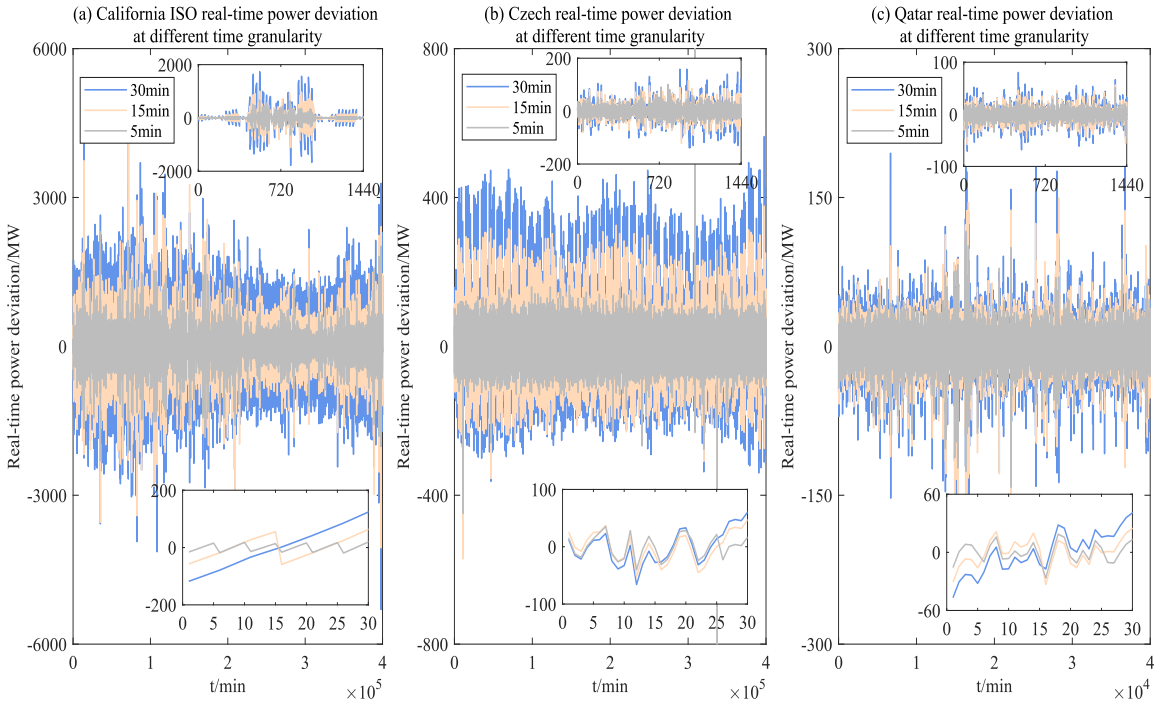

Figure 4-5. Increasing time granularity reduces the real-time power deviation (RTPD).

Next, by zooming in on the local curve in Figure 4-5, we notice that RTPD has time series characteristics during the daily curve. In the California ISO grid, (a) During the early morning and night periods, the RTPD is relatively small; (b) During the period close to noon, the RTPD is also small; (c) From early morning to noon, whether RTPD is positive or negative, the value of RTPD first increases and then decreases; (d) From noon to the afternoon, whether it is positive or negative, the RTPD first increases and then decreases. In the Czech and Qatar grid, the moment corresponding to the lowest point of the RTPD corresponds to the peak/valley load period (in the Czech grid, it is 3:00-5:00 am and 4:30-6:30 pm; and in the Qatar grid, it is 4:30-6:00 am and 12:00-15:00). The main reason for the above timing characteristics in the RTPD daily curve is that its value is mainly affected by the power gradient. The greater the power gradient, the higher the RTPD, and vice versa. In

the California ISO grid, variability resources mainly include load demand, photovoltaic (capacity is as high as about 42% of the peak load), and wind power (capacity is about 18% of the peak load), therefore, the RTPD value is mainly affected by photovoltaic power and load demand, which looks like a butterfly curve. In the Qatar grid, the current proportion of photovoltaic installed capacity is not high (nearly 14% of the peak load). Still, it is foreseeable that as photovoltaic installed capacity increases, Its RTPD characteristics will show butterfly curve characteristics like the California ISO grid. This daily curve time series characteristic of real-time power deviation will play an important role in achieving a reasonable flexibility resources reserve and predicting flexibility power demand during power system scheduling and operation.

We further zoom in to observe the RTPD during the interval at different time granularity in Figure 4-5, we can find that the RTPD is positive or negative alternatively, and as time granularity increases, the alternative frequency is quicker. Based on equation (4.16), RTPD amplitude will cause power grid frequency fluctuations. But when RTPD is a positive or negative alternative occurs, the frequency change direction will change frequently, that is, it will reduce power grid frequency fluctuation amplitude, In other words, that improves the power grid frequency stability. Therefore, increasing time granularity reduces the RTPD amplitude and increases the RTPD direction change frequency, improving power grid frequency stability.

(1) Ex-ante real-time power deviation prediction

In the ex-ante real-time power deviation prediction process, we construct a training

dataset of RTPD based on our datasets. Then we use the Markov Chain Mixture distribution (MCM) model to predict real-time power deviation time series. For details on the processing of the training dataset and the MCM prediction method, see the Methods section. The predicted results are displayed in Figure 4-6.

The RTPD predicted daily curve is consistent with the test daily curve in terms of timing characteristics, that is: In the California ISO grid, (a) During the early morning and night periods, the RTPD is relatively small; (b) During the period close to noon, the RTPD is also small; (c) From early morning to noon, whether RTPD is positive or negative, the value of RTPD first increases and then decreases; (d) From noon to the afternoon, whether it is positive or negative, the RTPD first increases and then decreases, RTPD looks like the butterfly curve. In the Czech and Qatar grids, the moment corresponding to the lowest point of the RTPD corresponds to the peak/valley load period (in the Czech grid, it is 3:00-5:00 am and 4:30-6:30 pm; and in the Qatar grid, it is 4:30-6:00 am and 12:00-3:00 pm). In particular, the Qatar and Czech grid are also affected by the photovoltaic power gradient (PV capacity in Qatar and Czech are nearly 14% of peak load power). At nearly 12:00 am (that is the PV power is highest), the RTPD value will be relatively lower than before and after the time point. The above timing characteristics can also be obtained from Figure 4-5. The timing characteristics of the power gradient affecting the RTPD quantities can further improve the prediction accuracy.

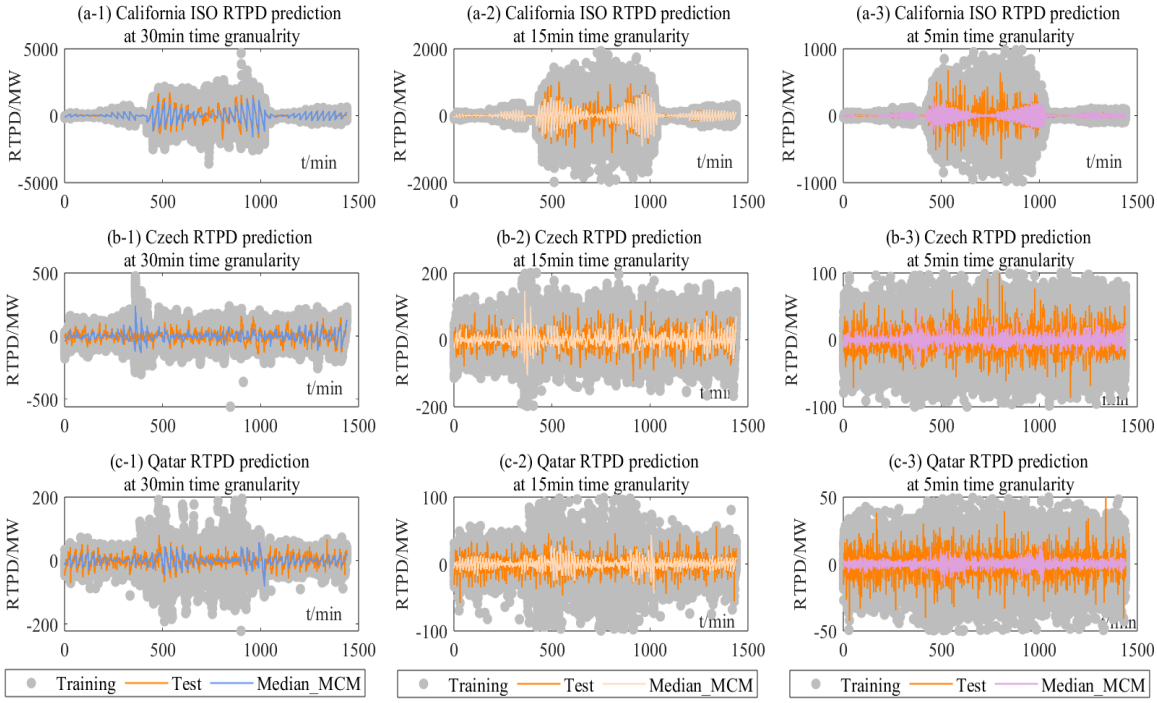

Figure 4-6. The real-time power deviation (RTPD) prediction at different time granularities.

Comparing the mean square error (MSE) between the prediction daily curve and the test daily curve at different time granularities, we find that, in the California ISO grid, the value of the MSE at the 30-minute granularity is more than six times and twice that at 5-minute granularity, and 15-minute granularity, respectively; in the Czech grid, the value of the MSE at the 30-minute granularity is nearly five times and twice that at the 5-minute granularity and 15-minute granularity, respectively; in the Qatar grid, the value of the MSE at the 30-minute granularity is nearly 1.6 times and 1.2 times that at the 5-minute granularity and 15-minute granularity, respectively. Increasing the time granularity will reduce the prediction error of RTPD in different countries. The main reason is that increasing the time granularity will, on the one hand, reduce the amplitude of the RTPD, thereby reducing the prediction amplitude; on the other hand, it can more accurately obtain the power deviation at the nearest

point, thereby improving the prediction accuracy.

(2) Real-time power scheduling and clearing process

During this process, power system operators will complete real-time scheduling control and clearing processes based on the predicted RTPD and combine them with flexible resource information in the electricity balance market. These flexibility resources can provide quick responses to ensure the power balance in the real-time market, these flexibility resources usually include chemical energy storage, quick load demand response, etc. This chapter assumes the different types of flexibility resources that participate in this process are shown in Table 4-1.

Table 4-1. Different types of flexibility resources provide balanced service information.

Type	Power/MW		Price/($/MWh)	
	Upward	Downward	Upward	Downward
Type A	50	60	200	250
Type B	100	120	300	320
Type C	100	100	320	360
Type D	120	150	350	400
Type E	4000	4500	400	500

Considering the flexible resource participation levels different in the electricity balance market, this thesis selects different cases to further discuss the impact of the abundance of flexible resource products on power system operation costs. 1) Case A represents that flexible resource products are barely abundant, just including Type A and Type E; 2) Case B represents that flexible resource includes Type A, Type B, and Type E; 3) Case C represents that flexibility resource includes all the types in Table 4-1.

Table 4-2. Real-time power scheduling costs in different cases and different time granularities ($).

Case	Countries	Time granularity		
		30min	15min	5min
Case A	California ISO	2.17E+06	1.03E+06	2.78E+05
	Czech	1.71E+05	7.94E+04	3.42E+04
	Qatar	5.68E+04	2.91E+04	1.30E+04
Case B	California ISO	2.07E+06	9.26E+05	2.26E+05
	Czech	1.47E+05	7.56E+04	3.42E+04
	Qatar	5.55E+04	2.91E+04	1.30E+04
Case C	California ISO	1.93E+06	8.43E+05	2.16E+05
	Czech	1.46E+05	7.56E+04	3.42E+04
	Qatar	5.55E+04	2.91E+04	1.30E+04

As the time granularity increases, the real-time power scheduling cost is significantly reduced, and as the richness of flexible resource products increases, the reduction effect becomes more significant. The results are shown in Table 4-2. For example, in Case A, the operation cost of the California ISO grid at the 5-minute granularity is approximately 13% of that at the 30-minute granularity; the operation costs of the Czech and Qatar grids at the 5-minute granularity are also approximately 20% of the 30-minute granularity, respectively; By comparing Case A, Case B, and Case C, we found that by increasing the richness of flexible resource products in the California ISO grid, the operation costs at the 30-minute granularity were reduced by approximately 4% and 11% respectively; the operation costs at the 5-minute granularity were reduced by approximately 19% and 23%; the main reason is that increasing time granularity reduces the RTPD on the one hand while increasing flexible resource richness significantly reduces the electricity marginal price, thereby reducing operation costs. However, in the Czech grid and Qatar grid, changes in flexible resource

abundance in this chapter have little impact on operation costs. The main reason is that the RTPD is relatively small in these two grids and the corresponding flexible resource products are relatively single. Therefore, when designing flexible resource products in the electricity market, it is necessary to design products based on the actual market needs in different countries.

Increasing time granularity reduces the amount of RTPD, thereby reducing real-time power operation costs and improving the economics of power grid operation; in addition, it also provides some new opportunities for the design of flexible resource markets that are more abundant, economical, and lightweight flexible products will play a greater role in the operation of power systems with high time granularity and bring greater economic benefits.

(3) Ex-post power deviation settlement

In general, uncertainties are inevitable in large electricity systems. Therefore, power system operators need to calculate the additional operation costs based on the actual data collected in the Supervisory Control and Data Acquisition (SCADA) systems afterward. The additional operation costs mainly include two parts: (1) power system reserve operation costs due to prediction errors, borne by the power system operator; (2) suppliers/consumers do not stick to their clearing given schedules during real-time power scheduling process, borne by themself. This thesis mainly evaluates the power system operation economy; therefore, the uncertainty of suppliers/consumers is ignored.

Table 4-3. Additional power system operation costs due to power deviation at different cases and different time granularities on test day ($).

Case	Countries	Time granularity		
		30min	15min	5min
Case A	California ISO	1.31E+06	7.50E+05	3.07E+05
	Czech	2.09E+05	1.30E+05	7.96E+04
	Qatar	5.40E+04	4.79E+04	4.16E+04
Case B	California ISO	1.22E+06	6.50E+05	2.51E+05
	Czech	1.93E+05	1.26E+05	7.96E+04
	Qatar	5.37E+04	4.79E+04	4.16E+04
Case C	California ISO	1.12E+06	6.00E+05	2.48E+05
	Czech	1.92E+05	1.26E+05	7.96E+04
	Qatar	5.37E+04	4.79E+04	4.16E+04

As the time granularity increases, the ex-post power deviation settlement cost from the power system operator is significantly reduced. As the richness of flexible resource products increases, the reduction effect becomes more significant. The results are shown in Table 4-3. For example, under Case A, the power deviation settlement cost of the California ISO grid at the 5-minute granularity is approximately 23% of that at the 30-minute granularity; By comparing Case A, Case B, and Case C, we found that by increasing the richness of flexible resource products in the California ISO grid, the ex-post power deviation settlement costs at the 30-minute granularity were reduced by approximately 7% and 14% respectively; the operation costs at the 5-minute granularity were reduced by approximately 18% and 20%; The ex-post power deviation settlement cost is mainly affected by two factors: 1) the power deviation caused by the prediction error; as the time granularity increases, more information near the prediction time point will be obtained in a more timely and effective manner. It is helpful to improve the prediction accuracy, as the results are displayed in Figure 4-6, 2) Ex-

post power deviation settlement electricity price; as the abundance of flexible resources products increases, the marginal settlement electricity price will be reduced.

In the whole electricity balance market operation process, increasing time granularity will improve RTPD prediction accuracy, reduce real-time power scheduling operation costs, reduce ex-post power deviation settlement costs, and significantly improve the power system operation economy. For example, the electricity balance market operation total cost of the California ISO grid at the 5-minute granularity is approximately 15% of that at the 30-minute granularity; the Czech and Qatar grid will also be reduced by nearly 70% and 50%, respectively. This improvement in the power system economy is not only reflected in the reduction of real-time power deviation quantities but also has an important impact on the flexible resource products market, giving more chances to the more abundant, economical, and lightweight flexible products, further reducing the settlement marginal electricity price. Therefore, increasing time granularity will have a profound impact on the operation economy of the power system

4.5. Summary

Through statistical analysis of high temporal resolution power data from three countries around the world, we found that with the time granularity increases, power step changes at different scheduled interval points and real-time power deviations during the scheduling interval will be significantly reduced, thereby reducing power market balancing costs and power grid frequency deviations. Specifically, when the time granularity is increased from

30 minutes to 5 minutes, the power step magnitude will be reduced (the power step change in the California ISO grid will be reduced by nearly five-sixths; the Czech and Qatar grid will also be reduced by almost 80%), and the RTPD will also be reduced (The RTPD in California ISO grid was reduced by nearly five-sixths; the Czech and Qatar grid also reduced by nearly half). Power grid frequency deviations are directly proportional to power change quantities; therefore, power grid frequency stability can be improved by increasing time granularity.

What is more, increasing time granularity will not only reduce the amount of real-time power deviations but also improve real-time power deviation prediction accuracy (shorter time will provide more accurate forecast information); reduce real-time power scheduling operation costs and reduce ex-post power deviation settlement cost, giving more chances to the more abundant, economical, and lightweight flexible products, reducing the settlement marginal electricity price and significantly improve the economics of power market operations with integration of massive renewable energy sources.

5. IMPACT ANALYSIS OF INCREASING SPACE GRANULARITY ON HIGH PENETRATION RENEWABLE ENERGY

Abstract: As variable renewable energy (VRE) penetration continues to increase, electricity transmission networks between regions with high penetration renewable energy generators and large load demand centers will become more congested. One of the possible methods to solve the above problem is to increase the space granularity, which includes the space granularity of renewable generation units and the space granularity of the subnetworks. This chapter mainly focuses on the evaluation of the impact of growing space granularity based on the above two levels. To reasonably construct subnetworks and increase the space granularity, this chapter proposes the stochastic energy network theory to characterize the supply-demand adaptation balance index (SDABI) and further proposes a subnetwork networking method to evaluate the impact of increasing space granularity on reducing power system operation costs, power flow losses, and power congestion. Finally, the IEEE 33-node system as a benchmark and combined with the power system operation evaluation indicators to evaluate the impact of increasing space granularity on power system operation cost, power flow losses, and power congestion to verify the effectiveness of the method.

Abbreviations	
VRE	Variable renewable energy
DERs	Distributed energy resources
ESS	Energy storage system
SDABI	Supply-demand adaptation balance index
SOC	State-of-charge
Nomenclature	
Sets and Indices	
$\boldsymbol{K}$	Sets of subnetworks
k	Index node in subnetworks
$\boldsymbol{I}$	Sets of wind turbines
$\boldsymbol{T}$	Schedule periods
t	Dispatching time interval
Variables	
$PS(s,t)$	The cumulative energy production during a period $[s,t]$
$LD(s,t)$	The cumulative energy consumption during a period $[s,t]$
$\varsigma^u(t)$/ $\varsigma^l(t)$	The upper/lower supply curve function
$\lambda^u(t)/\lambda^l(t)$	The upper/lower demand curve function
$\varepsilon_s^u(x)/\varepsilon_s^l(x)/\varepsilon_d^u(x)/\varepsilon_d^l(x)$	The bounding functions
$[x]^+$	Choose the maximum value between 0 and x
η_c	Energy storage battery charging efficiency
η_d	Energy storage battery discharging efficiency
$B_{\mathrm{ESS},i}$/ $P_{\mathrm{ESS},i}$	Rated energy/power capacity of the ESS in i-th wind turbine
$SOC_{\mathrm{ESS},i,t}$	ESS SOC at time t in i-th wind turbine
$SOC_{\mathrm{ESS},i,\min}$/ $SOC_{\mathrm{ESS},i,\max}$	Minimum/ maximum SOC of ESS in i-th wind turbine
$LoLD(s,t)$	Loss of load demand
$WoPS(s,t)$	Waste of power supply
SDABI(s,t)	Supply-demand adaptation balance index during (s,t)
F_1	Subnetworks' total operation cost
F_2	Backbone network operation cost
$V_{i,t,\min}$/ $V_{i,t,\max}$	Minimum/maximum voltage amplitude of node i at time t

N	Number of nodes in network topology
$N_{/K}$	Number of nodes in the backbone network
B	Number of branches in network topology
A	Network topology node adjacency matrix
$P_{ig,t}$	Active power generated from *i*-th wind turbine at time *t*
$P_{EM,t}$	Active power from the energy market at time *t*
$Q_{ij,t}$	Reactive power flow between node *i* and node *j* at time *t*
$P_{ij,t}$	Active power flow between node *i* and node *j* at time *t*
$c_{i,t}$	Cost of per kWh of *i*-th wind turbine at the *t*-th time spot
$c_{EM,t}$	Cost of per kWh of electricity market at the *t*-th time spot
ALP	The absolute sum of all line power

5.1. Introduction

To solve the problem of climate change, variable renewable energy (VRE) will account for an important proportion of primary energy in the future [3-5]. As VRE penetration continues to increase, Transmission networks between regions with high-penetration renewable energy generators and large load demand centers will become more congested [82]. Increasing the space granularity can effectively mitigate the congestion problems.

The congestion problems brought by the increase in the penetration of VRE are mainly due to two reasons. On the one hand, the centralized development and centralized access of VRE causes congestion of some adjacent power lines; on the other hand, it is caused by the space mismatch of supply and demand, causing congestion by repeated power flow. Increasing the space granularity is the main method to mitigate the above congestion problem. This space granularity mainly reflects on two aspects: one is increasing renewable generation units' space granularity, that is to reduce the amount of renewable energy injected

into a single node or increase the number of inject nodes for renewable generation units; another one is increasing transmission network space granularity, that is to reduce the complexity of the transmission network or reduce the repeated power flow transmission.

To solve the large number of renewable generation units resulting in congestion, the main idea is to adopt the distributed injection model, which increases the number of inject system nodes for renewable generation units. Increasing renewable generation units' space granularity can help system operators find the renewable generators' marginal electricity price, which will reduce the customers' energy costs [82]. In addition, increasing the renewable energy generation space granularity is also a key market design innovation in the electricity market, including node pricing widely used in the US market [83-85] and regional pricing widely used in the pan-European region [86-87]. By increasing space granularity and reducing the amount of renewable energy injected into a single node, this electricity market changes, on the one hand, improve the power congestion problem of adjacent lines connected to VRE injected nodes, on the other hand, increasing renewable generation units space granularity can better discover the marginal electricity price of the units, thereby reducing energy costs.

To increase transmission network space granularity, an innovative idea is to construct many space subnetworks. How to divide that transmission network topology into several subnetworks and then reduce the power transmission amount, repeated power flow and electricity power transfer distance is a vital problem. The subnetwork works in one of the following three working states during a period:

(1) Waste of power supply, in this state means that the power supply is more than the load demand during a period, and then the excess energy will be stored in the energy storage system until it reaches its rated capacity, resulting in excess energy [89-91].

(2) Loss of load demand, in this state means that the power supply plus energy stored in ESS is less than the load demand during a period, resulting in an energy shortage [92-93].

(3) Supply-demand adaptation balance, in this state means that the energy supply with the ESS can meet the energy demand during a period. To solve the above problems, the cumulative energy production of VREs needs to meet the cumulative energy consumption of all load nodes in the subnetwork, increasing the probability of a supply-demand adaptation balance state [91], [94-95].

Therefore, we define the supply-demand adaptation balance index (SDABI) to characterize energy balancing ability, in this chapter, we use the arrival process and departure process in the stochastic network theory to correspond to the energy production and energy consumption processes and then characterize the SDABI. Furthermore, based on the SDABI and power system operation information, we further proposed a subnetwork networking method, which can independently conduct spatial subnetworks based on the power supply and load demand information, combined with grid operation information and network topology, to achieve economic dispatch within the subnetwork and energy exchange between different subnetworks. The constructed subnetworks based on our model can improve the economy of the entire power grid operation, reduce power flow congestion,

etc.

Increasing space granularity in the power system, on the one hand, will change the distribution of renewable generation units, on the other hand, it will also change the network topology by using the space networking method. To evaluate the benefits of increasing space granularity reform, we choose three aspects:

(1) Power system operation economy.

(2) Power flow loss.

(3) Power transmission congestion evaluation.

This chapter constructs a spatial subnetwork networking method by establishing the SDABI model to improve the spatial granularity of the power grid. Then, we aim to provide evidence for reforming the power system spatial resolution by evaluating the beneficial impact of this method on operating indicators of the power system.

5.2. Data Setting and Description

The wind power and load demand datasets are shown in Figure 5-1 and Figure 5-2 below. The wind power includes 20 wind turbine units, and the load demand is distributed in the IEEE 33-node system. These datasets include a whole year of historical data, and the sampling rate is one hour. We use these datasets to analyze the SDABI and divide several subnetworks based on Algorithm 5-1, and then calculate the system operation evaluation indicators in the methods part to evaluate the impact of increasing space granularity.

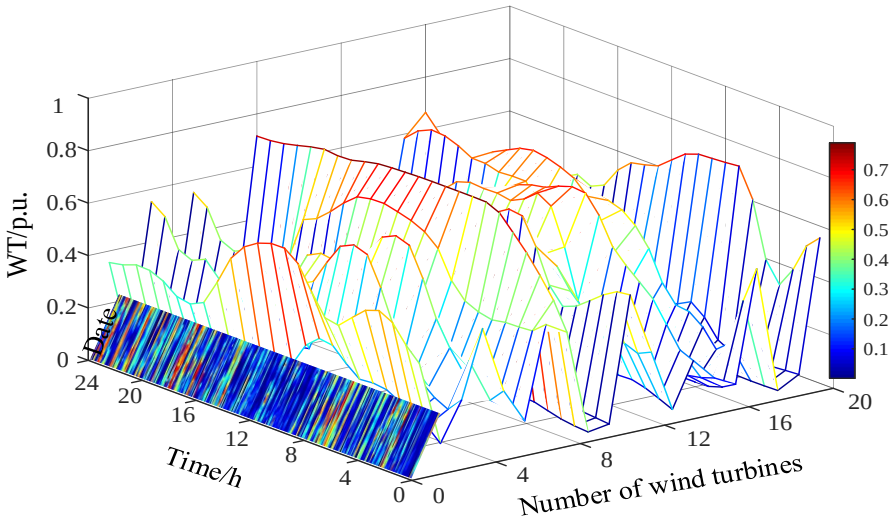

Figure 5-1. Per unit curve wind turbine power.

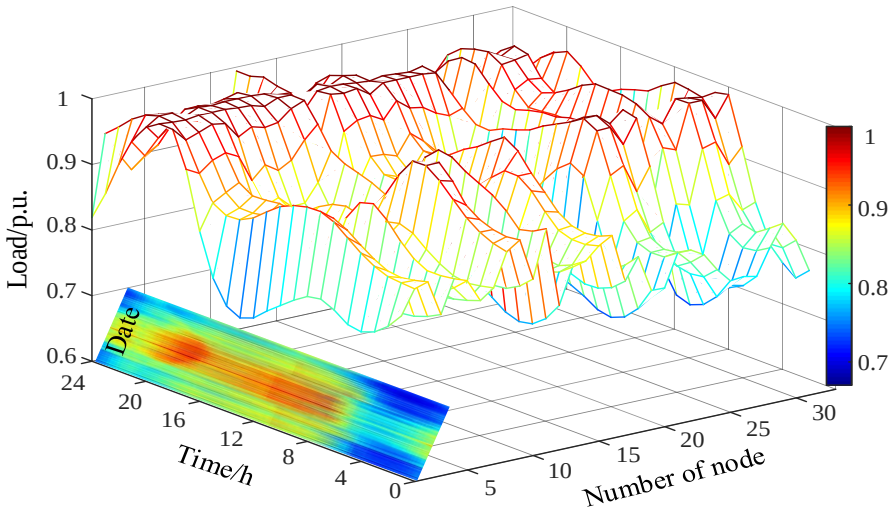

Figure 5-2. Per unit curve loads in different nodes.

Table 5-1 summarizes the number of units, marginal power generation price, rated power capacity, and equipped ESS information of different wind turbines. The initial SOC of ESS is 50%.

Table 5-1. Wind turbines information

Type	Number of wind turbines	Wind turbine LMP/($/kWh)	P/kW	ESS/(kW/kWh)
Type 1	{1-4}	0.080	100	100/200
Type 2	{5-7}	0.065	150	150/300
Type 3	{8-12}	0.045	200	200/400
Type 4	{13-20}	0.035	250	250/500

Table 5-2 summarizes the different cases to characterize the space granularity of 20 wind turbines. It has 6 cases including their having no renewable generation units and having 20 wind turbines injected into the different nodes. The wind turbines in different cases, from centralized access to a single node to separate access to multiple different nodes are in different cases. Different cases represent different space granularities of 20 wind turbines.

Table 5-2. Case description of different space granularity of 20 wind turbines

Case	Number of wind turbines	Input node number
case 0	-	-
case 1	{1-20}	{18}
case 2	{1-4};{5-10};{11-20}	{20};{6};{18}
case 3	{1-4};{5-10};{11-16};{17-20}	{20};{6};{18};{25}
case 4	{1-4};{5-7};{8-12};{13-16};{17-20}	{20};{6};{18};{25};{28}
case 5	{1-4};{5-7};{8-9};{10-12};{13-16};{17-20}	{20};{6};{18};{25};{28};{12}

5.3. Methods

5.3.1 Supply-Demand Adaptation Degree Index

To ensure that the subnetworks have the best supply-demand adaptability and reduce power exchange with the backbone network. We establish the supply-demand adaptation balance index (SDABI) to characterize the cumulative energy production of renewable energy generations to meet the cumulative energy consumption of all load nodes in the subnetwork, and the subnetwork will contain renewable generations, energy storage, load demand, etc. The subnetwork supply and demand states are shown in Figure 5-3 below.

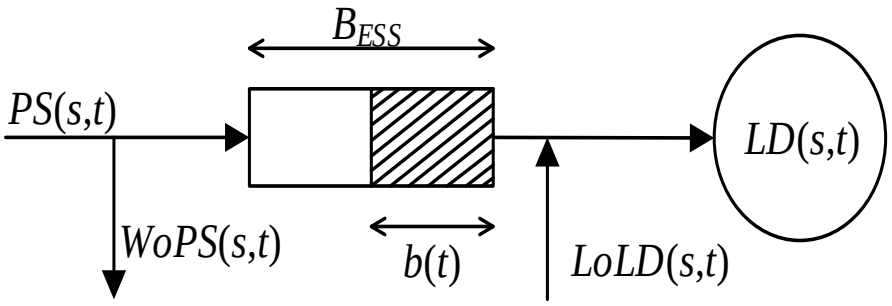

Figure 5-3. Schematic diagram of energy status in subnetwork.

From Figure 5-3, there are three different energy statuses in the subnetwork, including *WoPS*, *LoLD*, and power supply and load demand energy balance. $PS(s,t)$ and $LD(s,t)$ represent the value of energy production and energy consumption during the period $[s,t]$; $b(t)$ represents the energy stored in ESS at time t; B_{ESS} represents the energy rated capacity of ESS; $WoPS(s,t)$ represents the waste of power supply during $[s,t]$, and $LoLD(s,t)$ represents loss of load demand during $[s,t]$.

(1) Energy supply and energy demand.

In this section, we assume that in the subnetwork, the energy production looks like the arrival process, and the energy consumption process looks like the departure process, based on the stochastics network theory, respectively. Therefore, we can characterize the energy production and consumption process shown in equations (5.1)-(5.4), respectively.

$$Pr\left\{\sup_{0\le s\le t}[PS(s,t)-\xi^{u}(t-s)]>\pi\right\}\le\varepsilon_{s}^{u}(\pi) \tag{5.1}$$

$$Pr\left\{\sup_{0\le s\le t}[\xi^{l}(t-s)-PS(s,t)]>\pi\right\}\le\varepsilon_{s}^{l}(\pi) \tag{5.2}$$

$$Pr\left\{\sup_{0\le s\le t}[LD(s,t)-\lambda^{u}(t-s)]>\pi\right\}\le\varepsilon_{d}^{u}(\pi) \tag{5.3}$$

$$Pr\left\{\sup_{0\le s\le t}[\lambda^{l}(t-s)-LD(s,t)]>\pi\right\}\le\varepsilon_{d}^{l}(\pi) \tag{5.4}$$

where the energy production process function shown above (5-1) and (5-2), which can be characterized by parameter set $\{PS, \zeta^{u}, \zeta^{l}, \varepsilon_{s}^{u}, \varepsilon_{s}^{l}\}$; the energy production function $PS(s,t)$ can be obtained by accumulated power generation energy from renewable generations during $[s,t]$, the upper and lower curve functions $\zeta^{u}(t)$ and $\zeta^{l}(t)$ of the energy supply can be obtained through linearization, the rate is equal to the long-term average rate over a certain period in the historical fit data. The boundary function $\varepsilon_{s}^{u}(\pi)$ and $\varepsilon_{s}^{l}(\pi)$ can be fit by exponential functions based on historical data and upper and lower curve functions [91], [95]. The energy consumption process function shown in above (5-3) and (5-4), which can be characterized by parameter set $\{LD, \lambda^{u}, \lambda^{l}, \varepsilon_{d}^{l}, \varepsilon_{d}^{l}\}$; the energy consumption function $LD(s,t)$ can be obtained by accumulated power consumption by load nodes in the whole subnetwork during $[s,t]$, the upper and lower curve functions $\lambda^{u}(t)$ and $\lambda^{l}(t)$ of the energy demand can be obtained through linearization, the rate is equal to the long-term average rate over a certain period in the historical fit data. The boundary functions $\varepsilon_{d}^{u}(\pi)$ and $\varepsilon_{d}^{l}(\pi)$ can be fit by exponential functions based on historical data, and upper and lower curve functions [91], [95]. For different subnetworks containing different renewable energy capacities/load demand capacities, the characterization methods are the same, but the value of the functions and parameters set in equation (5.1)-(5.4) may be different. We can get all the above functions and set parameters based on the historical renewable energy supply and demand information.

(2) ESS Charging/Discharging Process

From the schematic diagram of subnetwork supply and demand states shown in Figure 5-3, the ESS would work in two working states: (1) The charging state, which indicates that

the cumulative energy production is larger than the cumulative energy consumption during [s,t], and the excess part is stored in the ESS until the ESS reaches its rated capacity. (2) The discharging state, which indicates that the cumulative energy production is less than the cumulative energy consumption during [s,t], and the shortage part will be emitted by the ESS until the ESS storage reaches its minimum required capacity. Therefore, the energy stored by the ESS at time t can be expressed as follows:

$$b(t) = min\begin{bmatrix} B_{ESS}, b(t-1) \\ +\left[\left(PS(t-1,t) - LD(t-1,t)\right)\right]\eta_c \end{bmatrix} \tag{5.5}$$

$$b(t) = [b(t-1) - [LD(t-1,t) - PS(t-1,t)]\eta_d]^+ \tag{5.6}$$

(3) Supply-demand Adaptation Balance Index (SDABI)

The supply-demand adaptation balance index refers to the cumulative energy production of renewable energy generations that can meet the cumulative energy consumption of all load nodes in the subnetwork. The subnetwork including renewable generation and load nodes works in one of the following three states during a period: (1) **waste of power supply (WoPS)**, in this state means that the cumulative energy production is larger than the cumulative energy consumption during the period, and the excess energy is stored in the ESS until the ESS reaches the rated energy capacity, resulting in excess energy; (2) **loss of load demand (LoLD)**, in this state means that the cumulative energy production plus energy stored in ESS is less than the cumulative energy consumption during a period, resulting in energy shortage. (3) **supply-demand adaptation balance**, in this state means that the cumulative energy production plus the ESS can meet the cumulative energy consumption

during a period. Based on these three states, we can use *WoPS*(t), *LoLD*(t), and SDABI(t) to represent the excess energy process, shortage energy process, and balanced energy process. Based on the above analysis, we can characterize these states as below.

$$WoPS(t) = \begin{bmatrix} b(t-1) + PS(t-1,t) - \\ LD(t-1,t) - B_{ESS} \end{bmatrix}^{+} \tag{5.7}$$

$$LoLD(t) = [LD(t-1,t) - PS(t-1,t) - b(t-1)]^{+} \tag{5.8}$$

Furthermore, we can calculate these states' probability as shown below.

$$Pr\big(WoPS(t)\big) = Pr\{WoPS(t) > 0\} \le \varepsilon_s^u \otimes \varepsilon_d^l \left(B_{ESS} - \sup_{0\le s\le t} [\xi^u(s) - \lambda^l(s)]\right) \tag{5.9}$$

$$Pr\big(LoLD(t)\big) = Pr\{LoLD(t) > 0\} \le \varepsilon_d^u \otimes \varepsilon_s^l \left(B_{ESS} - \sup_{0\le s\le t} [\lambda^u(s) - \xi^l(s)]\right) \tag{5.10}$$

$$Pr\ (\text{SDABI}(T)) = \frac{1}{T}\sum_{t=1}^{T}\Big(1 - Pr\big(LoLD(t)\big) - Pr\big(WoPS(t)\big)\Big) \le$$
$$\frac{1}{T}\sum_{t=1}^{T}\begin{pmatrix} 1 - \varepsilon_d^u \otimes \varepsilon_s^l \left(B_{ESS} - \sup\limits_{0\le s\le t} [\lambda^u(s) - \xi^l(s)]\right) \\ -\varepsilon_s^u \otimes \varepsilon_d^l \left(B_{ESS} - \sup\limits_{0\le s\le t} [\xi^u(s) - \lambda^l(s)]\right) \end{pmatrix} \tag{5.11}$$

Based on equation (5.11) and relevant assumptions, when the cumulative energy consumption is much less than the cumulative energy production of renewable energy resources, as the load demand increases (that is, the number of load nodes in the sub-network increases), *Pr*(*LoLD*(*t*)) will decrease, $Pr\ (\text{SDABI}(T))$ will increase; when the cumulative energy consumption is much greater than the cumulative energy production of renewable energy resources, as the load demand decreases (that is, the number of load nodes in the sub-network decreases), *Pr*(*WoPS*(*t*)) will decrease, $Pr\ (\text{SDABI}(T))$ will increase; Therefore, when $Pr\ (\text{SDABI}(T))$ is the largest, it means that the space sub-network has the best energy

balance ability.

5.3.2 Spatial Subnetwork Networking Method

For a given network, when changing the scale of the space subnetwork (adding more load nodes or reducing load nodes), it will affect the SDABI of the subnetwork, therefore, it is of great significance to select the scale of the space subnetwork reasonably based on the network topology information. We will introduce the method and steps for forming a reasonable space subnetwork based on SDABI as shown in Algorithm 5-1.

In Algorithm 5-1, when dividing the subnetworks, we do not need the location information of the distributed energy resources (DERs), based on the power flow calculation results, we can get the DERs node information, Through the historical statistical information of different node loads and the historical statistical power supply information of renewable generation units, and then we can construct several subnetworks which have the best $Pr(\mathrm{SDABI}(T))$. These subnetworks guarantee their highest supply-demand adaptation ability, that is these subnetworks have the best energy balance ability, they will not cause more energy waste due to excessive renewable power generation, it will also not cause load loss due to energy shortage.

Algorithm 5-1: SDABI-based subnetwork networking method

Step 1) *Input distribution network topology information* Ω{N, B, A} *and distribute energy resources information* DERs.

N: Node matrix.

B: Branch matrix.

A: Node affinity matrix.

N_S: DERs node matrix.

Step 2) *Construct subnetwork node set based on* DERs *power supply nodes and power flow information:*

Use the following equation to calculate power flow based on **Ω** and DERs, to get power flow results$\{P_{ij},Q_{ij},V_i\}$ without DERs and $\{P_{ij}^*,Q_{ij}^*,V_i^*\}$ with DERs.

$$\begin{cases} P_{ij,t} = g_{ij}\left(V_{i,t}^2 - V_{i,t}V_{j,t}\cos\theta_{ij,t}\right) - b_{ij}V_{i,t}V_{j,t}\sin\theta_{ij,t} \\ Q_{ij,t} = -g_{ij}V_{i,t}V_{j,t}\sin\theta_{ij,t} - b_{ij}V_{i,t}^2 - V_{i,t}V_{j,t}cos\theta_{ij,t} \end{cases} \tag{5.12}$$

Construct possible subnetwork node subset based on the following equation and A.

$$\Delta P_{ij} = P_{ij} - P_{ij}^* \geq \alpha \tag{5.13}$$

$$\Delta V_i = V_i^* - V_i \leq \beta \tag{5.14}$$

(Each subnetwork contains only one DERs node, and the DERs node is the starting point, and the rest of the nodes are all load nodes.)

Step 3) *Modify the subnetwork networking scheme based on SDABI:*

Traverse the load nodes in any subnetwork, and select the corresponding α^u and α^l based on the load nodes set, until satisfy the following equation,

$$\max \frac{1}{T}\sum_{t=1}^{T}\begin{pmatrix} 1 - \varepsilon_d^u \otimes \varepsilon_s^l\left(B_{ESS} - \sup\limits_{0\leq s\leq t}\left[\lambda^u(s) - \xi^l(s)\right]\right) \\ -\varepsilon_s^u \otimes \varepsilon_d^l\left(B_{ESS} - \sup\limits_{0\leq s\leq t}\left[\xi^u(s) - \lambda^l(s)\right]\right) \end{pmatrix} \tag{5.15}$$

5.3.3 Evaluation Indicators of Power System Operation

We evaluate the influence of increasing space granularity from three aspects, including operation economy [124], power flow loss [125], and power flow congestion [126]. The details of the evaluation indicators are as follows.

(1) Power system operation economy evaluation

The operation is a two-stage analysis process. The first stage needs to analyze the operation of each space subnetwork, considering that the renewable generation units in different subnetworks are equipped with energy storage systems (ESS), and the ESS can store energy when the renewable generation units are higher than the load demand and emit energy when the renewable generation units are lower than the load demand, therefore, the first stage is a multi-period optimization power flow model combined with ESS. The second stage needs to combine the net load conditions of different space subnetworks (different generalized nodes) for operation analysis [127].

a) Objective: The operation process has two objectives, the first one is to minimize the operation cost of subnetworks, and the second one is to minimize the operation cost of the backbone network. which are written as

$$\boldsymbol{P1}: min \quad F_1 = \sum_{t \in T} \sum_{i \in I} \left(c_{i,t} P_{ig,t} \right) \tag{5.16}$$

$$\boldsymbol{P2}: min \quad F_2 = \sum_{t \in T} \left(c_{EM,t} P_{EM,t} \right) \tag{5.17}$$

where F_1 represents the subnetwork (includes wind turbines) power generation operation

cost, that is equal to electricity price times wind power generation amount, $c_{i,t}$ represents the per unit electricity price from the i-th wind turbine at the t-th time spot; $P_{ig,t}$ represents active power generated from i-th wind turbine at time t. F_2 represents the backbone network (includes electricity market transaction) operation cost, which is equal to the electricity price from the electricity market times power transaction amount, $c_{EM,t}$ represents the per unit electricity price from the electricity market at the t-th time spot; $P_{EM,t}$ represents transaction power from the electricity market.

b) Constraints:

Power flow constraints:

$$\begin{cases} P_{ij,t} = g_{ij}\left(V_{i,t}^2 - V_{i,t}V_{j,t}\cos\theta_{ij,t}\right) - b_{ij}V_{i,t}V_{j,t}\sin\theta_{ij,t} \\ Q_{ij,t} = -g_{ij}V_{i,t}V_{j,t}\sin\theta_{ij,t} - b_{ij}V_{i,t}^2 - V_{i,t}V_{j,t}cos\theta_{ij,t} \end{cases} \tag{5.18}$$

where $P_{ij,t}$ and $Q_{ij,t}$ represent active power and reactive power flow between node i and node j at time t; $V_{i,t}$ represents the voltage at node i at time t; $\theta_{ij,t}$ represents the phase angle difference between node i and node j at time t.

Node voltage constraints:

$$V_{i,t,min} \leq V_{i,t} \leq V_{i,t,max} \tag{5.19}$$

ESS operation constraints:

Assume that the wind turbines in our model will be equipped with ESS. ESS usually operates in three different states, including charging, discharging, or neither charging nor discharging. Therefore, the operating state of ESS can be present by equation (5.20).

$$sc_{i,t} + sd_{i,t} \leq 1, \forall i \in I, t \in T \tag{5.20}$$

where $sc_{i,t}$ and $sd_{i,t}$.represent the i-th ESS is charged or discharged at t-th time point, respectively. They are binary variables. Considering the operating state of ESS, the power output of ESS should be constrained by the following equations.

$$0 \leq P_{ESSC,i,t} \leq sc_{i,t} * P_{ESS,i} \tag{5.21}$$

$$0 \leq P_{ESSD,i,t} \leq sd_{i,t} * P_{ESS,i} \tag{5.22}$$

where $P_{ESS,i}$ represents rated power capacity of the ESS in i-th wind turbine; $P_{ESSC,i,t}$ and $P_{ESSD,i,t}$ represent charging power and discharging power of ESS at t-th time spot, respectively.

What is more, to meet the needs of ESS to continuously participate in dispatching, the state of charge of ESS needs to meet the following constraints.

$$B_{ESS,i}SOC_{i,t} = \begin{cases} B_{ESS,i}SOC_{i,(t-1)} + \Delta t P_{ESS,i,t}\eta_c, P_{ESS,i,t} \geq 0 \\ B_{ESS,i}SOC_{i,(t-1)} + \dfrac{\Delta t P_{ESS,i,t}}{\eta_d}, P_{ESS,i,t} < 0 \end{cases} \tag{5.23}$$

$$\begin{cases} SOC_{i,min} \leq SOC_{i,t} \leq SOC_{i,max} \\ SOC_{i,0} = SOC_{i,T} \end{cases} \tag{5.24}$$

where $B_{ESS,i}$ represents rated energy capacity of the ESS in i-th wind turbine; $SOC_{i,t}$ represents state of charge of ESS at t-th time, it has maximum value and minimum value; η_c and η_d represent charging and discharging efficiency of ESS.

(2) Power flow loss evaluation

Based on Algorithm 5-1, we can construct different sub-networks and different sub-networks will be seen as generalized nodes (pro-consumer) to participate in the backbone network operation after they have finished the dispatching process based on their own topology and power supply/load demand resources. Therefore, in our evaluation model, for

the whole system, the power flow loss includes two parts, one part is the power flow loss based on the sub-networks including ESS power flow calculation, and the second part is the power flow loss from the backbone network power flow calculation, in which the subnetworks will be seen as generalized nodes.

In each subnetwork, the power flow loss satisfies the following equation.

$$P_{\text{Loss},k} = \sum_{t\in T}\left(\sum_{i\in K} V_{i,t}\sum_{j\in i} V_{j,t}g_{ij}cos\theta_{ij,t}\right) \tag{5.25}$$

The power flow loss of the system mainly includes two parts, one part is the subnetworks power flow loss, and the other part is the backbone network power flow loss (subnetworks have been treated as generalized nodes), the system power flow loss satisfies the following equation.

$$P_{\text{Loss}} = \sum_{k\in K} P_{Loss,k} + \sum_{t\in T}\left(\sum_{i\in\frac{N}{K}} V_{i,t}\sum_{j\in i} V_{j,t}g_{ij}cos\theta_{ij,t}\right) \tag{5.26}$$

(3) Power transmission congestion evaluation

System congestion management strategies can be divided into two aspects: (1) network topology reconfiguration, this way through switch operation to realize network topology reconfiguration and improve network congestion; (2) power supply/load demand locally matching, this way through direct load control (DLC) and market mechanism to modify the load demand and power supply, respectively to improve power congestion [128]. In this chapter, we through increasing space granularity to reduce the power congestion, it does not need to change the switch state, that is, the system operating mode, nor does it need to change

the load demand. It is a brand-new mechanism for increasing network space granularity to achieve power flow congestion management. Increasing renewable generation units' space granularity and increasing subnetwork space granularity will both help to realize power supply/load demand locally matching.

To describe the impact of increasing space granularity on power congestion and repeated power flow, we define average line power (ALP) to calculate the absolute sum of all line power, and using this indicator can help us analyze the concentration degree of all line power near to zeros and the total power flow of the power lines. The ALP indicator can be easily calculated using the equation below.

$$ALP = \left(\sum_{b=1}^{B}\sum_{t\in T}\left|P_{b,t}\right|\right)\Big/(B*T) \tag{5.27}$$

where $P_{b,t}$ represents the power flow in the b-th line at time t; B represents the number of the branch.

5.4. Test Results

5.4.1 Evaluation of the Spatial Networking Method

Based on Algorithm 5-1 and wind turbines inject information in the IEEE 33-node system in Table 5-2, we can calculate power flow and then get the results of branch power flow deviation and voltage magnitude deviation in different nodes. Considering case 0 does not have the wind power injection, we get the results from case 1 to case 5 shown in Figure 5-4 below.

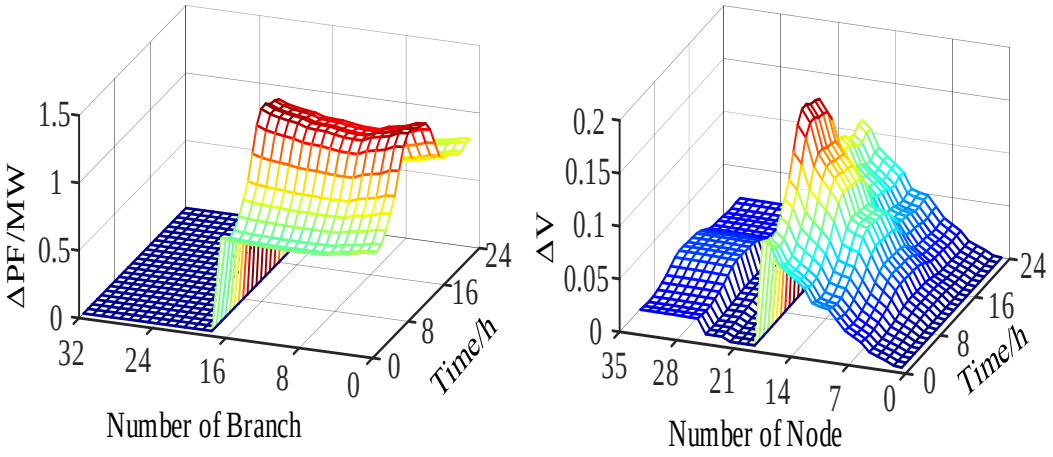

(a) case 1

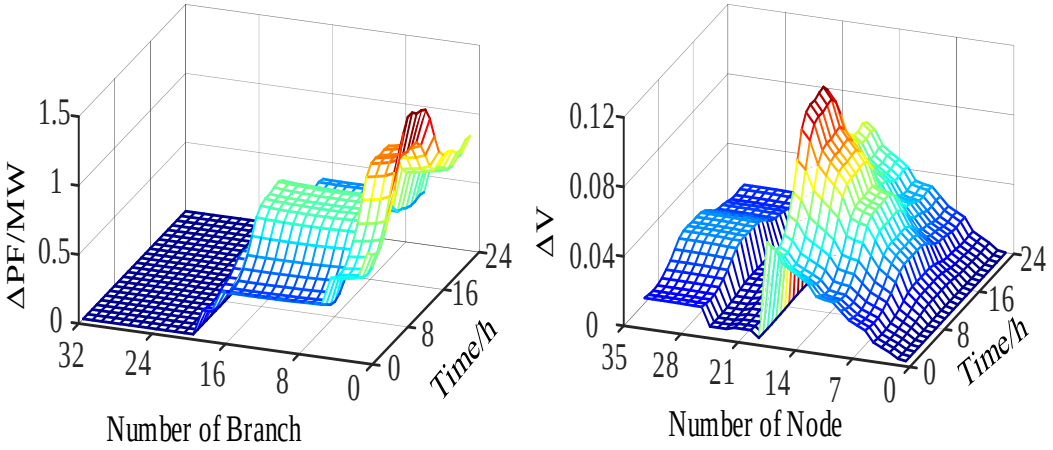

(b) case 2

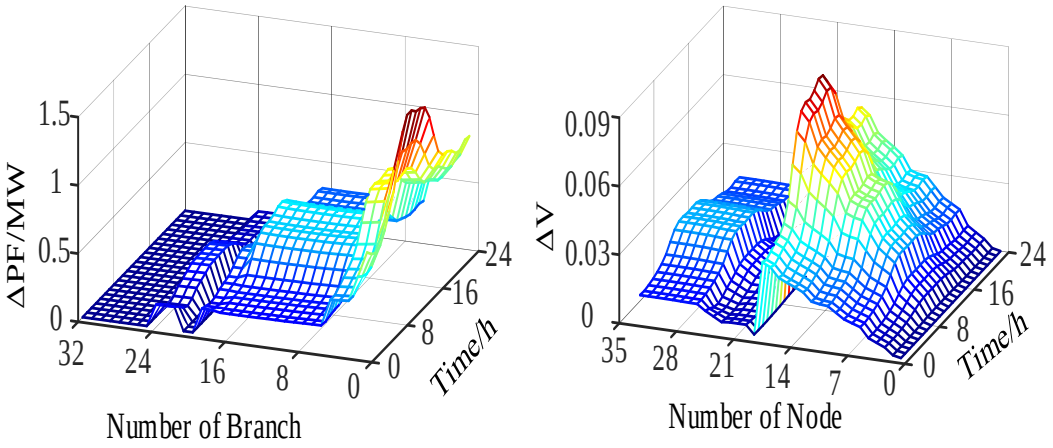

(c) case 3

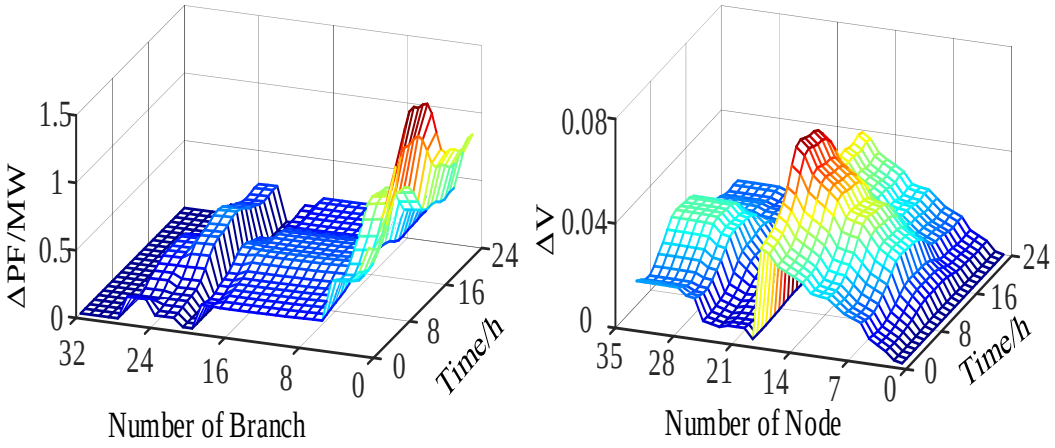

(d) case 4

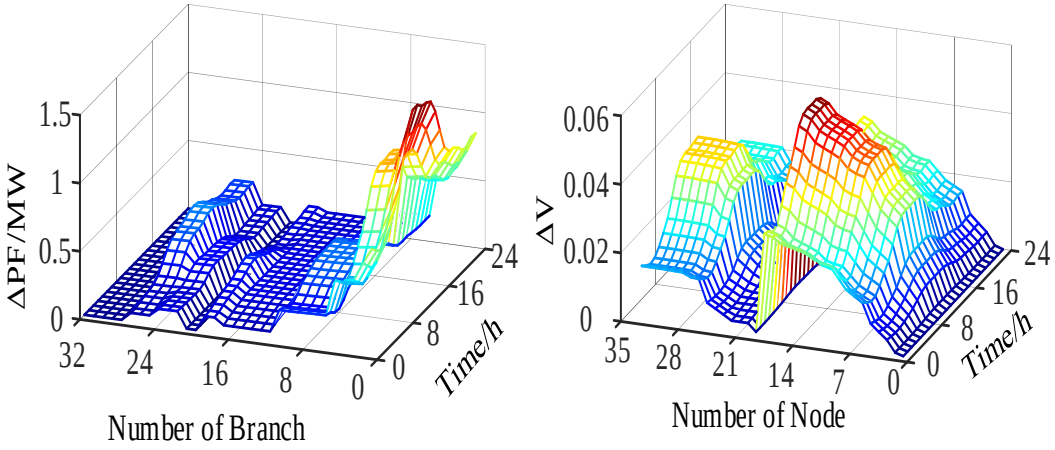

(e) case 5

Figure 5-4. Power flow and node voltage difference under different spatial distributions of wind turbines

From Figure 5-4. we can find that:

(1) In different cases, that is in different space granularity of wind turbines, there will be differences in the branch power flow and the node voltage magnitude. The main reason for the above differences is that the injection of wind turbines into different nodes will change the power flow of adjacent nodes and branches.

(2) Comparing the deviation branch power flow in case 1, case 2, case 3, case 4 and case 5, we can find that the branch power flow related to wind turbines inject node changes

significantly, and based on this feature, we can put it as the first node into subnetwork node subset. For example, in case 1, branch 17 power flow deviation has changed significantly, in case 3, branch 24, branch 19, branch 17, and branch 5 power flow deviation has changed significantly, and in case 5, branch 27, branch 24, branch 19, branch 17 and branch 5 power flow deviation have changed significantly. Therefore, based on the branch power flow deviation we can find the results where the wind turbines are injected are consistent with case setting.

(3) Comparing the deviation node voltage magnitude and adjacent node voltage amplitude in case 1, case 2, case 3, case 4 and case 5, we can find that the node voltage magnitude related to wind turbines inject node changes significantly, and based on this feature, we can put these nodes into subnetwork node subset. For example, in case 1, node-set {6-18} and {26-33} have changed significantly, in case 3, node-set {4-18} and node-set {20-33} voltage magnitude have changed significantly, in case 5, node-set {4-18} and {20-33} have changed significantly, based on the wind turbines inject nodes results and node adjacency matrix A, we can construct the possible load node-set containing a group of wind turbines as the subnetworks. In case 1, the subnetwork may contain nodes set {6-18}, in case 3, the subnetworks may contain nodes set {6, 26-33}, {7-18}, {23-25} and {20-22}, in case 5, the subnetworks may contain nodes set {6, 26-33}, {7-12}, {13-18}, {23-25} and {20-22}.

Then we set the above load node as the complete set, construct several subsets including the wind turbines inject node, traverse these subsets in turn, and select the largest $Pr(\mathrm{SDABI}(T))$ that contains the load node subset as the subnetwork. In different cases, the

subnetwork includes nodes' information as shown in Table 5-3.

Table 5-3. The subnetwork nodes result in different spatial distributions of wind turbines

Case	The subnetwork nodes	*Pr*(SDABI(*T*))
case 1	{7-18}	{0.482}
case 2	{20-21};{6,26-27};{13-18}	{0.526};{0.475};{0.438}
case 3	{20-21};{6,26-27};{14-18};{25}	{0.526};{0.475};{0.491};{0.403}
case 4	{20-21};{6};{16-18};{25};{28}	{0.526};{0.453};{0.428};{0.435};{0.486}
case 5	{20-21};{6};{18};{25};{28-29};{11-12}	{0.526};{0.453};{0.407};{0.412};{0.435};{0.486}

5.4.2Evaluation Indicators at Different Spatial Granularities

Increasing space granularity mainly has two aspects: (1) increasing wind turbines' space granularity, that is decreasing the number of wind turbines connected to the same one node; (2) increasing subnetworks' space granularity, that is increasing the number of subnetworks. Aiming at the evaluation operation indicators, we focus on the above two aspects, the results are as follows.

(1) Power system operation economy evaluation

Different cases characterize the different wind turbines' space granularity, and considering subnetworks means that we characterize the different subnetwork space granularity. Comparing Table 5-4 and Table 5-5 in different cases operation economy results, increasing space granularity can improve the power system operation economy, the details can be

described as follows:

(1) From Table 5-4, comparing the operation cost in different cases, such as F2 is lower in case 1 to case 5 than case 0. F_2 of case 5 is nearly 30% lower than case 0. That means wind power is injected into the power system; on the one hand, it will reduce the dependence on the main grid, on the other hand, it will improve the economy of power system operation. By comparing the power flow loss part in Table 5-4, the power flow loss of case 5 is about 48% of the power flow loss of case 1. That means by increasing wind turbines' space granularity, the power flow loss will also be reduced, further leading to a reduction in system operation cost.

(2) In the same cases, with the increasing subnetwork space granularity, F_2, system operation cost and power flow loss will all decrease.

Table 5-4. Without considering subnetworks in different cases

Case	F_2 ($)	(F_1+F_2) ($)	Power flow loss (MWh)
case 0	12565.2	12565.2	3.821
case 1	9112.1	10927.7	3.496
case 2	8902.8	10221.6	2.101
case 3	8879.8	10167.8	1.948
case 4	8861.3	10034.7	1.824
case 5	8836.8	10010.2	1.661

Table 5-5. With considering subnetworks in different cases

Case	F_2 ($)	(F_1+F_2) ($)	Power flow loss (MWh)
case 1	9082.9	10898.6	3.302
case 2	8886.3	10205.1	1.991
case 3	8867.7	10155.7	1.867

case 4	8854.5	10027.9	1.779
case 5	8829.4	10002.8	1.611

When the subnetwork is not considered, the system operation cost difference between different cases is mainly affected by two factors. One is the differences in local marginal electricity prices of wind turbines due to differences in space granularity. When the wind turbine's space granularity is smaller (that is, the more types of wind turbines are connected to the same node), the higher cost of wind turbine marginal electricity price will increase the DERs generation cost. The other one is the difference in power loss caused by the difference in space granularity of wind turbines, this difference is mainly reflected in the operation cost in the balanced market.

When the subnetwork is considered, the difference in operation cost in the same cases is mainly due to the difference in power loss caused by the difference in subnetwork space granularity. The main reason is that the increase in the subnetwork space granularity will reduce the transmission distance of the power flow, thereby reducing the power flow loss.

(2) Power flow loss evaluation

The injection of wind power will reduce the system power flow loss, and the system power flow loss will be significantly reduced regardless of the position of the wind turbine connected to the system and the change of the wind turbine space granularity. In Figure 5-5, we can find the injection of wind power minimizes the reduction in power flow loss and is close to 9%, what is more, with the increasing of the wind turbine space granularity, the power flow loss is further reduced, and reduction in case 5 is close to 57%.

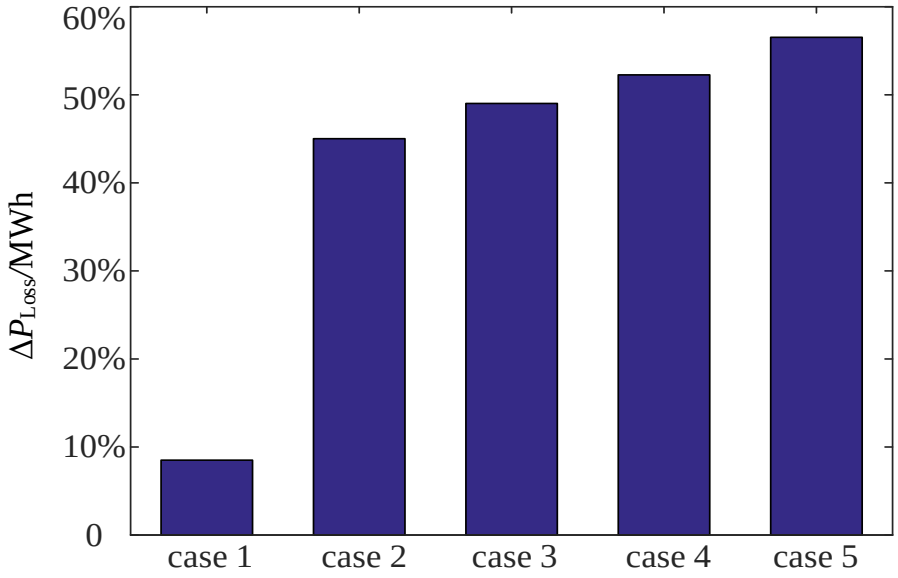

Figure 5-5. The relative difference of power loss deviation under different cases (without considering subnetworks)

Figure 5-6. The relative difference of power loss deviation under different cases (considering sub-networks)

From Figure 5-5 and Figure 5-6, we can find that increasing wind turbines' space granularity will reduce power flow loss, and then increasing subnetwork space granularity will also reduce power flow loss. In Figure 5-6, the power flow loss can be reduced by increasing the subnetwork space granularity. Compared with the same wind turbine space

granularity, the power flow loss can be reduced by at least 2.5% by increasing subnetwork space granularity.

(3) Power transmission congestion evaluation

Based on the historical data from wind power and load demand, we solved the IEEE 33 node system power flow in different branches under different cases, and the results as shown below. From Figure 5-7, we can find that:

(1) When we just consider the difference of wind turbines' space granularity (from the view of column), showing the difference in Figure 5-7 (*b*), (*d*) and (*f*) or Figure 5-7 (*a*), (*c*) and (*e*). With the increasing wind turbines' space granularity, the more concentrated the power flow range of the same branch is near 0, that is, the smaller the power flow of the same branch, the lower the possibility of power congestion of the branch. We can also find there is the same trend in Figure 5-8, the value of *ALP* will decrease with the increase of wind turbines' space granularity.

(2) When we consider the difference of subnetwork space granularity (from the view of row), shown the difference in Figure 5-7 (*a*) and (*b*), or Figure 5-7 (*c*) and (*d*), or Figure 5-7 (*e*) and (*f*). With the increasing subnetwork space granularity, the more concentrated the power flow range of the same branch is near 0, that is, the smaller the power flow of the same branch, the lower the possibility of power congestion of the branch. We can also find there is the same trend in Figure 5-8, the value of *ALP* considering networking will be lower than that without considering networking.

(3) Combining Figure 5-7 and Figure 5-8, we can find that with the increase of space

granularity, the power flow values will be more concentrated around 0 at the same branches, and at the same time, the *ALP* index will be smaller, that is, the lower the possibility of power congestion of the branches.

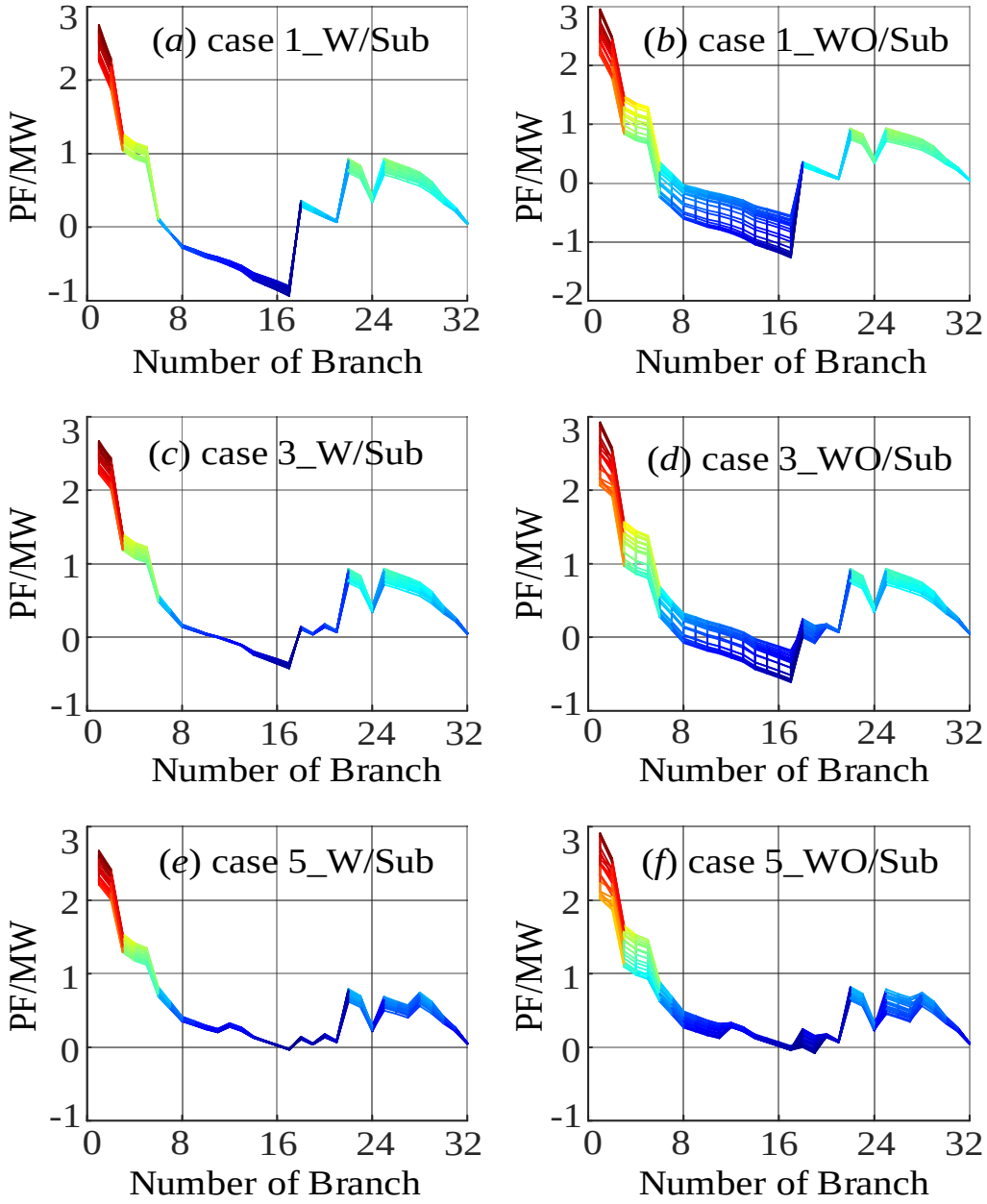

Figure 5-7. Power flows in different branches with and without subnetwork under different cases

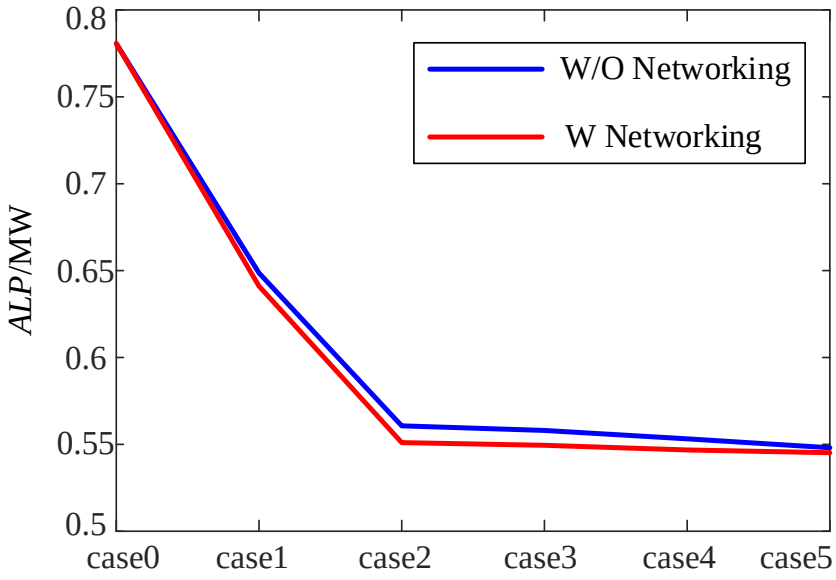

Figure 5-8. *ALP* indicators in different cases

5.5. Summary

In this chapter, we construct the supply-demand adaptation balance index and further propose a subnetwork networking method to increase the space granularity of networks, and then mainly evaluate the impact of growing space granularity on system operation cost, power flow loss, and power congestion evaluation. Increasing space granularity not only increases wind turbines' injection space granularity but also increases subnetworks' space granularity. The main conclusions are as follows:

Increasing space granularity by increasing the number of wind turbine injections and increasing subnetworks space granularity, on the one hand, will help to find the marginal generation price and reduce the customers' operation cost; on the other hand, it will decrease power flow loss and improve power congestion by improving the power flow distribution and reduce the repeat power flow. Compared with case 0, there is no wind turbine injection,

case 1 will reduce operating cost by about 13%, reduce power flow loss by about 8.5%, and further increase space granularity in case 5, which will further reduce operating cost by about 8.5% and reduce power flow loss about 54% than case 1.

The conclusions and methods of this chapter have important guiding and reference significance for the space layout of renewable generation units. At the same time, the relevant conclusions of increasing space granularity in this chapter are of great significance to the reform of power system operation.

6. CONCLUSIONS AND FUTURE WORKS

6.1. Conclusions

This study focuses on the reform of increasing spatial-temporal resolution in high-penetration renewable energy power systems. For the power fluctuation, this thesis proposed metrics including power incremental statistics, coefficient of variation, and peak power duration to characterize the power variability characteristics, based on these metrics, further analyze the mathematical relationship between these variations and net-load power curves and real-time power imbalance curve, finds that power variability will directly affect net-load power curves and the power gradient will affect the real-time power imbalance curve. For increasing temporal resolution reform, this thesis proposes an evaluation method for the electricity market at different time granularity, including ex-ante real-time power deviation prediction; real-time power scheduling operation and clearing; ex-post power deviation settlement. Based on this evaluation model, this thesis provides strong evidence that the higher the time granularity, the power step changes and the real-time power deviation quantities are smaller, and vice versus; For increasing spatial resolution reform, this study proposes the stochastic energy network theory to characterize the supply-demand adaptation balance index (SDABI) and further proposes a subnetwork networking method to evaluate the impact of increasing space granularity on reducing power system operation costs, power flow losses, and power congestion. This study for the first time provides scientific evidence to support the worldwide reform of the increasing spatial-temporal resolution with massive

renewable energy integration systems. The main conclusions are as follows:

1. **The statistical characteristics of power fluctuations of different types of resources can help system operators reasonably make the operations and reserve plans, which are mainly as follows:**
   1) The time series characteristics of PV power are relatively obvious, which directly affects the net load power curve. There is a higher flexible power requirement near noon (that is, around the maximum PV power), and this feature will increase as the PV penetration rate increases. It seems to look like the canyon curve; the timing characteristics of wind power in different countries are different, but the overall impact of wind power on the net load power curve is not as obvious as that of PV power.
   2) The real-time imbalanced power quantities of different types of resources are proportional to their power gradient. The real-time power imbalance caused by PV power has timing characteristics and looks like a butterfly curve, this characteristic will be more obvious with high penetration of PV generation.
   3) The different resource power fluctuation statistics characteristics in different countries can effectively help system operators rationally arrange flexible resource reserves, such as ramp power requirement and real-time power balance reserve based on these resource power fluctuations timing characteristics.
2. **Increasing the time granularity will significantly reduce power market balancing costs and power grid frequency deviations. Which are mainly as follows:**

1) With time granularity increases, power step changes at different scheduled interval points and real-time power deviations during the scheduling interval will be significantly reduced, thereby reducing power market balancing costs and power grid frequency deviations.

2) Specifically, when the time granularity is increased from 30 minutes to 5 minutes, the power step magnitude will be reduced (the power step change in the California ISO grid will be reduced by nearly five-sixths; the Czech and Qatar grid will also be reduced by almost 80%), and the real-time power deviation will also be reduced (The real-time power deviation in California ISO grid was reduced by nearly five-sixths; the Czech and Qatar grid also reduced by nearly half). Power grid frequency deviations are directly proportional to power change quantities; therefore, power grid frequency stability can be improved by increasing time granularity.

3. Increasing space granularity not only increases renewable energy generators' injection space granularity but also subnetworks' space granularity. This reform can reduce system operation costs, power flow loss, and mitigate power congestion. Which are mainly as follows:

1) Increasing space granularity by increasing the number of wind turbine injections and increasing subnetworks space granularity, on the one hand, will help to find the marginal generation price and reduce the customers' operation cost; on the other hand, it will decrease power flow loss and improve power congestion by improving the power flow distribution and reduce the repeat power flow.

2) Increase space granularity by the above two aspects, which will further reduce operating costs by about 8.5% and reduce power flow loss by nearly half.

6.2. Future Works

As variable renewable energy (VREs) penetrates the power grid on a massive scale, the grid will encounter greater fluctuations and intermittent than it does presently. Consequently, this paradigm shift will necessitate fundamental changes in power system planning, operation, and settlement approaches. To solve the above problems, we plan to conduct further research in the following aspects:

(1) Build a cross-domain energy power time series database for different research objects based on rich open-source meteorological data information: According to different levels of space granularity, we plan to build a cross-domain open dataset includes renewable energy time series data, load demand time series data, renewable generation installed capacity, and future resources evaluation information, etc.

(2) Using stochastic energy network theory to construct a new planning method based on the cross-domain open dataset: Given the power system planning problems caused by the randomness, volatility, and uncertainty of high-penetration renewable energy systems, we aim to combine the arrival process and departure process in the stochastic energy network theory to correspond to the energy production and energy consumption processes, and based on this theory we can characterize the three different operating states of the high penetration power grid, including waste of power supply,

loss of load demand and balance of energy supply and demand. Based on the probability characteristics of these three different work states, we can establish a high-energy reliable, and high-energy security power grid system unit.

(3) Design a new system flexible resource reserve and transaction strategies based on net-load power curve and real-time power imbalance curve timing characteristics: Using the cross-domain dataset, we can analyse the power development dynamic characteristic curves including net load power curves and real-time imbalanced power curves for research objects at different development degrees (that is different renewable penetration, different load consumption development, etc.), and provide scientific guidance for infrastructure construction (including lines, cables, substations, network infrastructure, etc.) and electricity market development models based on this dynamic development characteristic.

APPENDIX. IEEE 33-NODE DISTRIBUTION SYSTEM

A.1. IEEE 33-Node Distribution System Topology

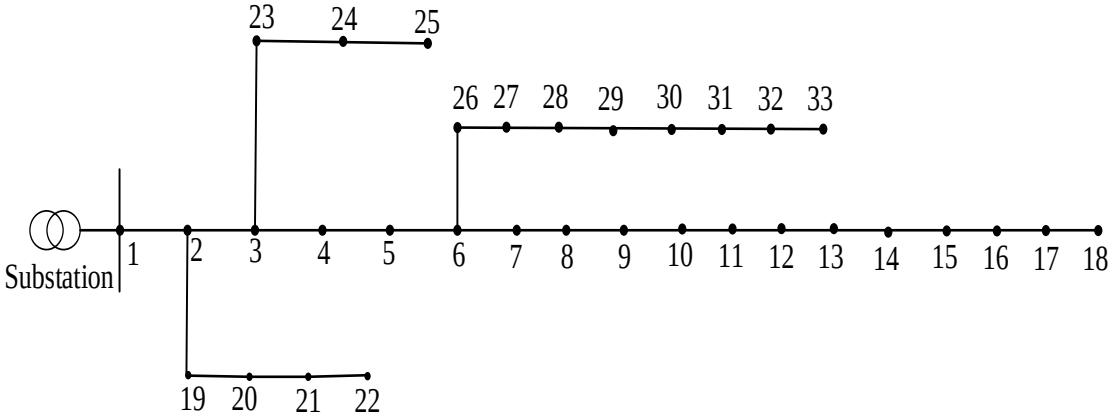

Figure A-1. IEEE 33-node system topology

A.2. IEEE 33-Node Distribution System Bus Data

Table A-1. IEEE 33-node system bus information

BN	BT	PD	QD	GS	BS	BA	VM	VA	BV	Zone	VMAX	VMIN
1	3	0	0	0	0	1	1	0	12.66	1	1	1
2	1	0.1	0.06	0	0	1	1	0	12.66	1	1.1	0.9
3	1	0.09	0.04	0	0	1	1	0	12.66	1	1.1	0.9
4	1	0.12	0.08	0	0	1	1	0	12.66	1	1.1	0.9
5	1	0.06	0.03	0	0	1	1	0	12.66	1	1.1	0.9
6	1	0.06	0.02	0	0	1	1	0	12.66	1	1.1	0.9
7	1	0.2	0.1	0	0	1	1	0	12.66	1	1.1	0.9
8	1	0.2	0.1	0	0	1	1	0	12.66	1	1.1	0.9
9	1	0.06	0.02	0	0	1	1	0	12.66	1	1.1	0.9
10	1	0.06	0.02	0	0	1	1	0	12.66	1	1.1	0.9
11	1	0.045	0.03	0	0	1	1	0	12.66	1	1.1	0.9
12	1	0.06	0.035	0	0	1	1	0	12.66	1	1.1	0.9
13	1	0.06	0.035	0	0	1	1	0	12.66	1	1.1	0.9
14	1	0.12	0.08	0	0	1	1	0	12.66	1	1.1	0.9
15	1	0.06	0.01	0	0	1	1	0	12.66	1	1.1	0.9
16	1	0.06	0.02	0	0	1	1	0	12.66	1	1.1	0.9
17	1	0.06	0.02	0	0	1	1	0	12.66	1	1.1	0.9

BN	BT	PD	QD	GS	BS	BA	VM	VA	BV	Zone	VMAX	VMIN
18	1	0.09	0.04	0	0	1	1	0	12.66	1	1.1	0.9
19	1	0.09	0.04	0	0	1	1	0	12.66	1	1.1	0.9
20	1	0.09	0.04	0	0	1	1	0	12.66	1	1.1	0.9
21	1	0.09	0.04	0	0	1	1	0	12.66	1	1.1	0.9
22	1	0.09	0.04	0	0	1	1	0	12.66	1	1.1	0.9
23	1	0.09	0.05	0	0	1	1	0	12.66	1	1.1	0.9
24	1	0.42	0.2	0	0	1	1	0	12.66	1	1.1	0.9
25	1	0.42	0.2	0	0	1	1	0	12.66	1	1.1	0.9
26	1	0.06	0.025	0	0	1	1	0	12.66	1	1.1	0.9
27	1	0.06	0.025	0	0	1	1	0	12.66	1	1.1	0.9
28	1	0.06	0.02	0	0	1	1	0	12.66	1	1.1	0.9
29	1	0.12	0.07	0	0	1	1	0	12.66	1	1.1	0.9
30	1	0.2	0.6	0	0	1	1	0	12.66	1	1.1	0.9
31	1	0.15	0.07	0	0	1	1	0	12.66	1	1.1	0.9
32	1	0.21	0.1	0	0	1	1	0	12.66	1	1.1	0.9
33	1	0.06	0.04	0	0	1	1	0	12.66	1	1.1	0.9

Note: BN represent bus number; BT represent bus type (PQ=1, PV=2, ref=3, isolated=4); PD represent real power demand; QD represent reactive power demand; GS represent shunt conductance; BS represent shunt susceptance; BA represent area number; VM represent voltage magnitude; VA represent voltage angle; BV represent base voltage; Zone represent loss zone; VMAX represent maximum voltage magnitude; VMIN represent minimum voltage magnitude.

A.3. IEEE 33-Node Distribution System Branch Data

Table A-2. IEEE 33-node system branch data

FB	TB	R	X	B	Rate-A	Rate-B	Rate-C	TAP	SHIFT	STATUS	AMIN	AMAX
1	2	0.0057526	0.0029324	0	0	0	0	0	0	1	-360	360
2	3	0.0307595	0.0156668	0	0	0	0	0	0	1	-360	360
3	4	0.0228357	0.01163	0	0	0	0	0	0	1	-360	360
4	5	0.0237778	0.0121104	0	0	0	0	0	0	1	-360	360
5	6	0.0510995	0.0441115	0	0	0	0	0	0	1	-360	360
6	7	0.0116799	0.0386085	0	0	0	0	0	0	1	-360	360
7	8	0.044386	0.0146685	0	0	0	0	0	0	1	-360	360
8	9	0.0642643	0.0461705	0	0	0	0	0	0	1	-360	360
9	10	0.0651378	0.0461705	0	0	0	0	0	0	1	-360	360
10	11	0.0122664	0.0040555	0	0	0	0	0	0	1	-360	360
11	12	0.0233598	0.0077242	0	0	0	0	0	0	1	-360	360
12	13	0.0915922	0.0720634	0	0	0	0	0	0	1	-360	360
13	14	0.0337918	0.0444796	0	0	0	0	0	0	1	-360	360
14	15	0.036874	0.0328185	0	0	0	0	0	0	1	-360	360
15	16	0.0465635	0.0340039	0	0	0	0	0	0	1	-360	360
16	17	0.080424	0.1073775	0	0	0	0	0	0	1	-360	360
17	18	0.0456713	0.0358133	0	0	0	0	0	0	1	-360	360
2	19	0.0102324	0.0097644	0	0	0	0	0	0	1	-360	360
19	20	0.0938508	0.0845668	0	0	0	0	0	0	1	-360	360
20	21	0.0255497	0.0298486	0	0	0	0	0	0	1	-360	360

FB	TB	R	X	B	Rate-A	Rate-B	Rate-C	TAP	SHIFT	STATUS	AMIN	AMAX
21	22	0.0442301	0.0584805	0	0	0	0	0	0	1	-360	360
3	23	0.0281515	0.0192356	0	0	0	0	0	0	1	-360	360
23	24	0.0560285	0.0442425	0	0	0	0	0	0	1	-360	360
24	25	0.0559037	0.0437434	0	0	0	0	0	0	1	-360	360
6	26	0.0126657	0.0064514	0	0	0	0	0	0	1	-360	360
26	27	0.017732	0.0090282	0	0	0	0	0	0	1	-360	360
27	28	0.0660737	0.0582559	0	0	0	0	0	0	1	-360	360
28	29	0.0501761	0.0437122	0	0	0	0	0	0	1	-360	360
29	30	0.0316642	0.0161285	0	0	0	0	0	0	1	-360	360
30	31	0.0607953	0.060084	0	0	0	0	0	0	1	-360	360
31	32	0.0193729	0.0225799	0	0	0	0	0	0	1	-360	360
32	33	0.0212759	0.0330805	0	0	0	0	0	0	1	-360	360
21	8	0.1247851	0.1247851	0	0	0	0	0	0	0	-360	360
9	15	0.1247851	0.1247851	0	0	0	0	0	0	0	-360	360
12	22	0.1247851	0.1247851	0	0	0	0	0	0	0	-360	360
18	33	0.0311963	0.0311963	0	0	0	0	0	0	0	-360	360
25	29	0.0311963	0.0311963	0	0	0	0	0	0	0	-360	360

Note: FB represent “from” bus number; TB represent “to” bus number; R represent resistance (p.u.); X represent reactance (p.u.); B represent total line charging susceptance (p.u.); Rate-A set to 0 for unlimited; Rate-B set to 0 for unlimited; Rate-C set to 0 for unlimited; TAP represent transformer off nominal turns ratio, TAP=0 used to indicate transmission line rather than transformer; SHIFT represent transformer phase shift angle degree; STATUS represent initial branch status, in-service=1, out-of-service=0; AMIN represent minimum angle difference; AMAX represent maximum angle difference.

REFERENCES

[1] "The Paris Agreement." United Nations Climate Action, Retrieved 27 Oct 2024. Available: https://www.un.org/en/climatechange/paris-agreement.

[2] Schleussner, Carl-Friedrich. "The Paris Agreement – the 1.5 °C Temperature Goal". Climate Analytics. Retrieved 29 January 2022. Available: https://climateanalytics.org/comment/understanding-the-paris-agreements-long-term-temperature-goal

[3] IEA (2023), Global Energy and Climate Model, IEA, Paris, Available: https://www.iea.org/reports/global-energy-and-climate-model, Licence: CC BY 4.0

[4] IRENA (2024), Renewable capacity statistics 2024, International Renewable Energy Agency, Abu Dhabi. https://www.irena.org/Publications/2024/Mar/Renewable-capacity-statistics-2024

[5] IEA (2024), Renewables 2023, IEA, Paris https://www.iea.org/reports/renewables-2023, Licence: CC BY 4.0

[6] Nuveen INFRASTURCTURE, "Energy transition update: Levelized cost of electricity from renewables", May 2024.

[7] IRENA (2023), Renewable power generation costs in 2022, International Renewable Energy Agency, Abu Dhabi.

[8] Ashish Gulagi, Myron Alcanzare, Dmitrii Bogdanov, Eugene Esparcia, Joey Ocon, Christian Breyer, "Transition pathway towards 100% renewable energy across the sectors of power, heat, transport, and desalination for the Philippines," Renewable and Sustainable Energy Reviews, Volume 144, 2021, 110934, ISSN 1364-0321, https://doi.org/10.1016/j.rser.2021.110934.

[9] Sven Teske, "Achieving the Paris Climate Agreement Goals", Springer Cham, Licence: CC BY, DOI: https://doi.org/10.1007/978-3-030-05843-2

[10] Mark Z. Jacobson. et al, "100% Clean and Renewable Wind, Water, and Sunlight All-Sector Energy Roadmaps for 139 Countries of the World, " Joule, Volume 1, Issue 1, 2017, Pages 108-121, ISSN 2542-4351, https://doi.org/10.1016/j.joule.2017.07.005

[11] IRENA (2021), "World Energy Transitions Outlook: 1.5°C Pathway, " International Renewable Energy Agency, Abu Dhabi.

[12] IEA (2021), "Net Zero by 2050, " IEA, Paris https://www.iea.org/reports/net-zero-by-2050, Licence: CC BY 4.0

[13] IRENA Coalition for Action (2024), "100% renewable energy scenarios: Supporting ambitious policy targets," International Renewable Energy Agency, Abu Dhabi.

[14] P. Kundur et al., "Power System Stability and Control." New York, NY, USA: McGraw Hill Education, 1994.

[15] D. E. Olivares et al., "Trends in Microgrid Control," IEEE Transactions on Smart Grid, vol. 5, no. 4, pp. 1905-1919, July 2014, Doi: 10.1109/TSG.2013.2295514.

[16] Wang, Z., Liu, W. Wind energy potential assessment based on wind speed, its direction and power data. Sci Rep 11, 16879 (2021). https://doi.org/10.1038/s41598-021-96376-7

[17] K. Guerra. et al, Facing the high share of variable renewable energy in the power system: Flexibility and stability requirements, Applied Energy, Volume 310, 2022, 118561, ISSN 0306-2619, https://doi.org/10.1016/j.apenergy.2022.118561.

[18] E. Ela and M. O'Malley, "Studying the Variability and Uncertainty Impacts of Variable Generation at Multiple Timescales," IEEE Transactions on Power Systems, vol. 27, no. 3, pp. 1324-1333, Aug. 2012, Doi: 10.1109/TPWRS.2012.2185816.

[19] M Anvari et al. "Short-term fluctuations of wind and solar power systems. " 2016 New J. Phys. 18 063027.

[20] Blaabjerg, F., Chen, M. & Huang, L. "Power electronics in wind generation systems." Nat Rev Electr Eng 1, 234–250 (2024). https://doi.org/10.1038/s44287-024-00032-x

[21] Z. Chen, J. M. Guerrero, and F. Blaabjerg, "A Review of the State of the Art of Power Electronics for Wind Turbines," IEEE Transactions on Power Electronics, vol. 24, no. 8, pp. 1859-1875, Aug. 2009, Doi: 10.1109/TPEL.2009.2017082.

[22] Ana Fernández-Guillamón. et al. "Power systems with high renewable energy sources: A review of inertia and frequency control strategies over time," Renewable and Sustainable Energy Reviews, Volume 115, 2019, 109369. https://doi.org/10.1016/j.rser.2019.109369

[23] M. Yue and X. Wang, "Grid Inertial Response-Based Probabilistic Determination of Energy Storage System Capacity Under High Solar Penetration," IEEE Transactions on Sustainable Energy, vol. 6, no. 3, pp. 1039-1049, July 2015, Doi: 10.1109/TSTE.2014.2328298.

[24] Dewenter, T. & Hartmann, A. K. Large-deviation properties of the resilience of power grids. New J. Phys. 17, 015005 (2015).

[25] Q. -H. Wu et al., "Control and Stability of Large-scale Power System with Highly Distributed Renewable Energy Generation: Viewpoints from Six Aspects," CSEE Journal of Power and Energy Systems, vol. 9, no. 1, pp. 8-14, January 2023, Doi: 10.17775/CSEEJPES.2022.08740.

[26] Andrew D. Mills, et al. "Impacts of variable renewable energy on wholesale markets and generating assets in the United States: A review of expectations and evidence," Renewable and Sustainable Energy Reviews, Volume 120,2020,109670, ISSN 1364-0321, https://doi.org/10.1016/j.rser.2019.109670.

[27] Cody Hohl, Chiara Lo Prete, Ashish Radhakrishnan, Mort Webster, "Intraday markets, wind integration and uplift payments in a regional U.S. power system," Energy Policy, Volume 175, 2023, 113503, ISSN 0301-4215, https://doi.org/10.1016/j.enpol.2023.113503.

[28] N. Aparicio, I. MacGill, J. Rivier Abbad and H. Beltran, "Comparison of Wind Energy Support Policy and Electricity Market Design in Europe, the United States, and Australia," IEEE Transactions on Sustainable Energy, vol. 3, no. 4, pp. 809-818, Oct. 2012, Doi: 10.1109/TSTE.2012.2208771.

[29] S. Wu et al., "Multi-Timescale Trading Strategy for Renewable Power to Ammonia Virtual Power Plant in the Electricity, Hydrogen, and Ammonia Markets," IEEE Transactions on Energy Markets, Policy and Regulation, vol. 1, no. 4, pp. 322-335, Dec. 2023, Doi: 10.1109/TEMPR.2023.3287857.

[30] C. Pan, C. Shao, B. Hu, K. Xie, C. Li and J. Ding, "Modeling the Reserve Capacity of Wind Power and the Inherent Decision-Dependent Uncertainty in the Power System Economic Dispatch," IEEE Transactions on Power Systems, vol. 38, no. 5, pp. 4404-4417, Sept. 2023, Doi: 10.1109/TPWRS.2022.3210106.

[31] Y. Dvorkin, M. Lubin, S. Backhaus and M. Chertkov, "Uncertainty Sets for Wind Power Generation," IEEE Transactions on Power Systems, vol. 31, no. 4, pp. 3326-3327, July 2016, Doi: 10.1109/TPWRS.2015.2476664.

[32] IRENA (2019), Innovation landscape brief: Increasing time granularity in electricity markets, International Renewable Energy Agency, Abu Dhabi.

[33] Wu, C., Zhang, XP. & Sterling, M. "Solar power generation intermittency and aggregation." Sci Rep 12, 1363 (2022). https://doi.org/10.1038/s41598-022-05247-2

[34] M. G. Villalva, J. R. Gazoli and E. R. Filho, "Comprehensive Approach to Modeling and Simulation of Photovoltaic Arrays," IEEE Transactions on Power Electronics, vol. 24, no. 5, pp. 1198-1208, May 2009, Doi: 10.1109/TPEL.2009.2013862.

[35] R. Tonkoski, L. A. C. Lopes and T. H. M. El-Fouly, "Coordinated Active Power Curtailment of Grid Connected PV Inverters for Overvoltage Prevention," IEEE Transactions on Sustainable Energy, vol. 2, no. 2, pp. 139-147, April 2011, Doi: 10.1109/TSTE.2010.2098483.

[36] Todd Levin, Audun Botterud, W. Neal Mann, Jonghwan Kwon, Zhi Zhou, "Extreme weather and electricity markets: Key lessons from the February 2021 Texas crisis", Joule, Volume 6, Issue 1, 2022, Pages 1-7, ISSN 2542-4351, https://doi.org/10.1016/j.joule.2021.12.015.

[37] Ceferino, L., & Lin, N. (2023). Hurricane Risk of Solar Generation in the United States. Natural Hazards Review, 24(4), Article 04023029. https://doi.org/10.1061/NHREFO.NHENG-1764

[38] Larson, David P.; Nonnenmacher, Lukas; Coimbra, Carlos F.M. (2016-06-01). "Day-ahead forecasting of solar power output from photovoltaic plants in the American Southwest". Renewable Energy. 91: 11–20. Doi:10.1016/j.renene.2016.01.039. ISSN 0960-1481.

[39] Jan Kleissl, "Solar Energy Forecasting and Resource Assessment-1st Edition". Academic Press, June 2013.

[40] T. Yao et al., "Intra-Hour Photovoltaic Generation Forecasting Based on Multi-Source Data and Deep Learning Methods," IEEE Transactions on Sustainable Energy, vol. 13, no. 1, pp. 607-618, Jan. 2022, Doi: 10.1109/TSTE.2021.3123337.

[41] Fei Wang, Xiaoxing Lu, Shengwei Mei, et al. "A satellite image data based ultra-short-term solar PV power forecasting method considering cloud information from neighboring plant," Energy, Volume 238, Part C, 2022, 121946, ISSN 0360-5442, https://doi.org/10.1016/j.energy.2021.121946.

[42] Fujita, K.S., Ancona, Z.H., Kramer, L.A., Straka, M., Gautreau, T.E., Garrity, C.P., Robson, D., Diffendorfer, J.E., and Hoen, B., 2023, United States Large-Scale Solar Photovoltaic Database v1.0 (November 2023): U.S. Geological Survey and Lawrence Berkeley National Laboratory data release, https://doi.org/10.5066/P9IA3TUS.

[43] Andreas, A.; Stoffel, T.; (1981). NREL Solar Radiation Research Laboratory (SRRL): Baseline Measurement System (BMS); Golden, Colorado (Data); NREL Report No. DA-5500-56488. http://dx.doi.org/10.5439/1052221

[44] Jianwu Zeng, Wei Qiao, "Short-term solar power prediction using a support vector machine," Renewable Energy, Volume 52, 2013, Pages 118-127, ISSN 0960-1481, https://doi.org/10.1016/j.renene.2012.10.009.

[45] M. Massaoudi et al., "An Effective Hybrid NARX-LSTM Model for Point and Interval PV Power Forecasting," IEEE Access, vol. 9, pp. 36571-36588, 2021, Doi: 10.1109/ACCESS.2021.3062776.

[46] S. Al-Dahidi, O. Ayadi, M. Alrbai and J. Adeeb, "Ensemble Approach of Optimized Artificial Neural Networks for Solar Photovoltaic Power Prediction," IEEE Access, vol. 7, pp. 81741-81758, 2019, Doi: 10.1109/ACCESS.2019.2923905.

[47] Alberto Dolara, Sonia Leva, Giampaolo Manzolini, "Comparison of different physical models for PV power output prediction," Solar Energy, Volume 119, 2015, Pages 83-99, ISSN 0038-092X, https://doi.org/10.1016/j.solener.2015.06.017.

[48] Eduardo Abdon Sarquis Filho, Carlos Alberto Ferreira Fernandes, Paulo José da Costa Branco, "A complete framework for the simulation of photovoltaic arrays under mismatch conditions," Solar Energy, Volume 213, 2021, Pages 13-26, ISSN 0038-092X, https://doi.org/10.1016/j.solener.2020.10.055.

[49] Pierluigi Guerriero, Lorenzo Codecasa, Vincenzo d'Alessandro, Santolo Daliento, "Dynamic electro-thermal modeling of solar cells and modules, " Solar Energy, Volume

179, 2019, Pages 326-334, ISSN 0038-092X, https://doi.org/10.1016/j.solener.2018.12.067.

[50] Dampaak Abdulai, Samuel Gyamfi, Felix Amankwah Diawuo, Peter Acheampong, Data analytics for prediction of solar PV power generation and system performance: A real case of Bui Solar Generating Station, Ghana, Scientific African, Volume 21, 2023, e01894, ISSN 2468-2276, https://doi.org/10.1016/j.sciaf.2023.e01894.

[51] V. Prema, K. Uma Rao, Development of statistical time series models for solar power prediction, Renewable Energy, Volume 83, 2015, Pages 100-109, ISSN 0960-1481, https://doi.org/10.1016/j.renene.2015.03.038.

[52] K. Doubleday, S. Jascourt, W. Kleiber and B. -M. Hodge, "Probabilistic Solar Power Forecasting Using Bayesian Model Averaging," IEEE Transactions on Sustainable Energy, vol. 12, no. 1, pp. 325-337, Jan. 2021, Doi: 10.1109/TSTE.2020.2993524.

[53] Hanis Nasuha Amer, Nofri Yenita Dahlan, Azlin Mohd Azmi, Mohd Fuad Abdul Latip, Mohammad Syazwan Onn, Afidalina Tumian, "Solar power prediction based on Artificial Neural Network guided by feature selection for Large-scale Solar Photovoltaic Plant, " Energy Reports, Volume 9, Supplement 12, 2023, Pages 262-266, ISSN 2352-4847, https://doi.org/10.1016/j.egyr.2023.09.141.

[54] Salim Moslehi, T. Agami Reddy, Srinivas Katipamula, "Evaluation of data-driven models for predicting solar photovoltaics power output, " Energy, Volume 142, 2018, Pages 1057-1065, ISSN 0360-5442, https://doi.org/10.1016/j.energy.2017.09.042.

[55] H. S. Jang, K. Y. Bae, H. -S. Park and D. K. Sung, "Solar Power Prediction Based on Satellite Images and Support Vector Machine," IEEE Transactions on Sustainable Energy, vol. 7, no. 3, pp. 1255-1263, July 2016, Doi: 10.1109/TSTE.2016.2535466.

[56] H. Long, R. Geng, W. Sheng, H. Hui, R. Li and W. Gu, "Small-Sample Solar Power Interval Prediction Based on Instance-Based Transfer Learning," IEEE Transactions on Industry Applications, vol. 59, no. 5, pp. 5283-5292, Sept.-Oct. 2023, Doi: 10.1109/TIA.2023.3284776.

[57] M. -Y. Chen, H. -S. Chiang and C. -Y. Chang, "Solar Photovoltaic Power Generation Prediction based on Deep Learning Methods," 2022 IET International Conference on Engineering Technologies and Applications (IET-ICETA), Changhua, Taiwan, 2022, pp. 1-2, Doi: 10.1109/IET-ICETA56553.2022.9971676.

[58] M. Elsaraiti and A. Merabet, "Solar Power Forecasting Using Deep Learning Techniques," IEEE Access, vol. 10, pp. 31692-31698, 2022, Doi: 10.1109/ACCESS.2022.3160484.

[59] K. Y. Bae, H. S. Jang and D. K. Sung, "Hourly Solar Irradiance Prediction Based on Support Vector Machine and Its Error Analysis," IEEE Transactions on Power Systems, vol. 32, no. 2, pp. 935-945, March 2017, Doi: 10.1109/TPWRS.2016.2569608.

[60] V. Prema, M. S. Bhaskar, D. Almakhles, N. Gowtham and K. U. Rao, "Critical Review of Data, Models and Performance Metrics for Wind and Solar Power Forecast," IEEE Access, vol. 10, pp. 667-688, 2022, Doi: 10.1109/ACCESS.2021.3137419.

[61] Kumar, K., Prabhakar, P., & Verma, A. (2024). Wind power forecasting technologies: A review. Energy Storage and Conversion, 2(2), 538. https://doi.org/10.59400/esc.v2i2.538

[62] T. Hong, P. Pinson, Y. Wang, R. Weron, D. Yang and H. Zareipour, "Energy Forecasting: A Review and Outlook," IEEE Open Access Journal of Power and Energy, vol. 7, pp. 376-388, 2020, Doi: 10.1109/OAJPE.2020.3029979.

[63] N. Chen, Z. Qian, I. T. Nabney and X. Meng, "Wind Power Forecasts Using Gaussian Processes and Numerical Weather Prediction," IEEE Transactions on Power Systems, vol. 29, no. 2, pp. 656-665, March 2014, Doi: 10.1109/TPWRS.2013.2282366.

[64] Maclaurin, Galen, Nick Grue, Anthony Lopez, Donna Heimiller, Michael Rossol, Grant Buster, and Travis Williams. 2019. The Renewable Energy Potential (reV) Model: A Geospatial Platform for Technical Potential and Supply Curve Modeling. Golden, CO: National Renewable Energy Laboratory. NREL/TP-6A20-73067. https://www.nrel.gov/docs/fy19osti/73067.pdf

[65] G. W. Chang, et al. "A hybrid model for forecasting wind speed and wind power generation," 2016 IEEE Power and Energy Society General Meeting (PESGM), Boston, MA, USA, 2016, pp. 1-5.Doi: 10.1109/PESGM.2016.7742039.

[66] R. Fan, et al. "A New Power Prediction Accuracy Evaluation Method of Renewable Energy Plant," 2019 IEEE Sustainable Power and Energy Conference (iSPEC), Beijing, China, 2019, pp. 610-612. Doi: 10.1109/iSPEC48194.2019.8975125.

[67] FENG Shuanglei, WANG Weisheng, LIU Chun, et al. Study on the physical approach to wind power prediction[J]. Proceedings of the CSEE, 2010, 30(2): 1-6.

[68] CASSOLA F, BURLANDO M. Wind speed and wind energy forecast through Kalman filtering of numerical weather prediction model output[J]. Applied Energy, 2012, 99(6): 154-166. https://doi.org/10.1016/j.apenergy.2012.03.054.

[69] MEN Z, YEE E, LIEN F S, et al. Short-term wind speed and power forecasting using an ensemble of mixture density neural networks[J]. Renewable Energy, 2016, 87(3): 129-135. https://doi.org/10.1016/j.renene.2015.10.014.

[70] M. Cui, J. Zhang, Q. Wang, V. Krishnan and B. -M. Hodge, "A Data-Driven Methodology for Probabilistic Wind Power Ramp Forecasting," in IEEE Transactions on Smart Grid, vol. 10, no. 2, pp. 1326-1338, March 2019, Doi: 10.1109/TSG.2017.2763827.

[71] B. Sweetman and S. Dai, "Transformation of Wind Turbine Power Curves Using the Statistics of the Wind Process," IEEE Transactions on Sustainable Energy, vol. 12, no. 4, pp. 2053-2061, Oct. 2021, Doi: 10.1109/TSTE.2021.3078774.

[72] Lei Liu, eet al. Ultra-short-term wind power forecasting based on deep Bayesian model with uncertainty, Renewable Energy, Volume 205, 2023, Pages 598-607, ISSN 0960-1481, https://doi.org/10.1016/j.renene.2023.01.038.

[73] Ilhami Colak, Seref Sagiroglu, Mehmet Yesilbudak, Data mining and wind power prediction: A literature review, Renewable Energy, Volume 46, 2012, Pages 241-247, ISSN 0960-1481, https://doi.org/10.1016/j.renene.2012.02.015.

[74] Yue Sun et al. Probabilistic model of wind power output considering temporal autocorrelation and cross-correlation with forecast output. 2021 J. Phys.: Conf. Ser. 1754 012190. DOI 10.1088/1742-6596/1754/1/012190

[75] Ehsan Taslimi Renani, Mohamad Fathi Mohamad Elias, Nasrudin Abd. Rahim, Using data-driven approach for wind power prediction: A comparative study, Energy Conversion and Management, Volume 118, 2016, Pages 193-203, ISSN 0196-8904, https://doi.org/10.1016/j.enconman.2016.03.078.

[76] J. Zhang and C. Wang, "Application of ARMA Model in Ultra-short-Term Prediction of Wind Power," 2013 International Conference on Computer Sciences and Applications, Wuhan, China, 2013, pp. 361-364, Doi: 10.1109/CSA.2013.91.

[77] Beizhen Zhao, Xin He, Shaolin Ran, Yong Zhang, Cheng Cheng, Spatial correlation learning based on graph neural network for medium-term wind power forecasting, Energy, Volume 296, 2024, 131164, ISSN 0360-5442, https://doi.org/10.1016/j.energy.2024.131164.

[78] J. Zeng and W. Qiao, "Short-Term Wind Power Prediction Using a Wavelet Support Vector Machine," IEEE Transactions on Sustainable Energy, vol. 3, no. 2, pp. 255-264, April 2012, Doi: 10.1109/TSTE.2011.2180029.

[79] Zhengjing Ma, Gang Mei, A hybrid attention-based deep learning approach for wind power prediction, Applied Energy, Volume 323, 2022, 119608, ISSN 0306-2619, https://doi.org/10.1016/j.apenergy.2022.119608.

[80] J. Zeng and W. Qiao, "Support vector machine-based short-term wind power forecasting," 2011 IEEE/PES Power Systems Conference and Exposition, Phoenix, AZ, USA, 2011, pp. 1-8, Doi: 10.1109/PSCE.2011.5772573.

[81] Huai-zhi Wang, Gang-qiang Li, Gui-bin Wang, Jian-chun Peng, Hui Jiang, Yi-tao Liu, Deep learning based ensemble approach for probabilistic wind power forecasting, Applied Energy, Volume 188, 2017, Pages 56-70, ISSN 0306-2619, https://doi.org/10.1016/j.apenergy.2016.11.111.

[82] IRENA (2019), Innovation landscape brief: Increasing space granularity in electricity markets, International Renewable Energy Agency, Abu Dhabi. Available: https://www.irena.org/-/media/Files/IRENA/Agency/Publication/2019/Feb/IRENA_Increasing_space_granularity_2019.pdf

[83] CAISO (2005), Locational Marginal Pricing (LMP): Basics of nodal price calculation, California Independent System Operator.

[84] NYISO (2017a), Distributed energy resources roadmap for New York's wholesale electricity markets, New York Independent System Operator.

[85] Jun Yu, "Locational marginal pricing in ERCOT market," 2006 IEEE Power Engineering Society General Meeting, Montreal, QC, Canada, 2006, pp. 3 pp.-, Doi: 10.1109/PES.2006.1708980.

[86] ENTSO-E (2018), Regular reporting on bidding zone configuration, European Network of Transmission System Operators for Electricity Available: https://docstore.entsoe.eu/Documents/Events/2018/BZ_report/20181015_BZ_TR_FINAL.pdf.

[87] Quentin Lété, Yves Smeers, Anthony Papavasiliou, An analysis of zonal electricity pricing from a long-term perspective, Energy Economics, Volume 107, 2022, 105853, ISSN 0140-9883, https://doi.org/10.1016/j.eneco.2022.105853.

[88] Kevin Carden, et al. Estimation of the Market Equilibrium and Economically Optimal Reserve Margins for the ERCOT Region for 2024, the Electric Reliability Council of Texas (ERCOT), 2021.

[89] Y. Yang, W. Wu, B. Wang, and M. Li, "Chance-Constrained Economic Dispatch Considering Curtailment Strategy of Renewable Energy," IEEE Transactions on Power Systems, vol. 36, no. 6, pp. 5792-5802, Nov. 2021, Doi: 10.1109/TPWRS.2021.3081120.

[90] Wang, Z., Li, Q., Kong, S. et al. Analysis of renewable energy consumption and economy considering the joint optimal allocation of "renewable energy + energy storage + synchronous condenser". Sci Rep 13, 20376 (2023). https://doi.org/10.1038/s41598-023-47401-4.

[91] G. Ma, J. Li and X. -P. Zhang, "Energy Storage Capacity Optimization for Improving the Autonomy of Grid-Connected Microgrid," IEEE Transactions on Smart Grid, vol. 14, no. 4, pp. 2921-2933, July 2023, Doi: 10.1109/TSG.2022.3233910.

[92] Yanhua Zou, Marko Čepin, "Loss of load probability for power systems based on renewable sources, Reliability Engineering & System Safety, " Volume 247, 2024, 110136, ISSN 0951-8320, https://doi.org/10.1016/j.ress.2024.110136.

[93] E. Sortomme, M. M. Hindi, S. D. J. MacPherson and S. Venkata, "Coordinated Charging of Plug-In Hybrid Electric Vehicles to Minimize Distribution System Losses," IEEE Transactions on Smart Grid, vol. 2, no. 1, pp. 198-205, March 2011, Doi: 10.1109/TSG.2010.2090913.

[94] P. Xie, Z. Cai, P. Liu, X. Li, Y. Zhang, and D. Xu, "Microgrid System Energy Storage Capacity Optimization Considering Multiple Time Scale Uncertainty Coupling," IEEE

Transactions on Smart Grid, vol. 10, no. 5, pp. 5234-5245, Sept. 2019, Doi: 10.1109/TSG.2018.2879520.

[95] K. Wang, F. Ciucu, C. Lin and S. H. Low, "A Stochastic Power Network Calculus for Integrating Renewable Energy Sources into the Power Grid," IEEE Journal on Selected Areas in Communications, vol. 30, no. 6, pp. 1037-1048, July 2012, Doi: 10.1109/JSAC.2012.120703.

[96] H. Qiu, et al. Multi-Time-Scale Rolling Optimal Dispatch for AC/DC Hybrid Microgrids With Day-Ahead Distributionally Robust Scheduling, IEEE Transactions on Sustainable Energy, vol. 10, no. 4, pp. 1653-1663, Oct. 2019, Doi: 10.1109/TSTE.2018.2868548.

[97] Eric J. Hoevenaars, Curran A. Crawford, Implications of temporal resolution for modeling renewables-based power systems, Renewable Energy, Volume 41, 2012, Pages 285-293, ISSN 0960-1481, https://doi.org/10.1016/j.renene.2011.11.013.

[98] M. Emmanuel and J. Giraldez, "Net Electricity Clustering at Different Temporal Resolutions Using a SAX-Based Method for Integrated Distribution System Planning," IEEE Access, vol. 7, pp. 123689-123697, 2019, doi: 10.1109/ACCESS.2019.2938212.

[99] Soliman Abdel-hady Soliman, et al. Chapter 8 Dynamic Electric Load Forecasting, Butterworth-Heinemann, 2010, Pages 291-352, ISBN 9780123815439, https://doi.org/10.1016/B978-0-12-381543-9.00008-7.

[100] Jiwon Kim, Younghoon Kwak, Sun-Hye Mun, Jung-Ho Huh, Electric energy consumption predictions for residential buildings: Impact of data-driven model and temporal resolution on prediction accuracy, Journal of Building Engineering, Volume 62, 2022, 105361, ISSN 2352-7102, https://doi.org/10.1016/j.jobe.2022.105361.

[101] FERC Order No. 764 market changes. CAISO. Available: http://www.caiso.com/informed/Pages/StakeholderProcesses/CompletedClosedStakeholderInitiatives/FERCOrderNo764MarketChanges.aspx.

[102] New record set on French Intraday market. Available: https://www.epexspot.com/en/news/new-record-set-french-intraday-market

[103] Description of EPEX SPOT Markets Indices. Available: https://www.epexspot.com/sites/default/files/download_center_files/EPEX%20SPOT%20Indices%202019-05_final.pdf

[104] Qingyong Zhang, et al. TransformGraph: A novel short-term electricity net load forecasting model, Energy Reports, Volume 9, 2023, Pages 2705-2717, ISSN 2352-4847, https://doi.org/10.1016/j.egyr.2023.01.050.

[105] TODAY IN ENERGY: As solar capacity grows, duck curves are getting deeper in California, U.S. Energy Information Administration, June 2023.

[106] Bess Krietemeyer, Jason Dedrick, Ehsan Sabaghian, Tarek Rakha, "Managing the duck curve: Energy culture and participation in local energy management programs in the

United States, " Energy Research & Social Science, Volume 79, 2021, 102055, ISSN 2214-6296, https://doi.org/10.1016/j.erss.2021.102055.

[107] J. M. Morales et al., Integrating Renewables in Electricity Markets, International Series in Operations Research & Management Science 205. New York, NY, USA: Springer, 2014.

[108] Stoker, J. J. (1969), Differential Geometry, New York: Wiley, ISBN 0-471-82825-4

[109] Zheng, X., Xu, N., Trinh, L. et al. A multi-scale time-series dataset with benchmark for machine learning in decarbonized energy grids. Sci Data 9, 359 (2022). https://doi.org/10.1038/s41597-022-01455-7

[110] https://www.ceps.cz/en/all-data

[111] Mohamed Alashqar, et al. Comprehensive economic analysis of PV farm -A case study of Alkarsaah PV farm in Qatar, Front. Energy Res. Sec. Smart Grids, 01 September 2022 Volume 10 - 2022 | https://doi.org/10.3389/fenrg.2022.987773

[112] M Anvari et al. Short-term fluctuations of wind and solar power systems, 2016 New J. Phys. 18 063027. DOI: 10.1088/1367-2630/18/6/063027

[113] Papoulis, A. (1984). Probability, Random Variables, and Stochastic Processes, 2nd ed. New York: McGraw Hill. pp. 145–149.

[114] X. -P. Zhang and Z. Yan, "Energy Quality: A Definition," IEEE Open Access Journal of Power and Energy, vol. 7, pp. 430-440, 2020, Doi: 10.1109/OAJPE.2020.3029767.

[115] G. Ma and X. -P. Zhang, "Real-Time Power Imbalance Time Series With Solar Power Penetration: Butterfly Curve," IEEE Transactions on Sustainable Energy, vol. 15, no. 2, pp. 1414-1417, April 2024, Doi: 10.1109/TSTE.2024.3368268.

[116] Munkhammar J, Widén J, van der Meer D. Probabilistic forecasting of high-resolution clear-sky index time-series using a Markov-chain mixture distribution model. Sol Energy 2019;184:688–95. http://dx.doi.org/10.1016/j.solener.2019.04.014.

[117] Joakim Munkhammar, Very short-term probabilistic and scenario-based forecasting of solar irradiance using Markov-chain mixture distribution modeling, Solar Energy Advances, Volume 4, 2024, 100057, ISSN 2667-1131, https://doi.org/10.1016/j.seja.2024.100057.

[118] Joakim Munkhammar, Dennis van der Meer, Joakim Widén, Very short-term load forecasting of residential electricity consumption using the Markov-chain mixture distribution (MCM) model, Applied Energy, Volume 282, Part A, 2021, 116180, ISSN 0306-2619, https://doi.org/10.1016/j.apenergy.2020.116180.

[119] I. G. Marneris, P. N. Biskas and E. A. Bakirtzis, "An Integrated Scheduling Approach to Underpin Flexibility in European Power Systems," IEEE Transactions on Sustainable Energy, vol. 7, no. 2, pp. 647-657, April 2016, Doi: 10.1109/TSTE.2015.2497081.

[120] Ofgem, Pay-as-bid or pay-as-clear pricing for energy balancing services in the Balancing Mechanism. Available: https://www.ofgem.gov.uk/sites/default/files/docs/2012/10/pay-as-bid-or-pay-as-clear-presentation.pdf

[121] Ofgem, Electricity Balancing Significant Code Review (EBSCR). 2015. Available: https://www.neso.energy/document/61496/download

[122] Rydin Gorjão, L., Jumar, R., Maass, H. et al. Open database analysis of scaling and spatio-temporal properties of power grid frequencies. Nat Commun 11, 6362 (2020). https://doi.org/10.1038/s41467-020-19732-7

[123] Schäfer, B., et al. Non-Gaussian power grid frequency fluctuations characterized by Lévy-stable laws and superstatistics. Nat Energy 3, 119–126 (2018). https://doi.org/10.1038/s41560-017-0058-z

[124] J. H. Talaq, F. El-Hawary, and M. E. El-Hawary, "A summary of environmental/economic dispatch algorithms," IEEE Transactions on Power Systems, vol. 9, no. 3, pp. 1508-1516, Aug. 1994, Doi: 10.1109/59.336110.

[125] R. D. Zimmerman, C. E. Murillo-Sánchez and R. J. Thomas, "MATPOWER: Steady-State Operations, Planning, and Analysis Tools for Power Systems Research and Education," IEEE Transactions on Power Systems, vol. 26, no. 1, pp. 12-19, Feb. 2011, Doi: 10.1109/TPWRS.2010.2051168.

[126] K. Chakravarthi, P. Bhui, N. K. Sharma and B. C. Pal, "Real Time Congestion Management Using Generation Re-Dispatch: Modeling and Controller Design," IEEE Transactions on Power Systems, vol. 38, no. 3, pp. 2189-2203, May 2023, Doi: 10.1109/TPWRS.2022.3186434.

[127] Sun, Y.; Cai, Z.; Zhang, Z.; Guo, C.; Ma, G.; Han, Y. Coordinated Energy Scheduling of a Distributed Multi-Microgrid System Based on Multi-Agent Decisions. Energies 2020, 13, 4077. https://doi.org/10.3390/en13164077

[128] X. Yan, C. Gu, X. Zhang, and F. Li, "Robust Optimization-Based Energy Storage Operation for System Congestion Management," IEEE Systems Journal, vol. 14, no. 2, pp. 2694-2702, June 2020, Doi: 10.1109/JSYST.2019.2932897.